The Abdus Salam International Centre for Theoretical Physics

United Nations Educational, Scientific and Cultural Organization

IAEA International Atomic Energy Agency

2332-31

School on Synchrotron and FEL Based Methods and their Multi-Disciplinary Applications

19 - 30 March 2012

Basic concepts for LEEM and XPEEM and applications

Andrea Locatelli

Sincrotrone Trieste, Italy

Basic concepts for LEEM and XPEEM and applications

A. Locatelli

Why do we need photomission electron microscopy?

- To combine SPECTROSCOPY and MICROSCOPY to characterise the structural, chemical and magnetic properties of surfaces, interfaces and thin films
- Applications in diverse fields such as surface science, catalysis, material science, magnetism but also geology, soil sciences, biology and medicine.

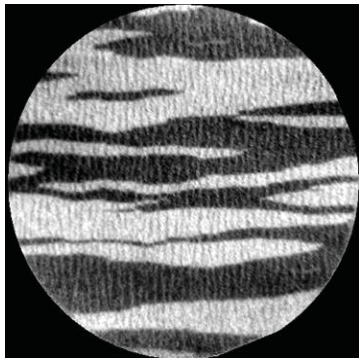

Magnetic state

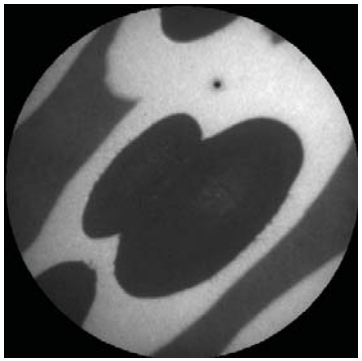

Composition maps

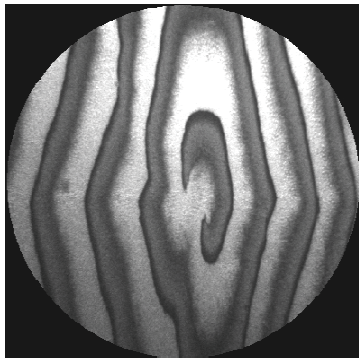

Surface reactions

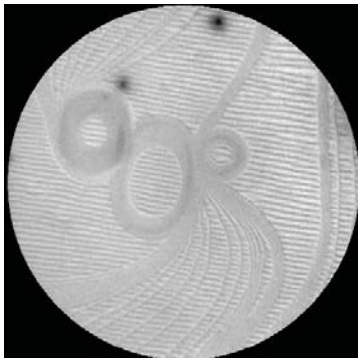

Self-organisation

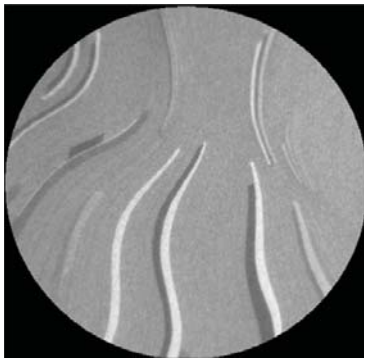

Thin film growth

Applications examples

Surface science

DOI: 10.1103/PhysRevLett.86.5088

Concentration maps, chemical stare, electronic strucutre of surfaces and interfaces

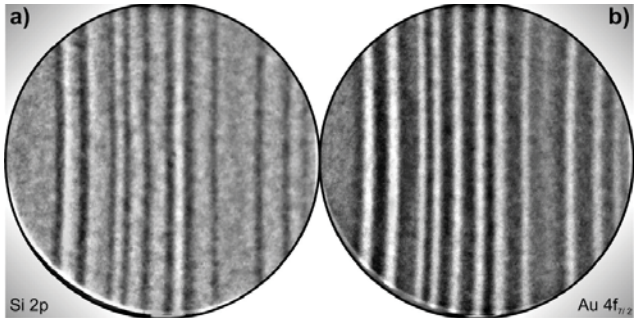

Ultrafast processes

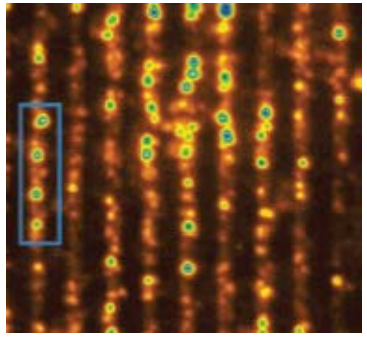

Nano Lett., Vol. 5, No. 6, **2005**

Surface plasmons

Magnetism

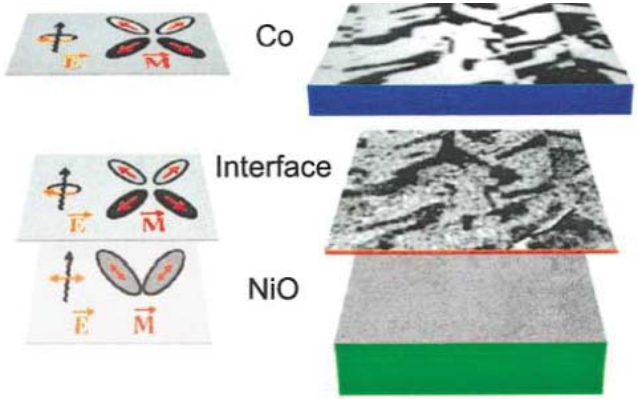

DOI: 10.1103/PhysRevLett.87.247201

Biology

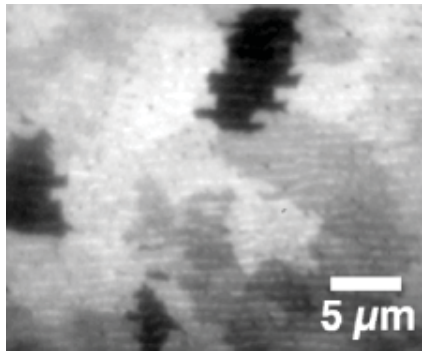

PRL **98,** 268102 (2007)

Biominerals: nacre

1. basic concepts of synchrotron based microscopy

Photoemission electron microscopy: spectroscopic modes

1	UV threshold microscopy	photoelectrons	with
2	XPS, UPS:	"	energy
3	Auger Spectroscopy:	Auger electrons AE	filter

4 XAS, XANES, XMCD, XMLD: Secondary electrons SE

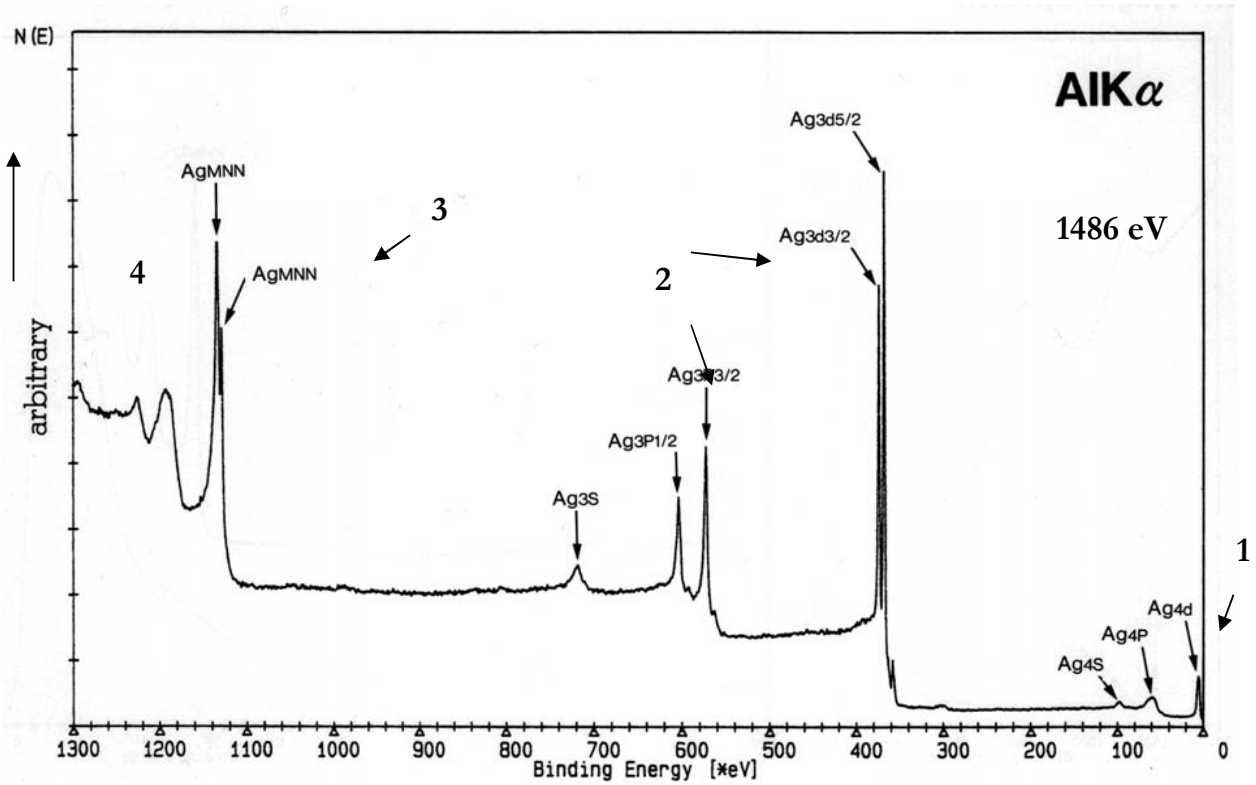

Principal spectroscopies implemented by PEEM

XAS (XANES, XMLD, XMCD)

- Elemental sensitivity; work function sensitivity.
- Sensitivity to emitter (site location, valence state, bond orientation, nearest-neighbour)
- Magnetic sensitivity
- Buried layer and interfaces accessible

When the photon energy matches a core level energy, a resonance in the secondary emission intensity is observed, originating from electronic transitions from core levels into unoccupied valence states via excitation processes occurring during the filling of the core holes. Such resonances are unique fingerprints that enable us to get precious information about the emitter chemical state, site location and valence state (x-ray absorption near edge spectroscopy). Due to the very low energy of the secondary electrons (less than 10 eV) and the increase of the inelastic mean free path of electrons at very low energy, XAS and XANES are used to probe buried interfaces or films up to a depth of ~10nm.

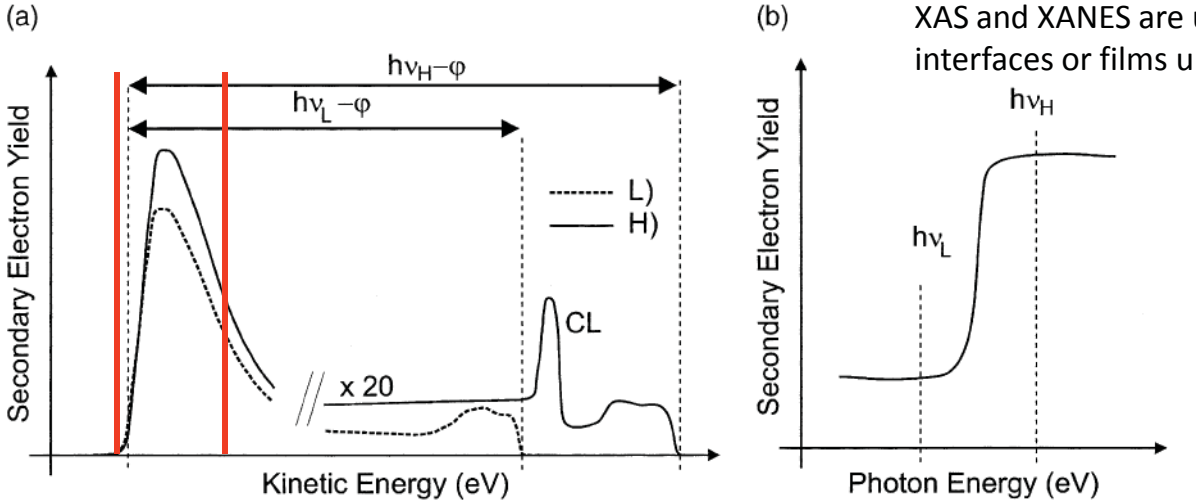

Principal spectroscopies implemented by PEEM

XPS and UPS

- Elemental and chemical sensitivity, surface core level shifts.
- Valence band: LOCAL electronic structure (micro-ARPES);
- Sensitivity to local structure (micro-XPD).
- High surface sensitivity
- Energy filter needed
- in XPEEM

The PEEM detects electrons emitted from atomic core levels with kinetic energy $E_{kin} = h\nu - E_{bin} - \phi$, where E_{bin} is the core level binding energy, $h\nu$ the photon energy and ϕ the work function. Typically $h\nu$ is kept fixed, with energies in the range provided by the beamline (50-1000 eV). The energy filter is used to select the kinetic energy E_{kin} of photoelectrons, which allows measuring the binding energies of emitting atoms or accessing the surface electronic structure, including surface states and resonances. The intensity of the photoemission signal is proportional to the number of emitters in the topmost layers within their energy-dependent escape depth, and thus provides straightforward and quantitative information about the surface chemical composition.

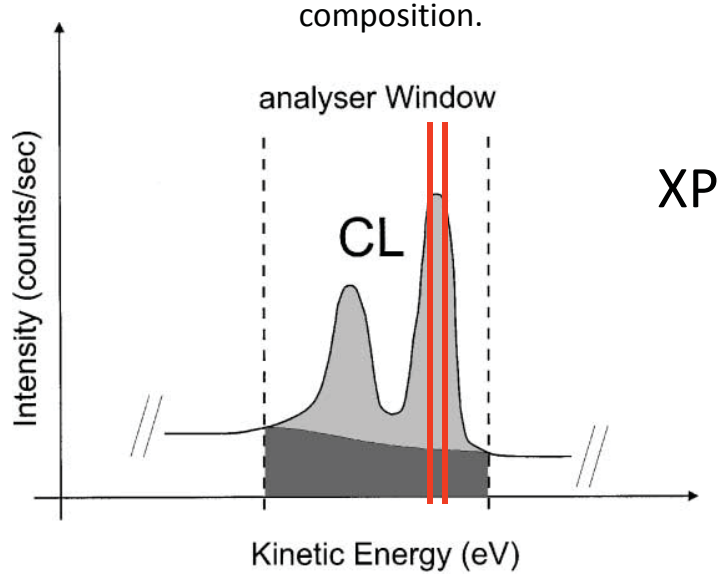

XPS mode: $h\nu$ const
$h\nu$ in / e^- out

X- ray microscopy: surface sensitivity

Inelastic mean free path ("universal curve") determines sampling depth

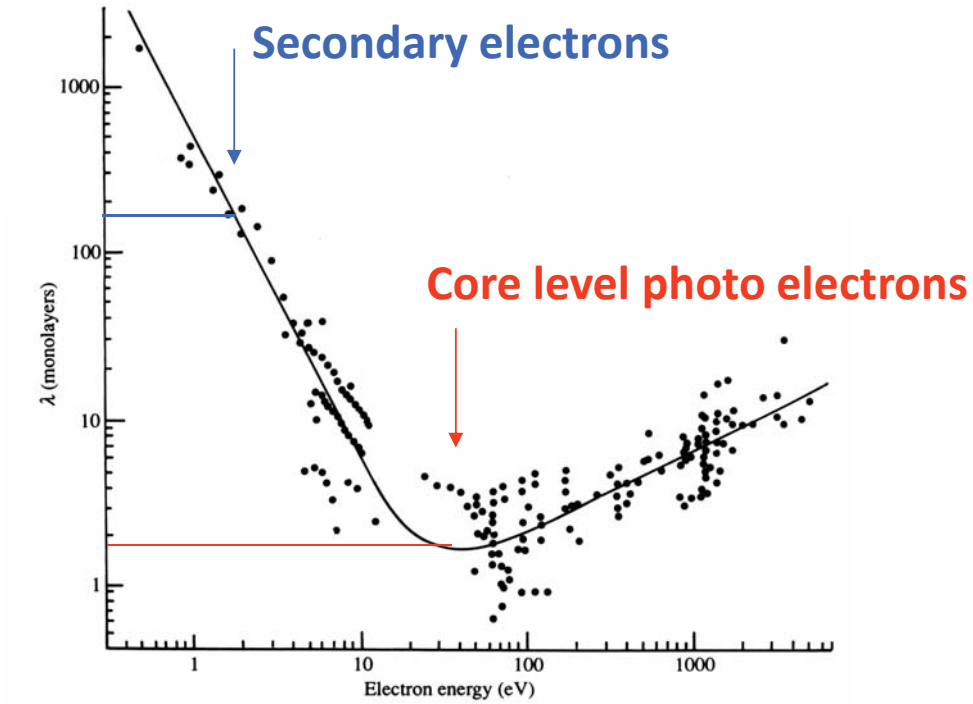

XAS, XANES, XMCD, XMLD can probe thin films and buried interfaces to max. depth of max 10 nm

Sensitivity to the topmost surface layers, especially at K. E. 50-150 eV

Reviews on spectromicroscopy

[1.1] Gunther S, Kaulich B, Gregoratti L, Kiskinova M 2002 *Prog. Surf. Sci.* **70** 187–260.

[1.2] Bauer E and Schmidt T, 2003 *"Multi-Method High Resolution Surface Analysis with Slow Electrons"* in: High Resolution Imaging and Spectroscopy of Materials, Eds. Ernst F. and Ruehle M. (Springer, Berlin Heidelberg 2003) 363-390.

[1.3] Bauer E 2001 *J. Electron Spectrosc. Relat. Phenom.* **114-116** 976-987.

[1.4] Bauer E 2001 J. Phys.: Condens. Matter **13** 11391-11405.

2. PEEM instrument and methods

Method characteristics

X-ray photo emission electron microscopy (XPEEM)

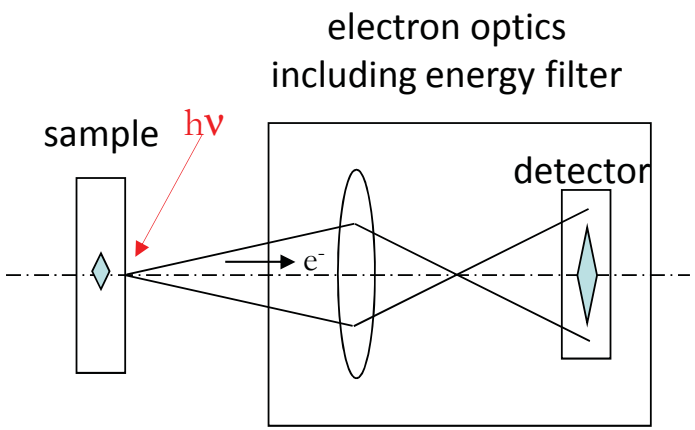

- Direct imaging, parallel detection
- Dynamic processes ok!
- Lateral resolution is determined by electron optics (10-50 nm); with aberration correction: few nm will be possible.
- Requires smooth sample morphology.
- Combination with LEEM/LEED
- Spectroscopic PEEM! Intermediate spectroscopic ability(200 meV).
- Diffraction imaging possible.
- Sensitive in plane magnetisation!
- Vacuum better than $1 \cdot 10^{-5}$ mbar

The cathode lens

1. In emission microscopy θ (emission angle) is large. Electron lenses can accept only small θ because of large chromatic and spherical aberrations

2. Solution of problem: accelerate electrons to high energy before lens → Immersion objective lens or cathode lens

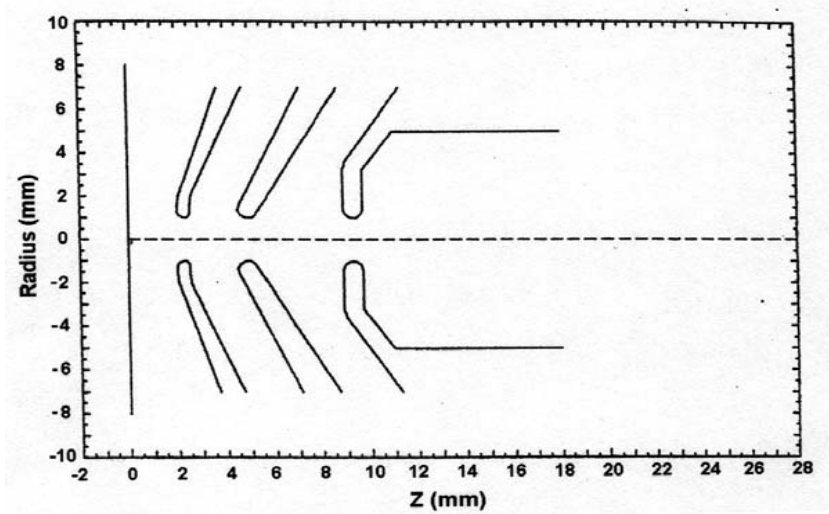

Accelerating field

Imaging lens

$$n \sin\theta = \text{const}$$
$$n \sim \sqrt{E}$$
$$\theta \rightarrow \alpha$$
$$\sin \alpha / \sin \alpha_0 = \sqrt{E_0/E}$$

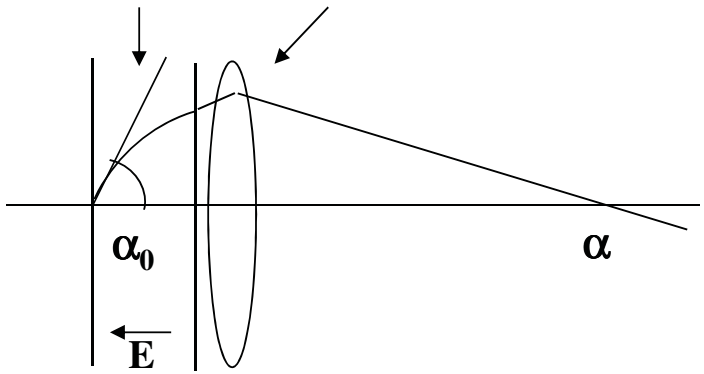

E_0 start energy

E final energy

Example for E = 20000 eV:

E_0	2 eV	200 eV
α for $\alpha_0 = 45^o$	0.4^o	4.5^o

Basic PEEM instruments

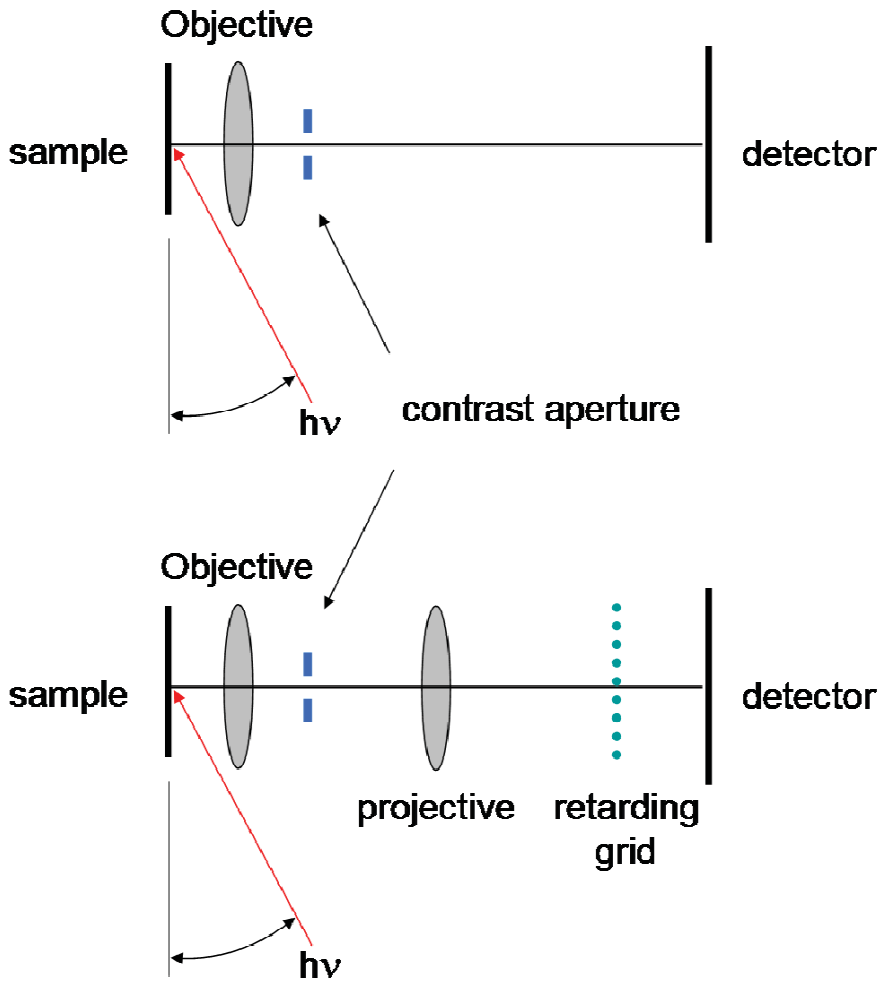

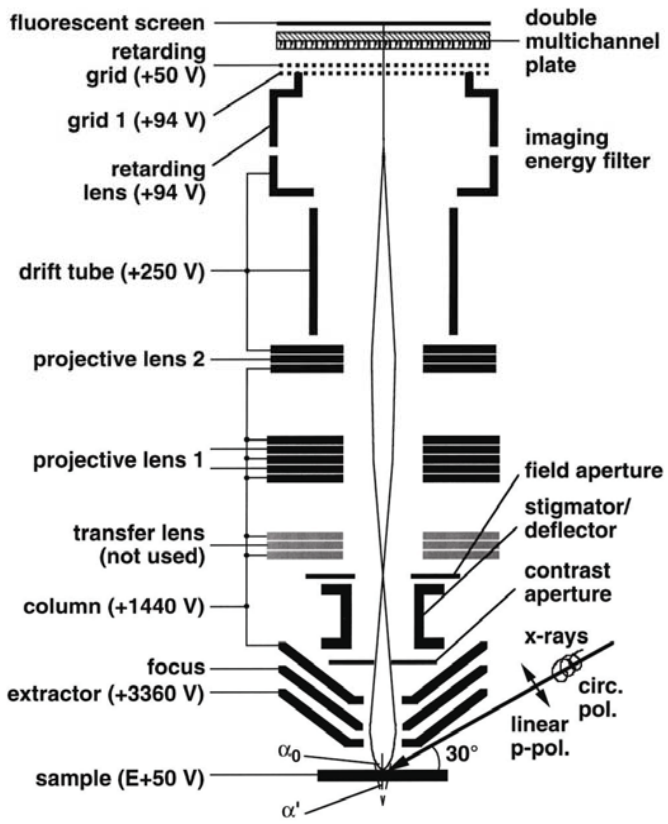

Focus PEEM with high pass filter

Properties accessible in XPEEM

ELEMENTAL COMPOSITION & CHEMICAL STATE

C1s image of SWCN

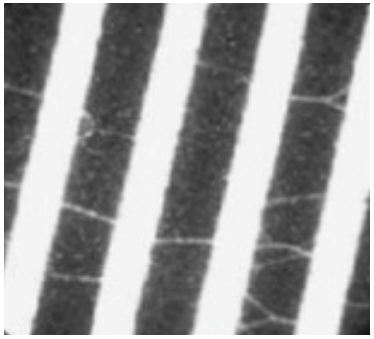

1 μm

S. Suzuki et al, J. El. Spec Rel. Phenom. 357-360, 144 (2005)

Pb on W110

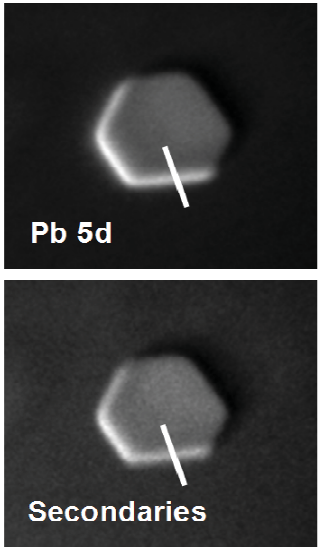

500 nm

MAGNETIC STATE using XMCD

Co nanodots on Si-Ge

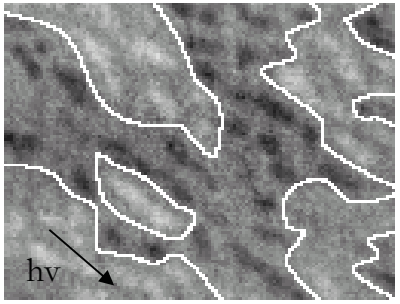

Co - L_3 edge

A. Mulders et al, Phys. Rev. B 71, 214422 (2005).

patterned structures

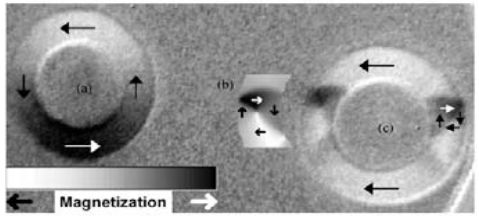

1.6 μm

M. Klaeui et al, Phys. Rev. B 68, 134426 (2003).

References on XPEEM

[2.1] Tonner B P, Harp G R 1988 *Rev. Sci. Instrum.* **59** 853.

[2.2] Swiech W et al 1997 *J. Electr. Spectr. Relat. Phenom.* **84** 171.

[3.3] Kleineberg U et al 1999 *J. Electr. Spectr. Relat. Phenom.* **103** 931.

[4.4] Chmelik J et al 1983 *Optik* **83**, 155.

[5.5] Cruise D R 1964 *J. Appl. Phys*. **35** 3080.

3. LEEM and SPELEEM

Low energy electron microscopy

In a LEEM, a beam of high energy electrons (5-20 keV) is decelerated through the objective lens in front of the specimen surface, onto which it impinges normally with energy in the range 0 to few hundred eV. The beam energy is varied by changing the bias voltage between sample and electron emitter. The elastically backscattered electrons are reaccelerated through the objective lens, following the inverse pathway.

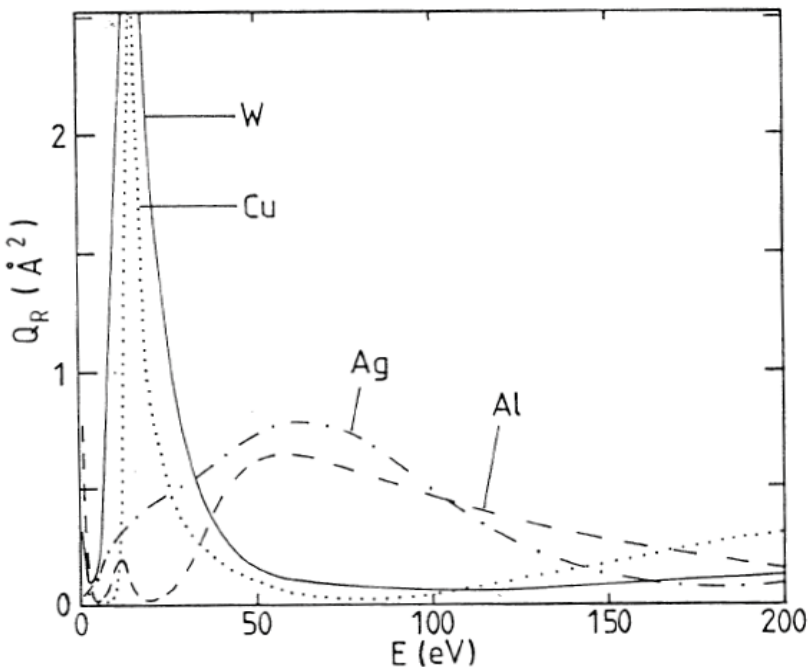

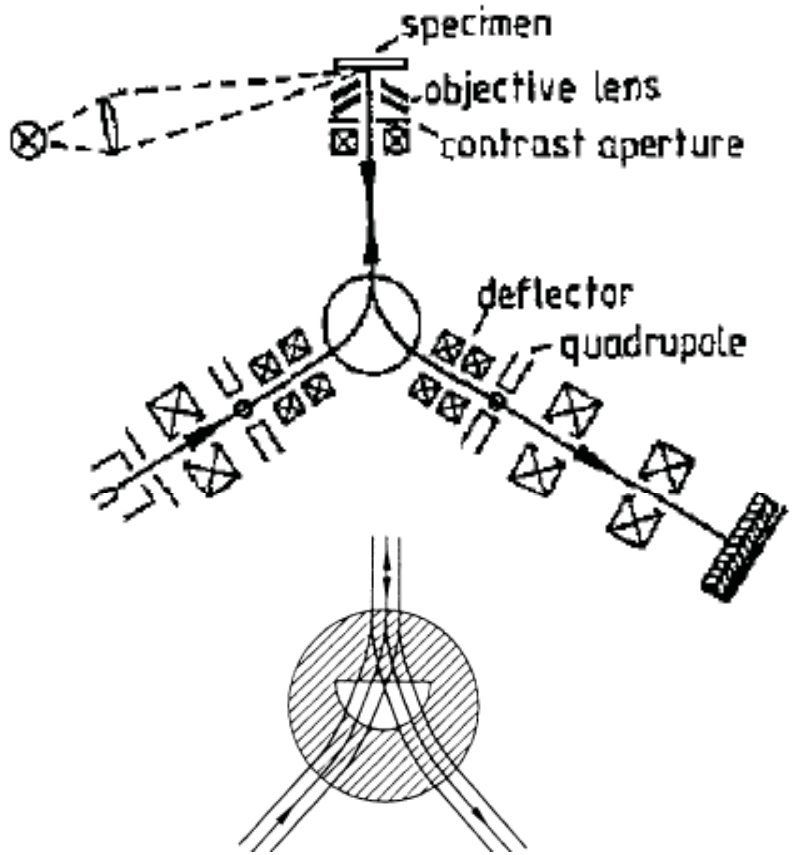

E. Bauer: *Low Energy Electron Microscopy*, Rep. Prog. Phys. 57 (1994) 895-938.

Spectroscopic Photoemission and low energy Electron Microscope

Spectroscopic imaging
XPEEM / LEEM

microprobe-diffraction
ARPES / LEED

microprobe-spectroscopy
XPS

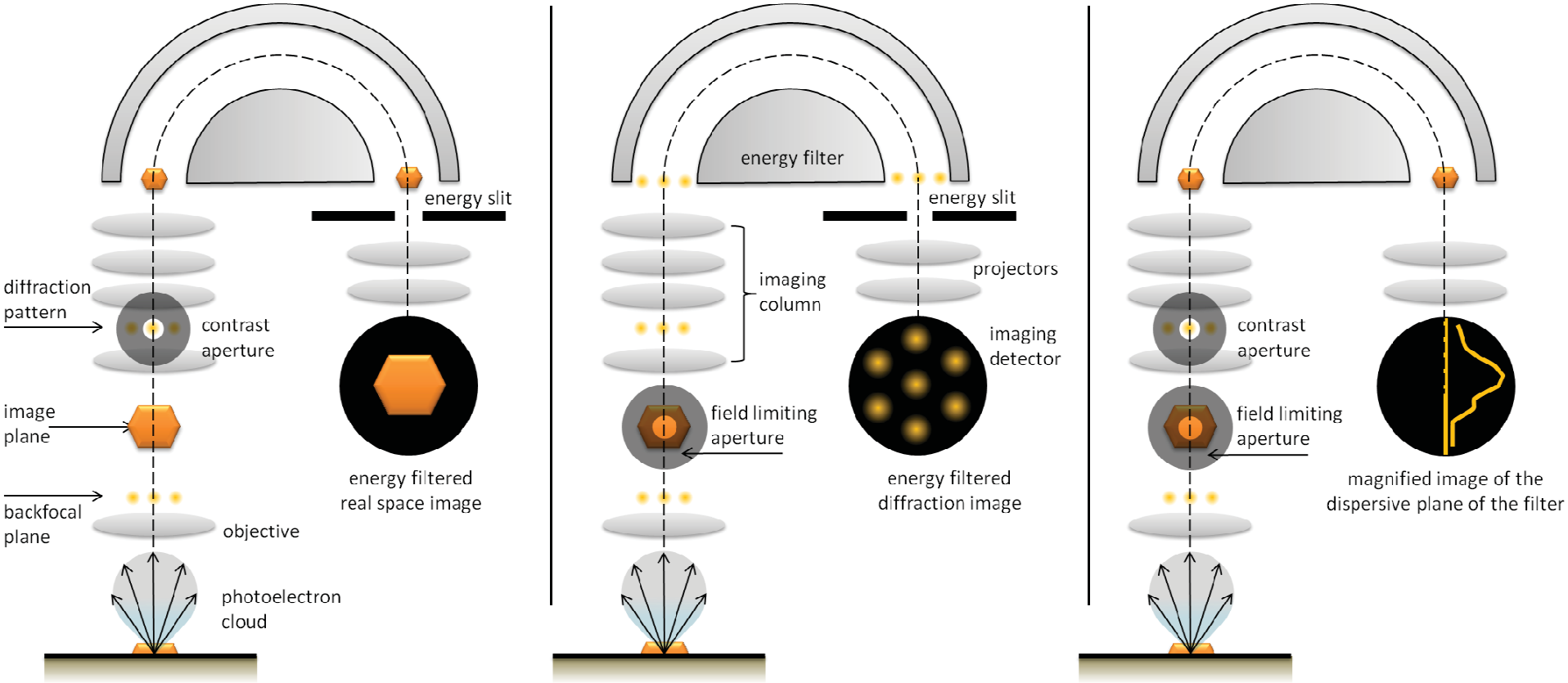

Microprobe measurements are limited to surface areas of 2 microns in diameter!

Spectroscopic Photoemission and low energy Electron Microscope

Performance: lateral resolution in imaging: 10nm (LEEM)
30 nm (XPEEM)
energy resolution: 0.3 eV (0.2 in microprobe spectroscopy)

Key feature: multi-method approach to the study of surfaces and interfaces, based on *imaging* and *diffraction* techniques.

Probe: *low energy electrons* (0-500 eV) ⟷ structure sensitivity
soft X-rays (50-1000 eV) ⟷ chemical state, magnetic state
electronic structure

Applications: *characterization* of materials at microscopic level
magnetic imaging of microstrucutres
growth process

Which properties does LEEM allow to probe?

Different contrast mechanisms are available in LEEM for strucutre characterization

SURFACE STRUCTURE

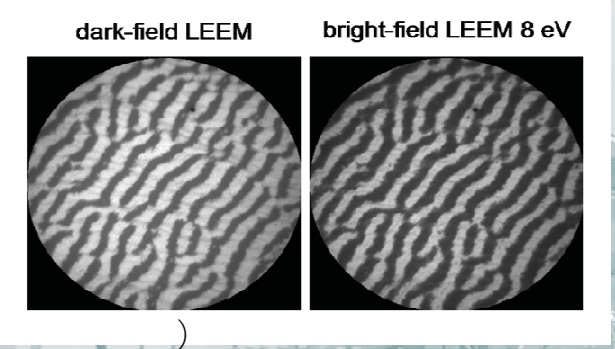

diffraction contrast

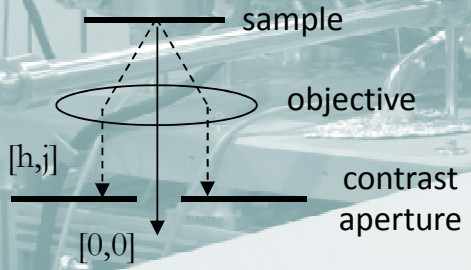

FILM THICKNESS

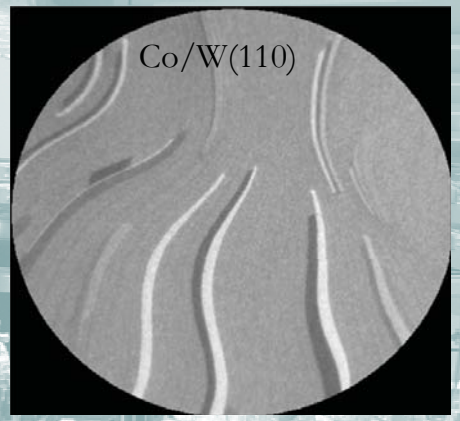

quantum size contrast

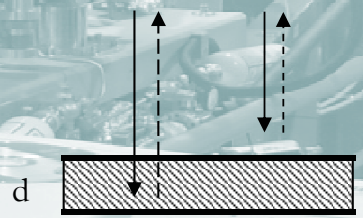

STEP MORPHOLOGY

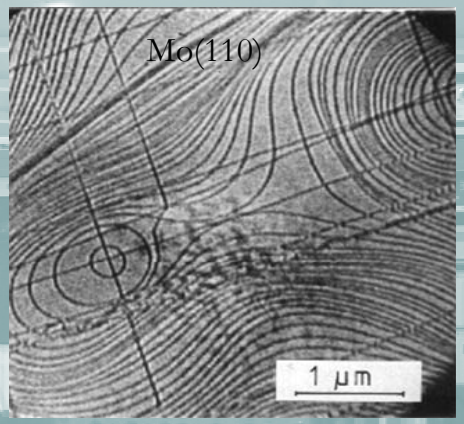

geometric phase contrast

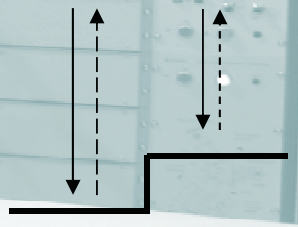

Darkfield LEEM: imaging domains

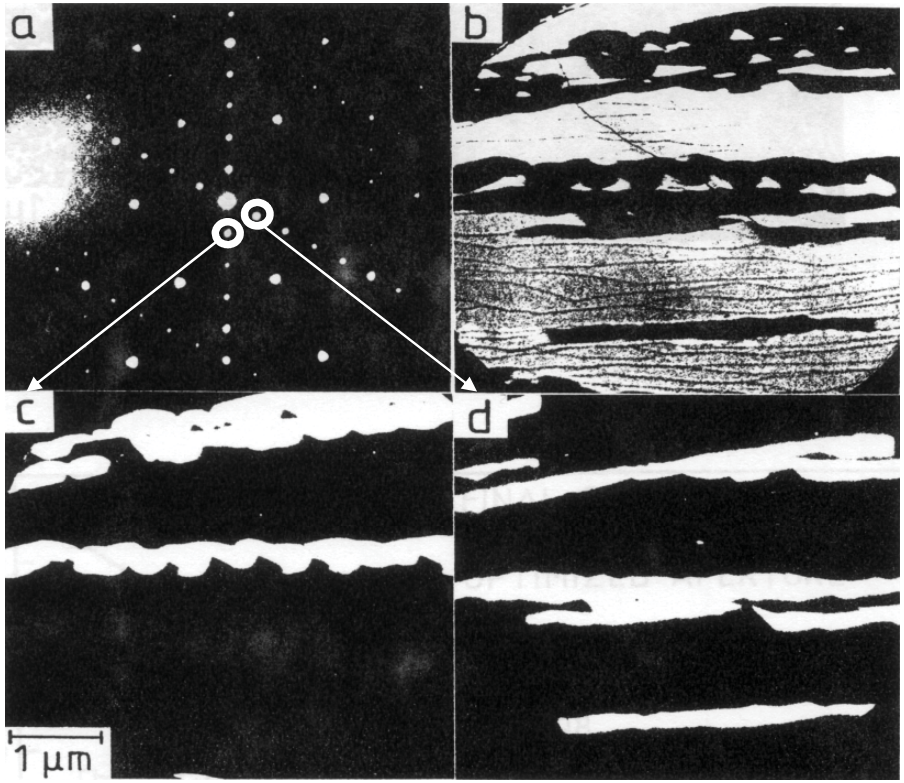

Au($\sqrt{3}\times\sqrt{3}$)-R30^o + Au(5 ×2) on Si(111)
b c,d

LEEM also much brighter and better resolution ⇒ dynamical phenomena
LEED much easier to interpret than PED ⇒ use for structure analysis

Video rate imaging using LEEM

very favourable backscattering cross section at low electron energy!

[001]

Ni growth on W(110): step flow and completion of ps ML

Ni growth on W(110): formation of a striped phase above 1 ps ML Ni

540 < T < 750 C

Complementary methods!

microprobe-XPS

LEED

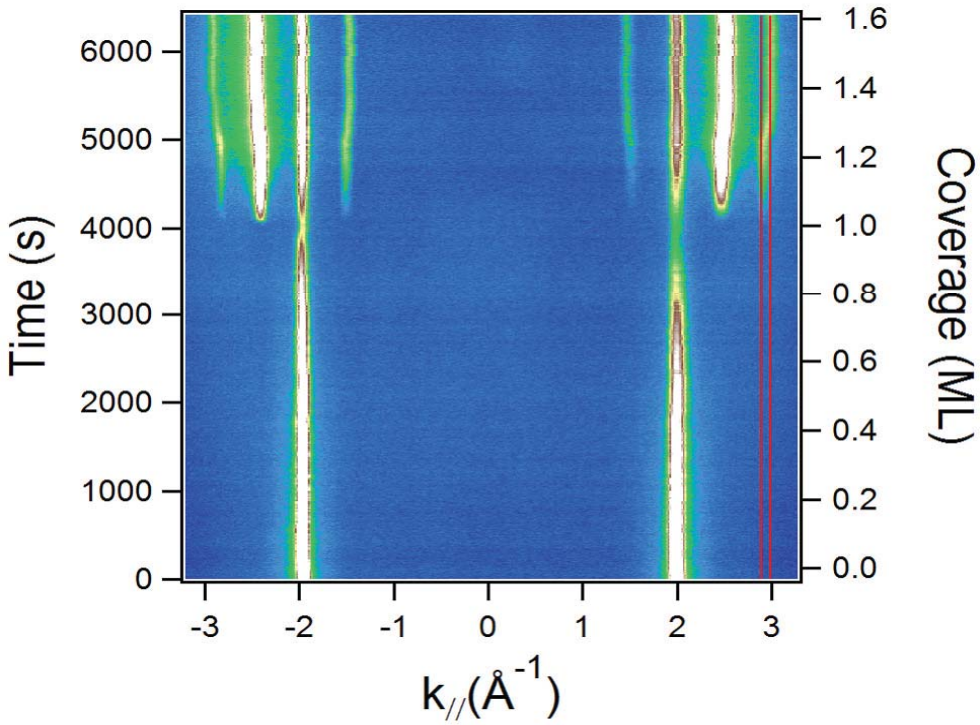

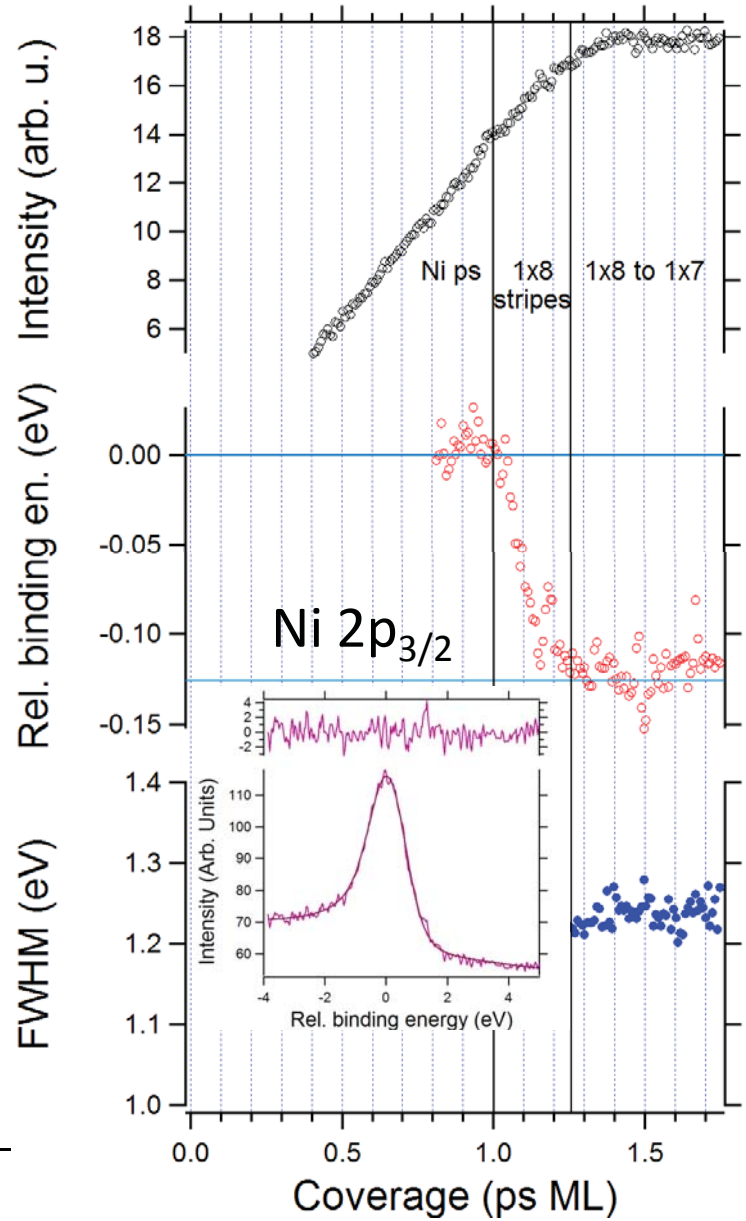

EELS microscopy (requires energy filter)

K-space

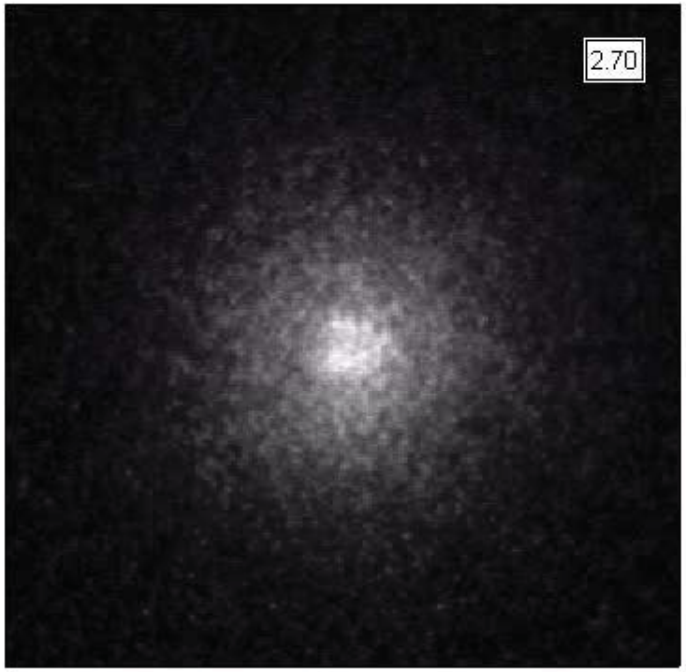

Ag-O(1x12)/W(110)

Imaging (20 nm lateral res.)

FoV 1.5 µm

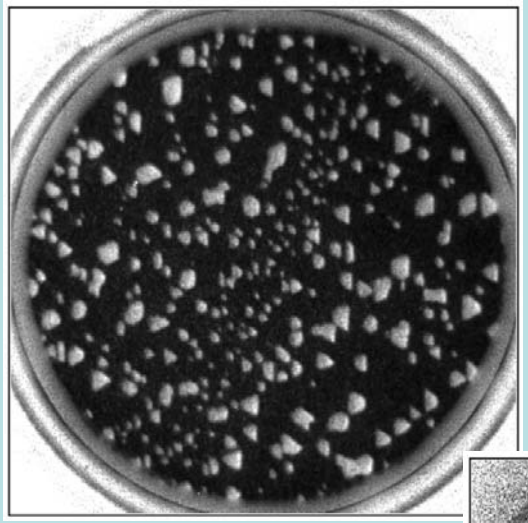

LEEM

EELS

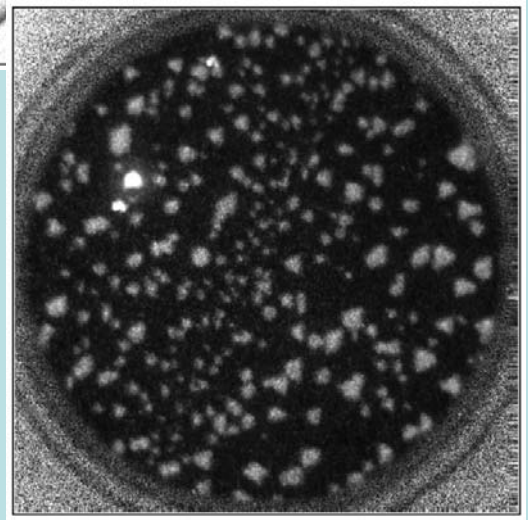

Mentes et al; e-Journal of Surface Science and Nanotechnology, Vol. 9 (2011) pp.72-79

References

[3.1] *Low Energy Electron Microscopy;*
E. Bauer;
Rep. Prog. Phys. 57, 895-938 (1994).
doi: 10.1088/0034-4885/57/9/002

[3.2] *LEEM basics;*
E. Bauer;
Surf. Rev. Lett. 5, 1275-1286 (1998).
doi: 110.1142/S0218625X98001614

[3.3] *Trends in low energy electron microscopy;*
M S Altman
Journal of Physics: Condensed Matter 22, 084017 (2010).
doi: 10.1088/0953-8984/22/8/084017

[3.4] *LEEM and SPLEEM;*
Ernst Bauer; in *Science of Microscopy*, pp. 606-656. edited by P. Hawkes and J. Spence, Kluwer/Springer Academic Publishers, 2007.

[3.5] Bauer E, *1991 Ultramicroscopy* **36** 52.

[3.6] Bauer E, Koziol C, Lilienkamp G, Schmidt Th 1997 *J. Electron Spectrosc. Relat. Phenom.* **84** 201-209.

[3.7] Schmidt Th, Heun S, Slesak J, Diaz J., Prince KC, Lilienkamp G, Bauer E ; *Surf. Rev. Lett.* **5** 1287-1296 (1998).

[3.8] Locatelli A, Abelle L, Mentes T O, Kiskinova M, Bauer E, *Surf. Interface Anal.* **38**, 1554-1557 (2006).

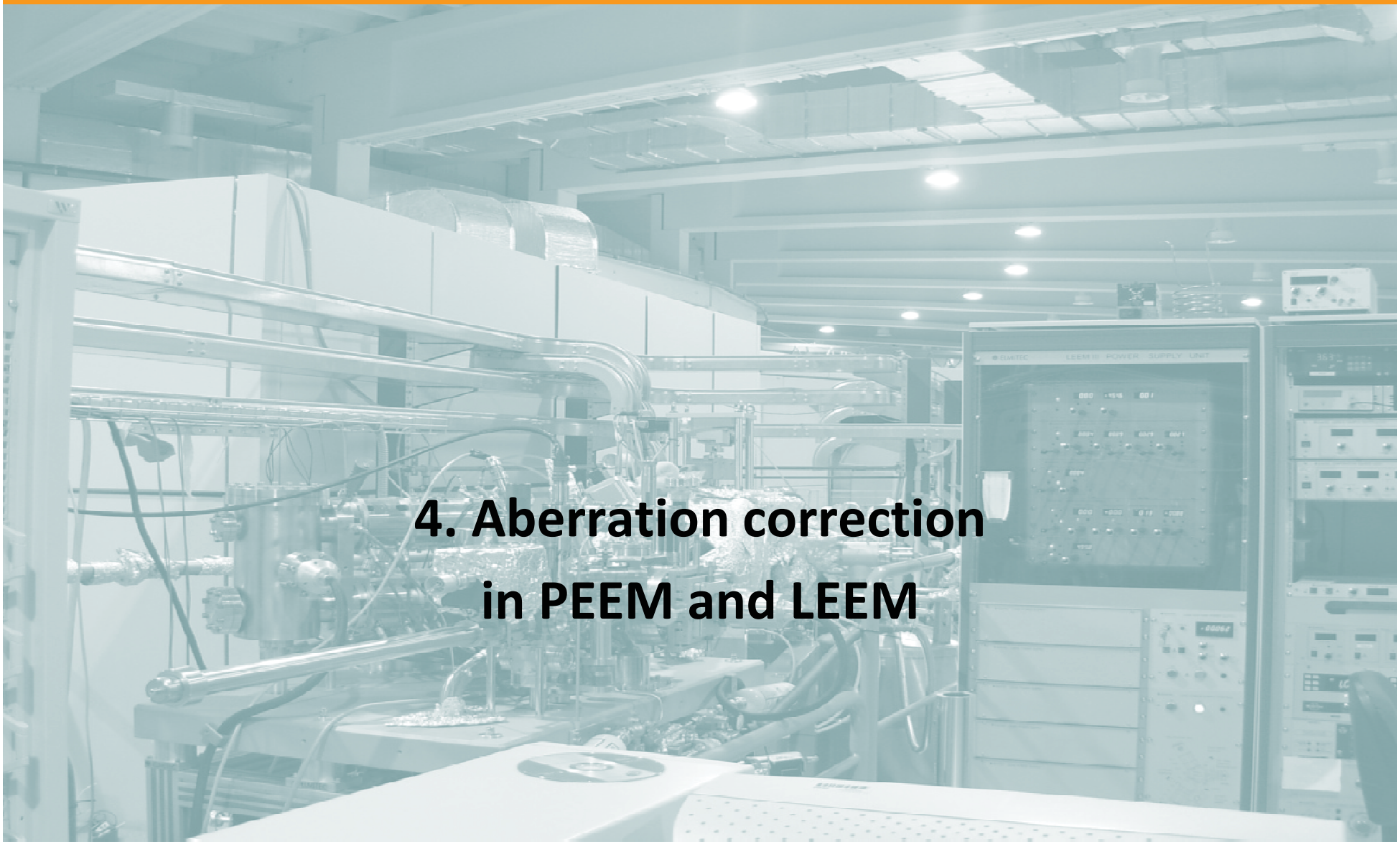

4. Aberration correction in PEEM and LEEM

Lateral resolution in PEEM: effect of aberrations

CROMATIC

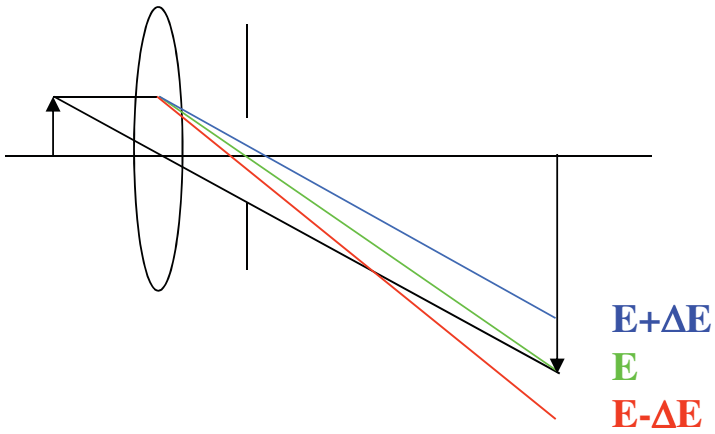

slower (faster) electrons
are more (less) deflected

$$D_{CH} \approx \varepsilon \alpha$$

SPHERICAL

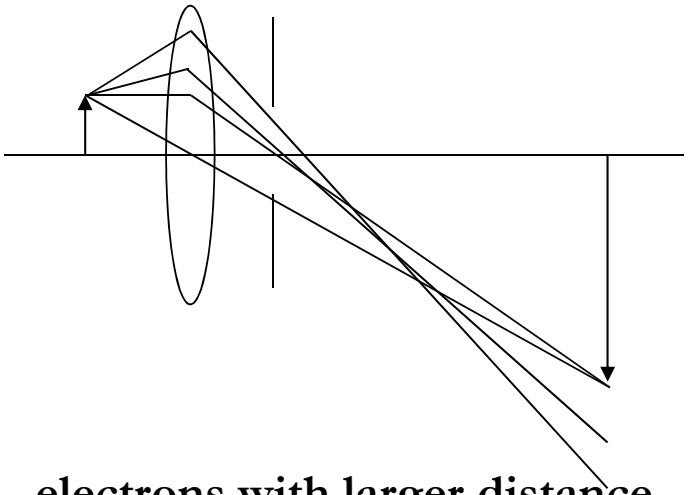

electrons with larger distance
from axis are more deflected
(stronger field!)

$$D_{SP} \approx \rho \alpha^3$$

α = acceptance angle, small

DIFFRACTION BY THE APERTURE

$$d_D = 0.6\, \lambda / r_A$$

Lateral resolution performance

- SPEM: Fresnel zone plate

$$\delta_m = \sqrt{\delta_i^2 + \delta_g^2 + \delta_c^2} =$$

$$= \sqrt{(1.22\,\Delta r/m)^2 + \left(\sigma \frac{q}{p}\right)^2 + \left(2r\frac{\Delta E}{E}\right)^2}$$

intrinsic ZP resolution (from Rayleigh criterion)	demagnified source	chromatic aberration
small outermost zone	small source size	monochromatic beam

e.g. Δr=100 nm and typical beamline
δ_i=122 nm
δ_g= 30 $\mu m^2 \times$ 8 mm/3 m=80 nm
δ_c=100 μm $\times$ 0.2eV/500eV=40 nm

30nm possible at the state of the art

- PEEM:
  - Objective lens and contrast aperture determine lateral resolution

Approximate resolution:

$$d = \sqrt{d_{SP}^2 + d_{CH}^2 + d_D^2}$$

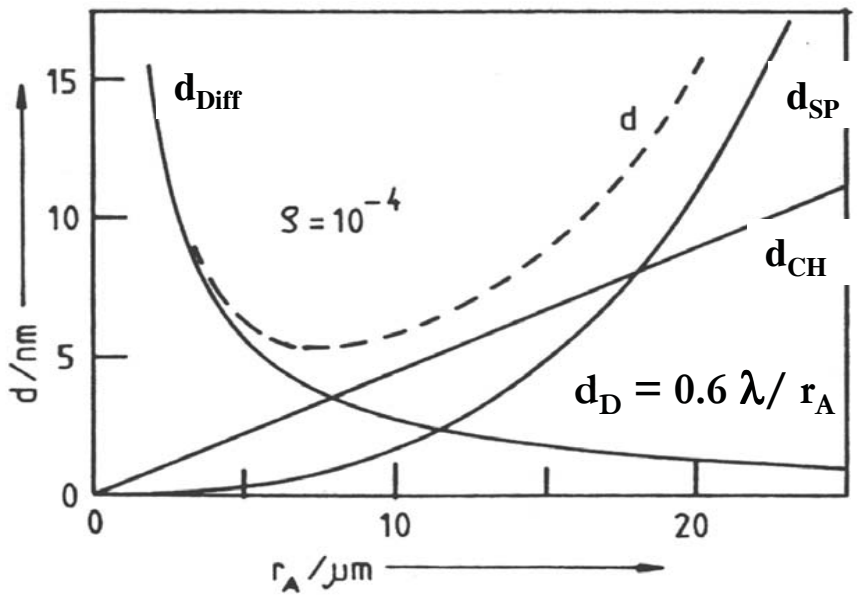

Aberration correction in light optics

Round **convex** lenses

Round **concave** lenses

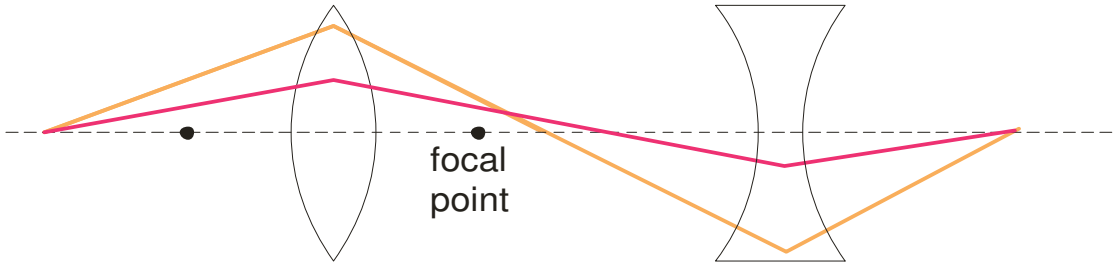

Spherical aberration

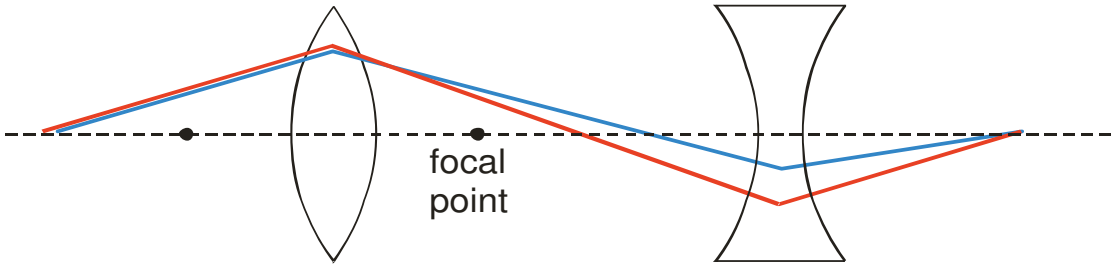

Chromatic aberration

Aberration correction in electron optics

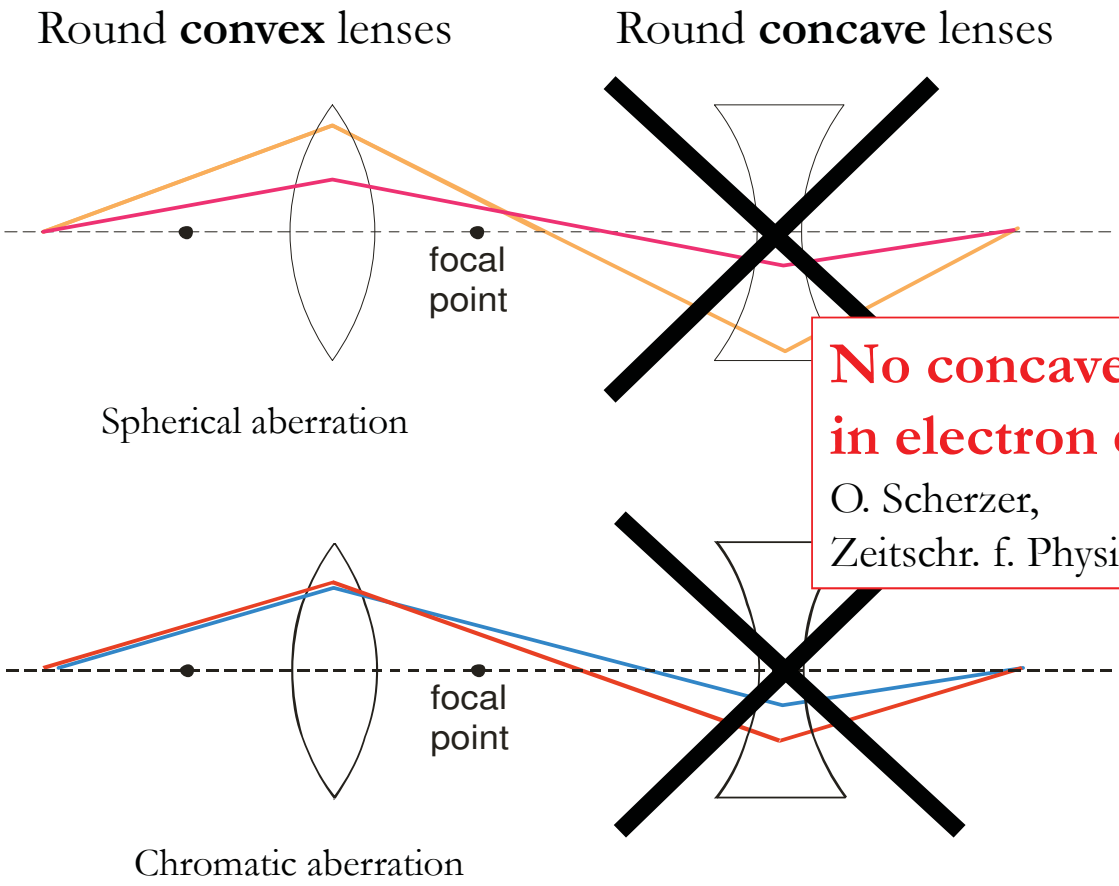

No concave lenses in electron optics!

O. Scherzer,
Zeitschr. f. Physik 101, 593, (1936)

Aberration correction by electron mirror

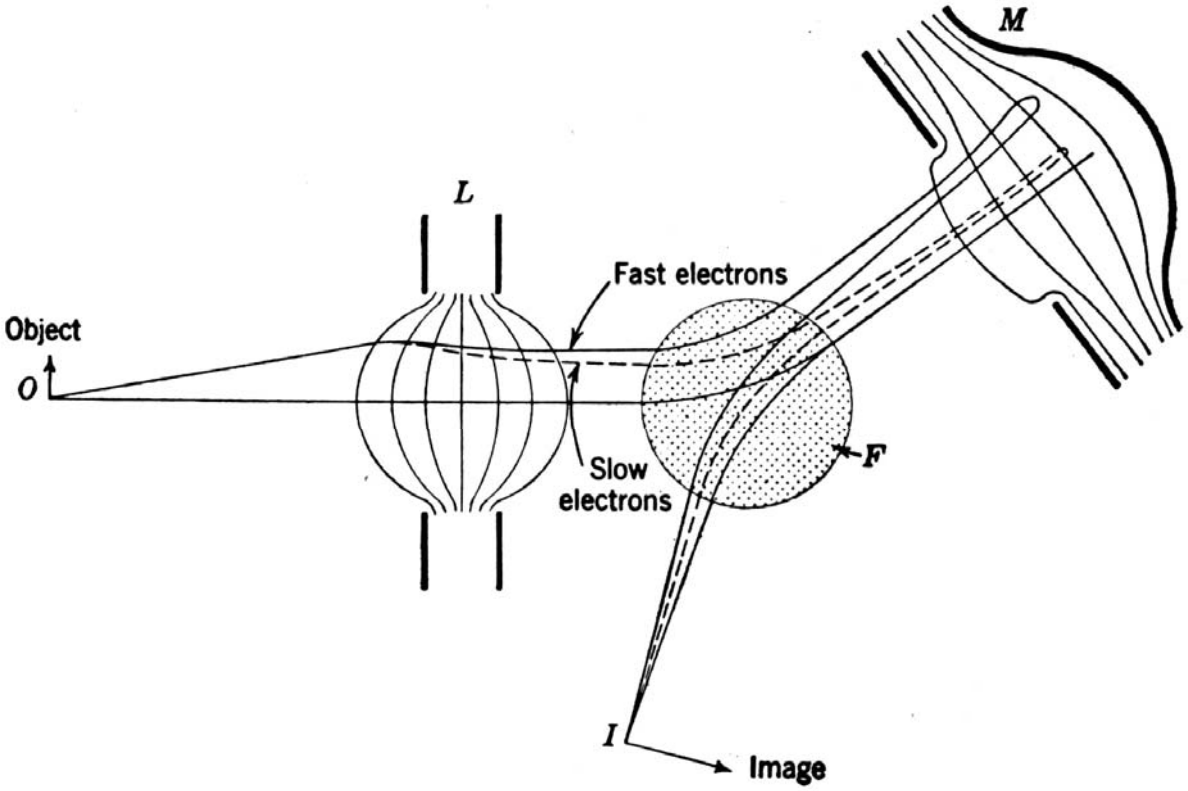

V.K. Zworykin et al, Electron Optics and the Electron Microscope, John Wiley, New York 1945

Improvement with mirror corrector

Simultaneous improvement in

Transmission and Resolution!!!

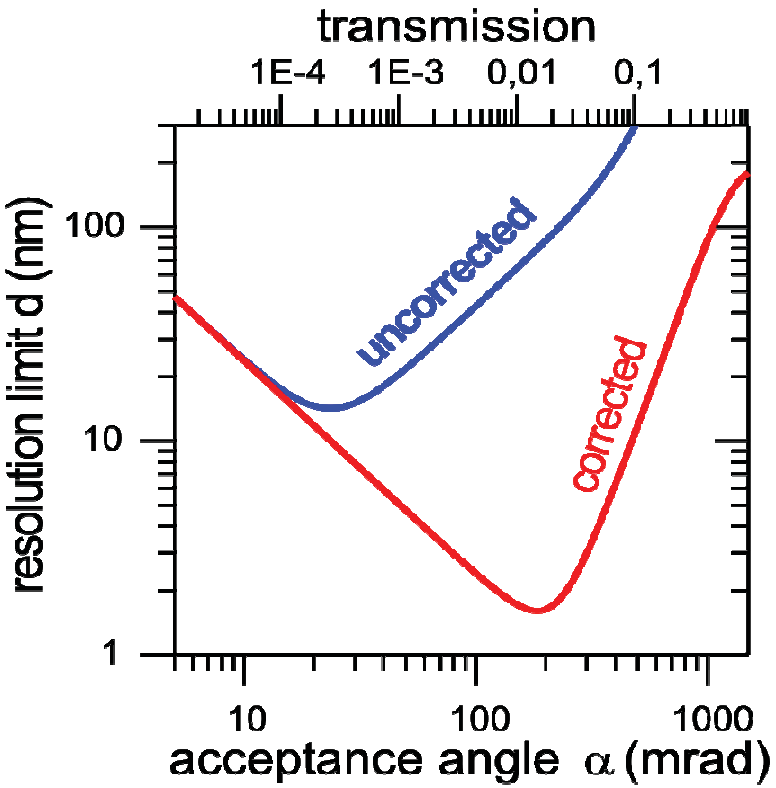

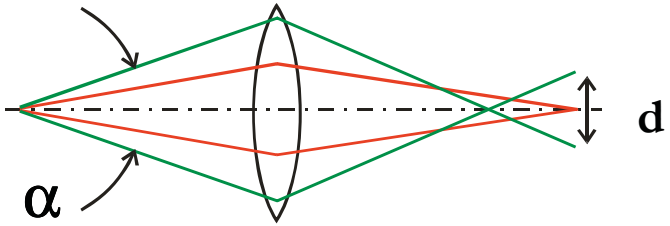

Resolution limit	without correction	with correction
Spherical aberr.	$\alpha^3 + \ldots$	α^5
Chromatic aberr.	$\Delta E\ \alpha + \ldots$	$\Delta E\ \alpha^2 + \Delta E^2\ \alpha$
Diffraction	$1/\alpha$	$1/\alpha$

D. Preikszas, H. Rose, J. Electr. Micr. 1 (1997) 1

Th. Schmidt, D. Preikszas, H. Rose et al., Surf.Rev.Lett 9 (2002) 223

XPEEM-LEEM with aberration correction: SMART

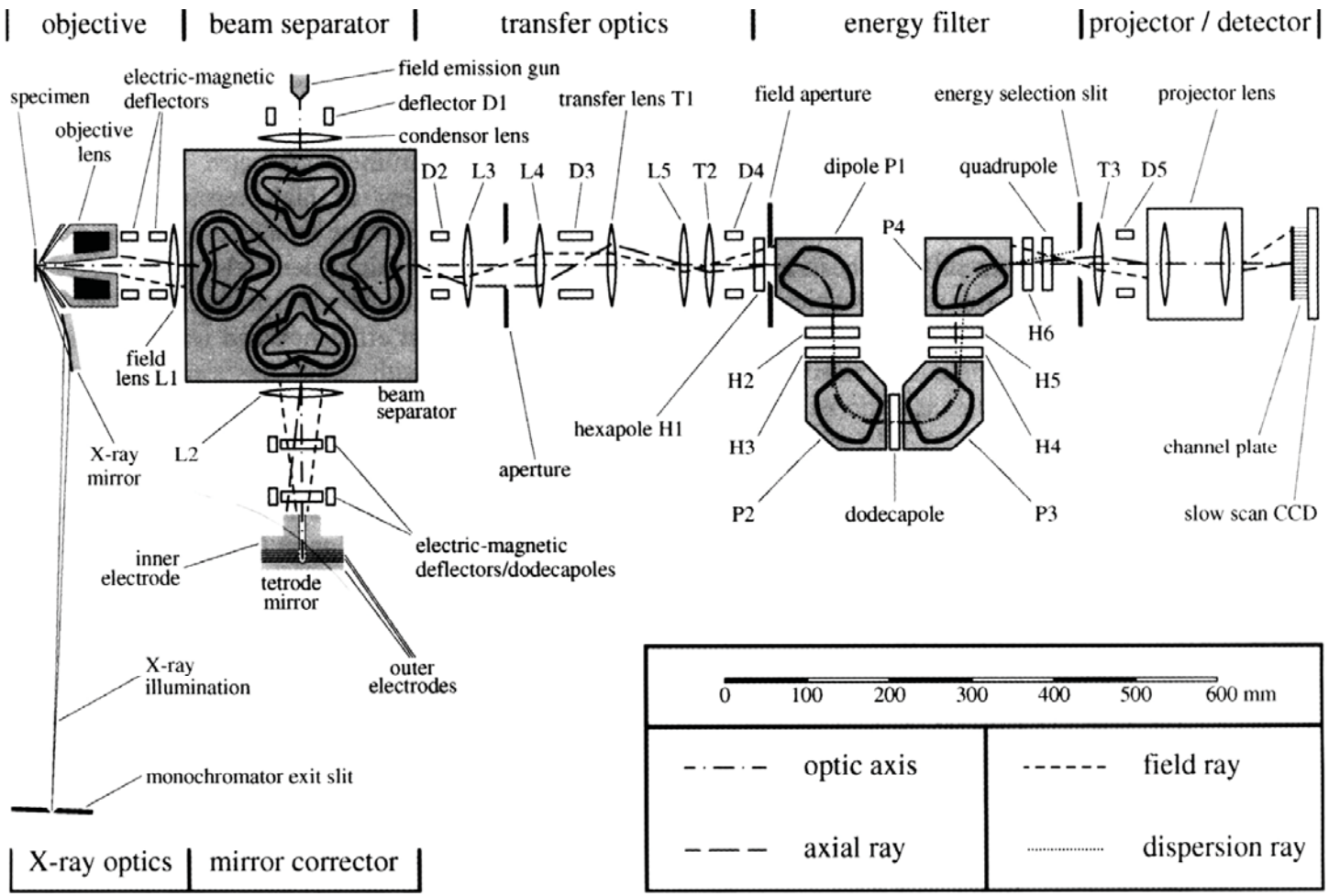

Latest Results of the SMART microscope @BESSY

Atomic steps on Au(111),
LEEM 16 eV, FoV = 444 nm x 444 nm
(18.09.06)

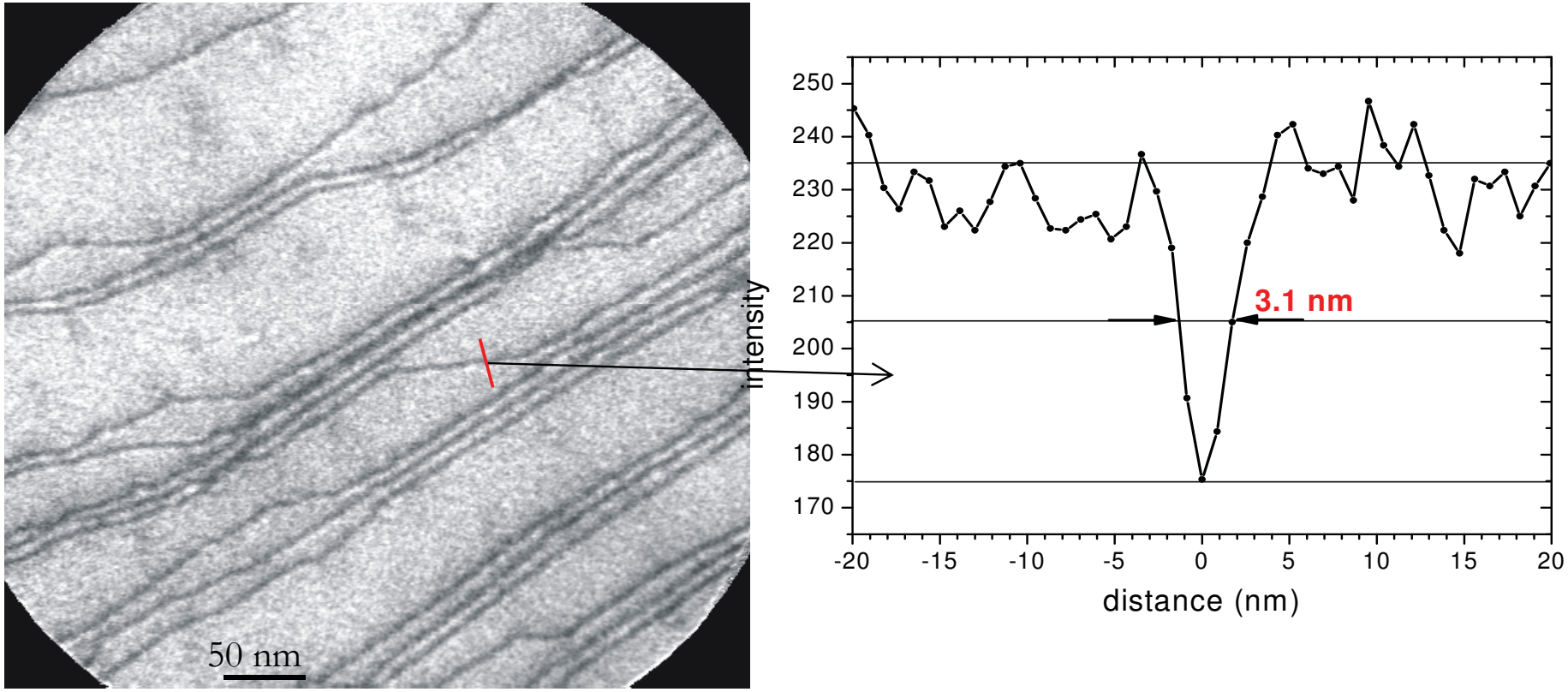

Courtesy of Th. Schmidt et al.; 5th Int. Conf. LEEM/PEEM, Himeji, 15.-19. Oct. 2006

Resolution limitation: space charge effects

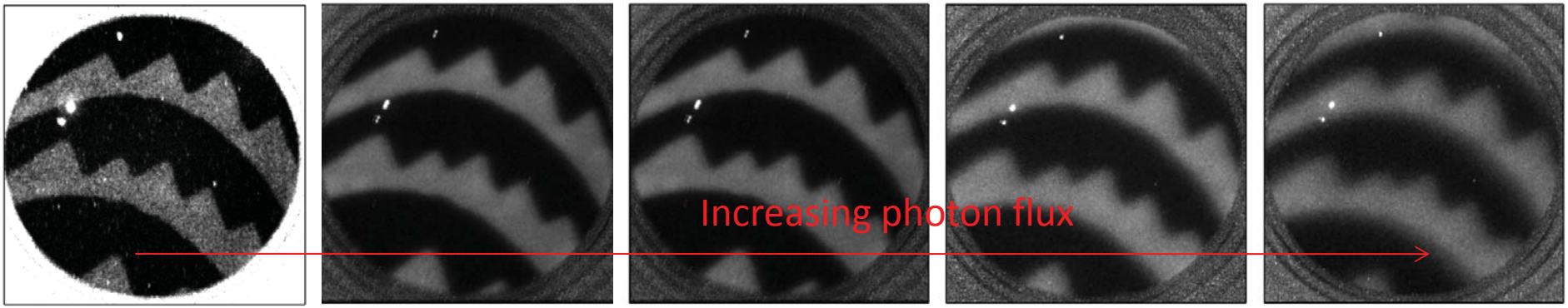

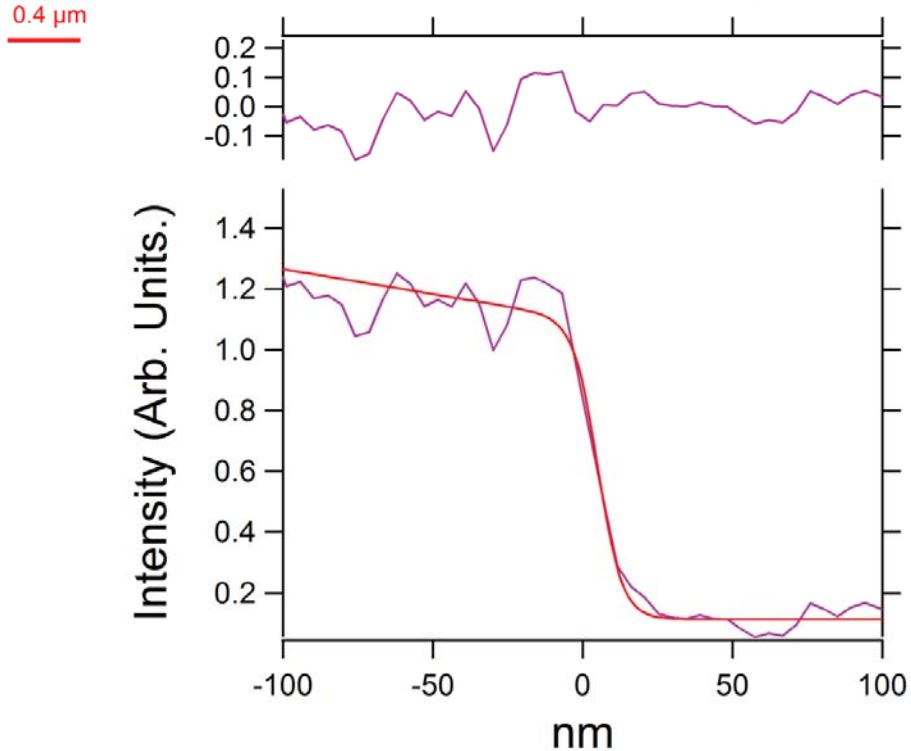

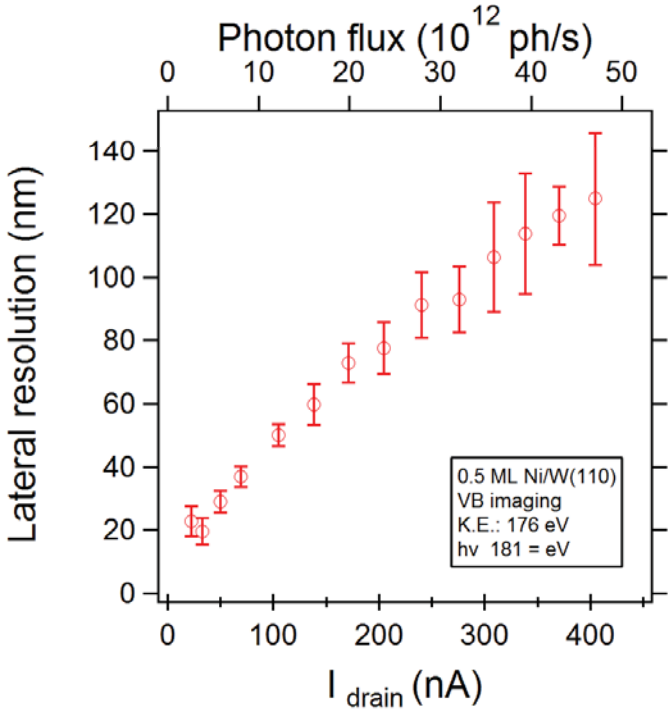

A. Locatelli et al, Ultramicroscopy, 2011

References on aberration correction in XPEEM/LEEM

[4.1] Wichtendahl R et al 1997 *J. Electr. Spectr. Relat. Phenom.* **84** 1249-1256.

[4.2] Fink R et al 1998 *Surf. Rev. Lett.* **5** 231-250.

[4.3] Schmidt Th et al 2002 *Surf. Rev. Lett.* **9** 223-232.

[4.4] J Feng et al 2005 *J. Phys.: Condens. Matter* **17** S1339-S1350.doi:10.1088/0953-8984/17/16/005

[4.5] Wan W , Feng J, Padmore H A and Robin D S 2004 *Nucl. Instrum. Methods Phys Res. A* **519**, 222-229.

[4.6] Wan W, Feng J and Padmore H A 2006 *Nucl. Instrum. Methods Phys Res. A* **564**, 537-543.

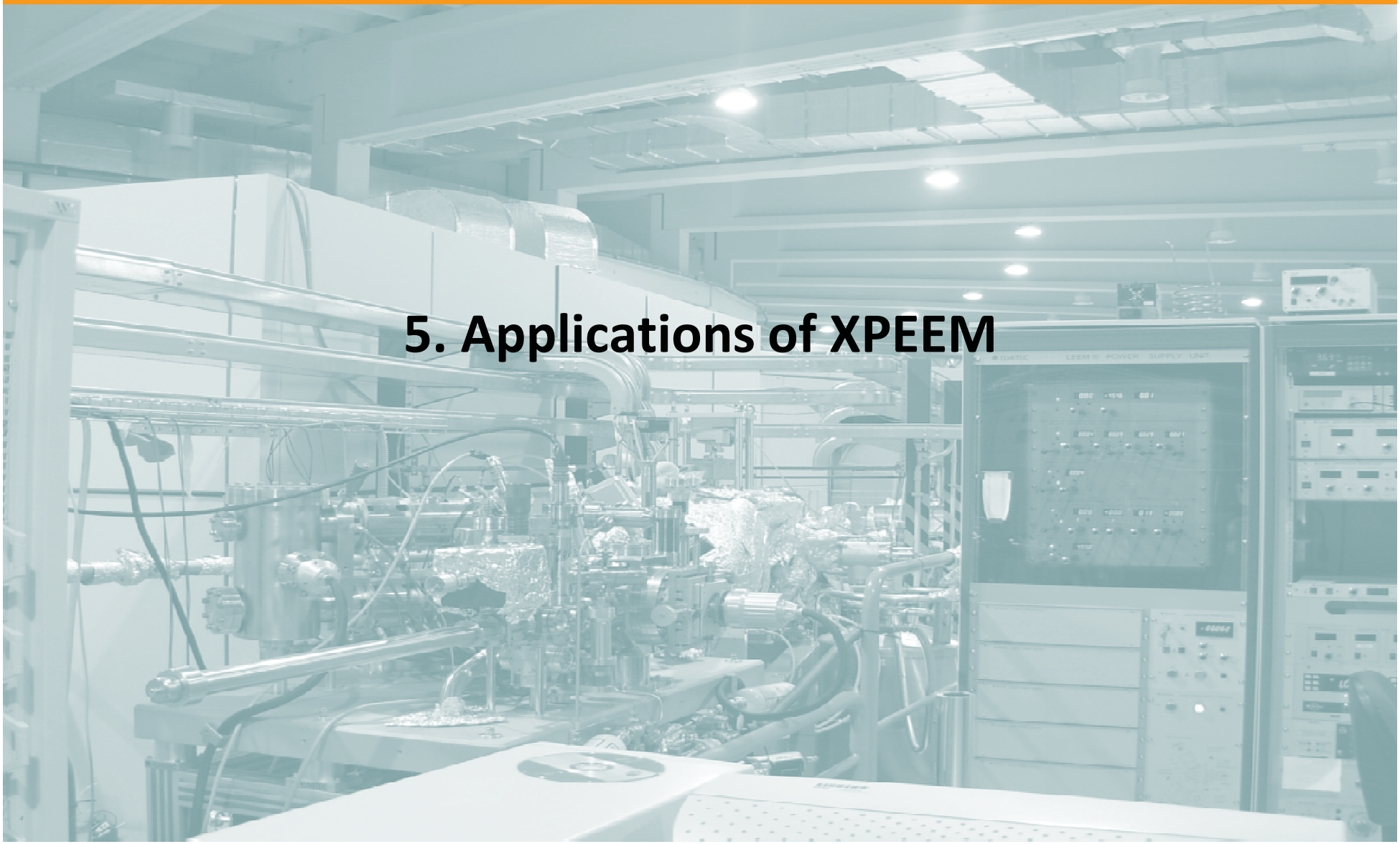

5. Applications of XPEEM

Reactivity and electron confinement in Mg thin films

Thickness dependent reactivity? Film oxidation

Previous work:

- QWR
- Spontaneous dissociation of O_2
- O goes below surface
- 2 layers Mg oxidized
- Coalescence MgO islands

Bungaro et al, PRL 79, 4433 (1997)
Goonewardene et al, Surf. Sci. 501, 102 (2002)

- Micro-XPS: Mg VB reveal oxidation extent and QWR

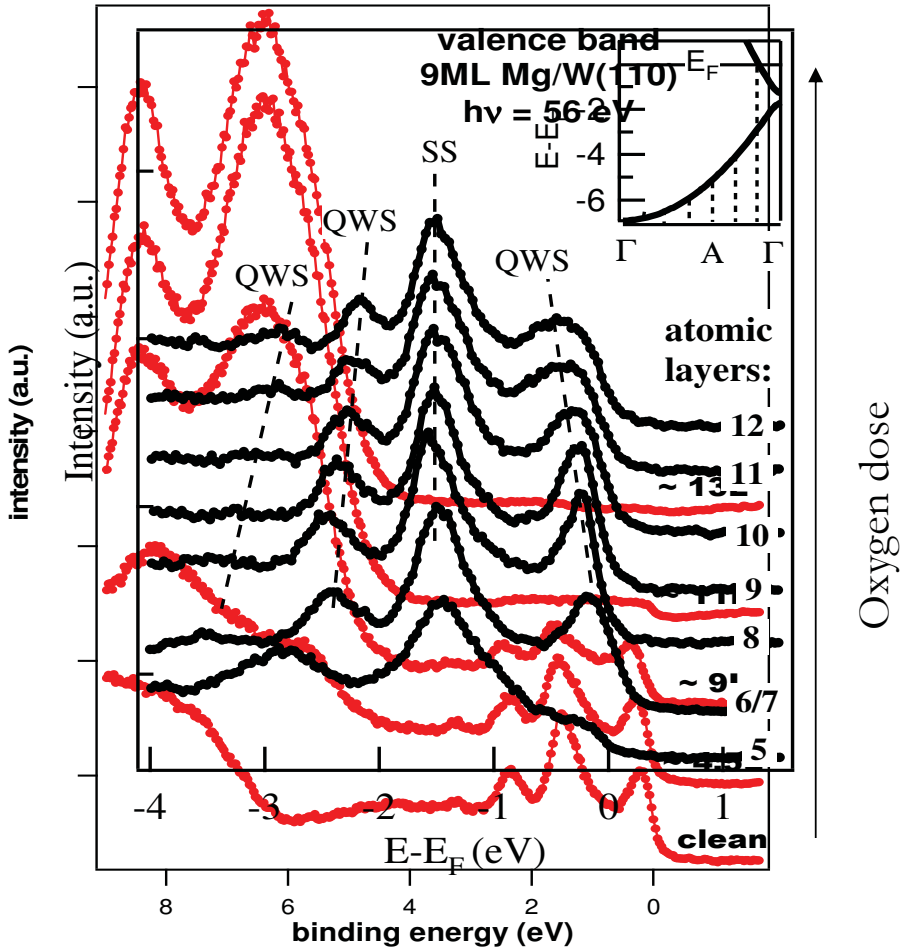

L. Aballe et al, Phys. Rev. Lett. 93, 196103 (2004)

Mg epitaxial growth

growth is followed *in-situ* by LEEM

Film thickness is measured by quantum interference contrast

[001]

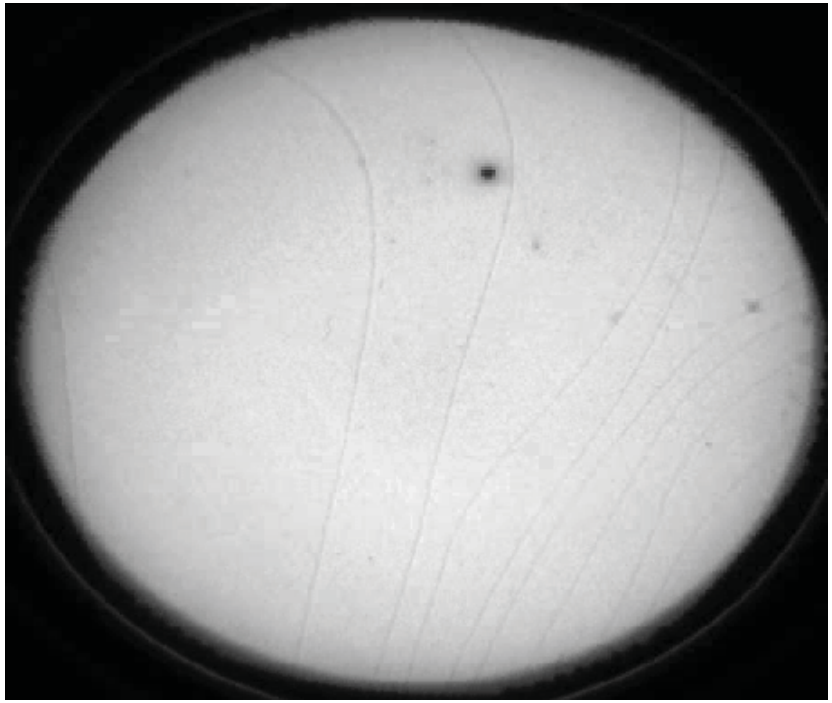

Mg/W(110) dep. 405 K, 0.1ML/min
11.1eV, 5 μm

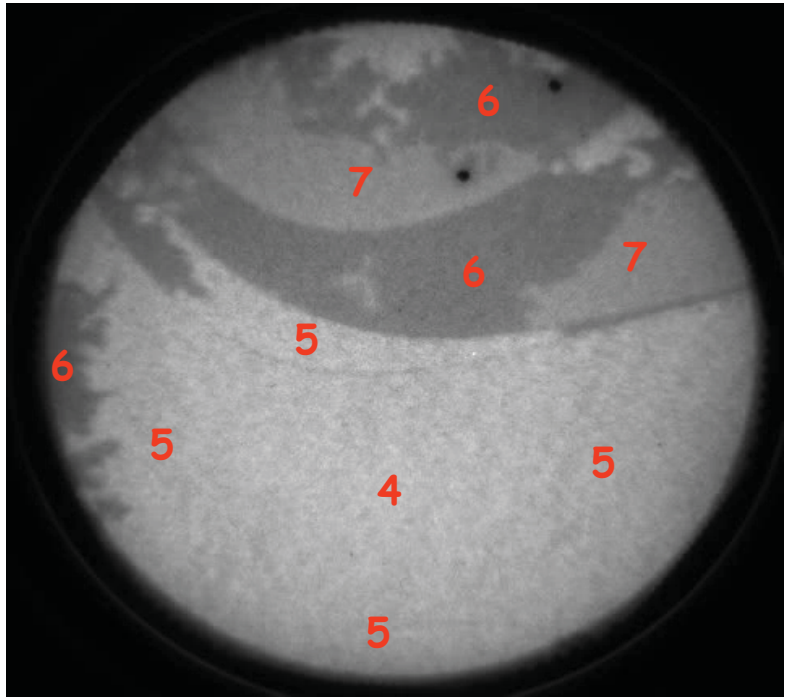

4 - 7 ML Mg/W(110)
0.1-10.1eV/0.2eV, 5 μm

Quantitative characterization of film oxidation

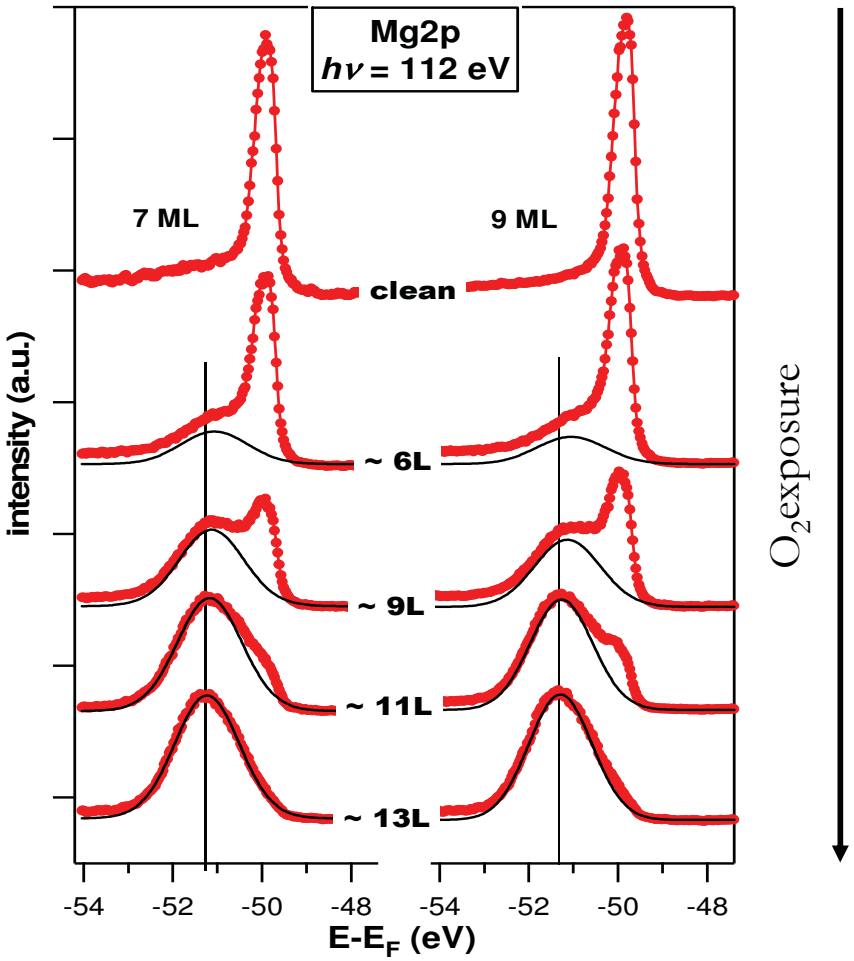

I_{ox}/I_{tot}

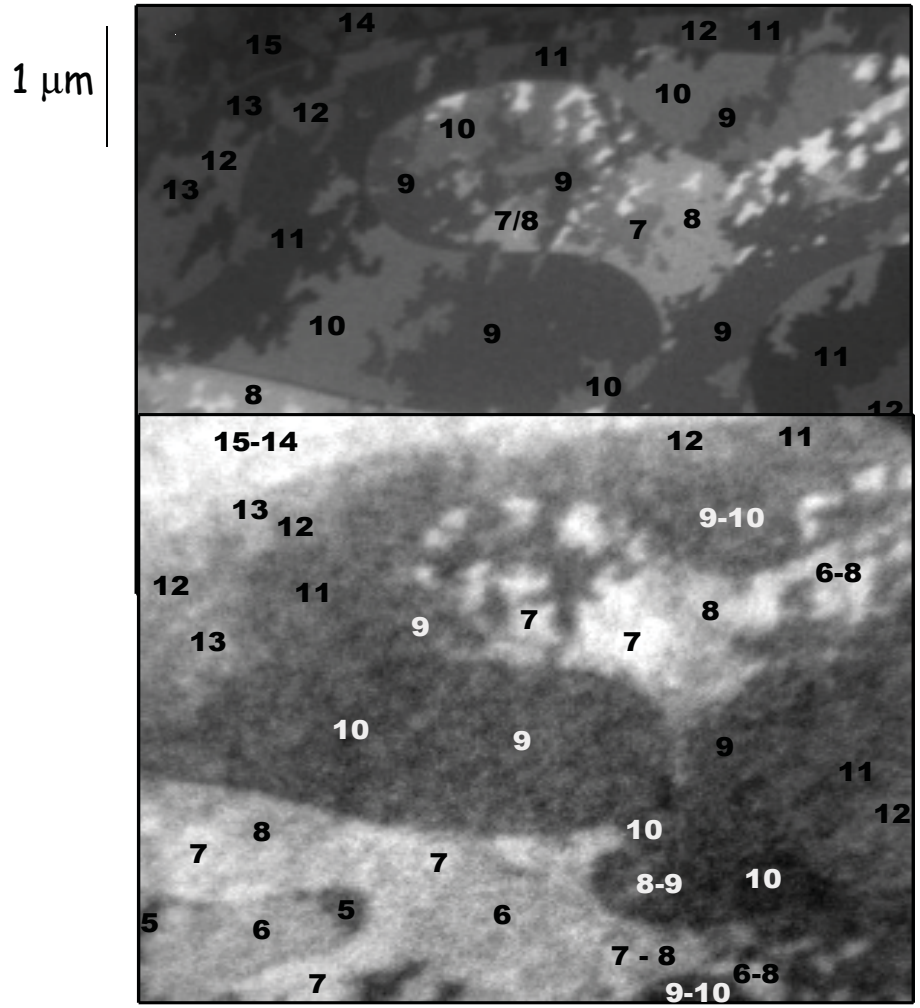

oxide component imaged by XPEEM reveals chemistry!

L. Aballe et al, Phys. Rev. Lett. 93, 196103 (2004)

Oxidation of Mg film and QWR

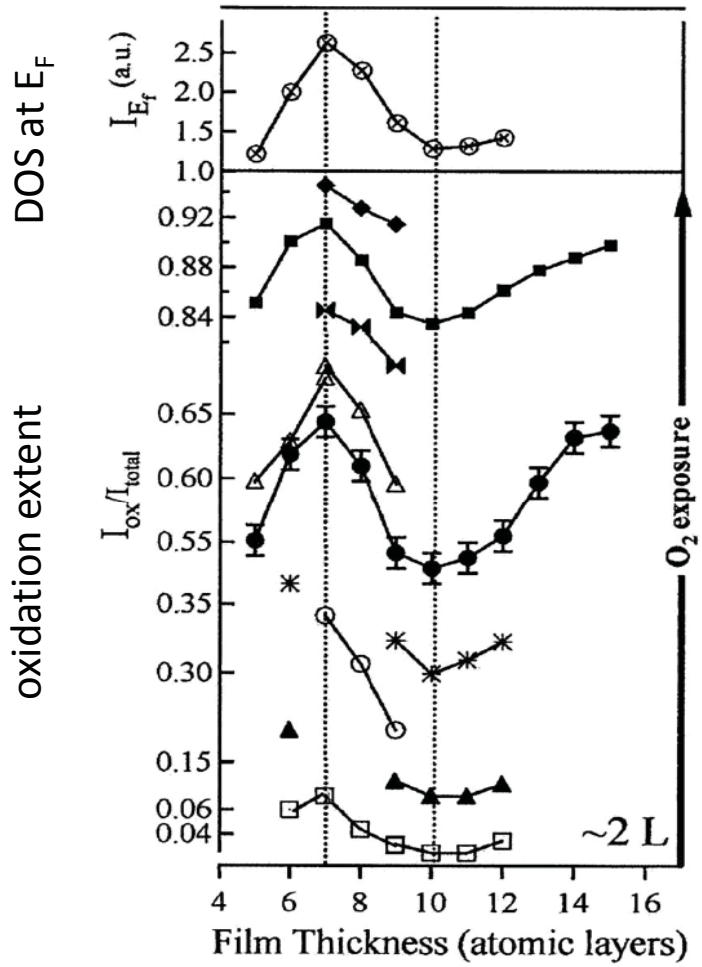

- strong variations in the oxidation extent are correleted to thickness and to the density of *bulk* states at E_F
- Control on film thickness enables modifying the molecule surface interaction
- Strong theoretical interest:

  Decay length of QWS into vacuum is critical: it reproduces peak of reactivity in experimental data.

  – N. Binggeli and M. Altarelli, PRL 96, 036805 (2005)

L. Aballe et al, Phys. Rev. Lett. 93, 196103 (2004)

Applications of XPEEM & SPEM

CHEMICAL IMAGING

Reorganisation processes driven by surface chemical reactions

Spatio-temporal concentration patterns in surface reactions

VOLUME 65, NUMBER 24 PHYSICAL REVIEW LETTERS 10 DECEMBER 1990

Spatiotemporal Concentration Patterns in a Surface Reaction: Propagating and Standing Waves, Rotating Spirals, and Turbulence

S. Jakubith, H. H. Rotermund, W. Engel, A. von Oertzen, and G. Ertl
Fritz-Haber-Institut der Max-Planck-Gesellschaft, Faradayweg 4-6, D-1000 Berlin 33, Germany
(Received 25 June 1990)

Belousov-Zabatinski reaction
(solution of, acidified bromate, malonic acid, ceric salt)

Pattern formation
in surface chemical reactions

oscillatory oxidation of carbon monoxide on a Pt(110) surface

standing fronts

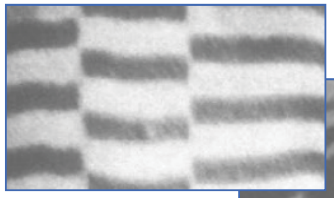

rotating spirals

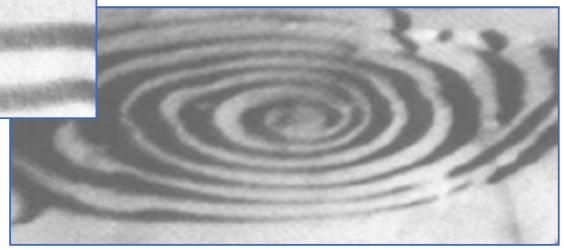

target waves

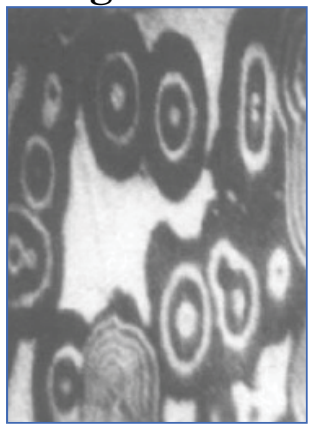

Jakubith et al, PRL 65, 3013 (1990)

Reaction diffusion patterns: NO+H_2 /Rh(110)

- First quantitative measurement of concentration profiles

  Schaak et al Phys. Rev. Lett.

$$H_2 + 2^* \leftrightarrow 2H_{ad},$$
$$NO + * \leftrightarrow NO_{ad},$$
$$NO_{ad} + * \rightarrow N_{ad} + O_{ad},$$
$$2N_{ad} \rightarrow N_2 + 2^*,$$
$$O_{ad} + 2H_{ad} \rightarrow H_2O + 3^*,$$

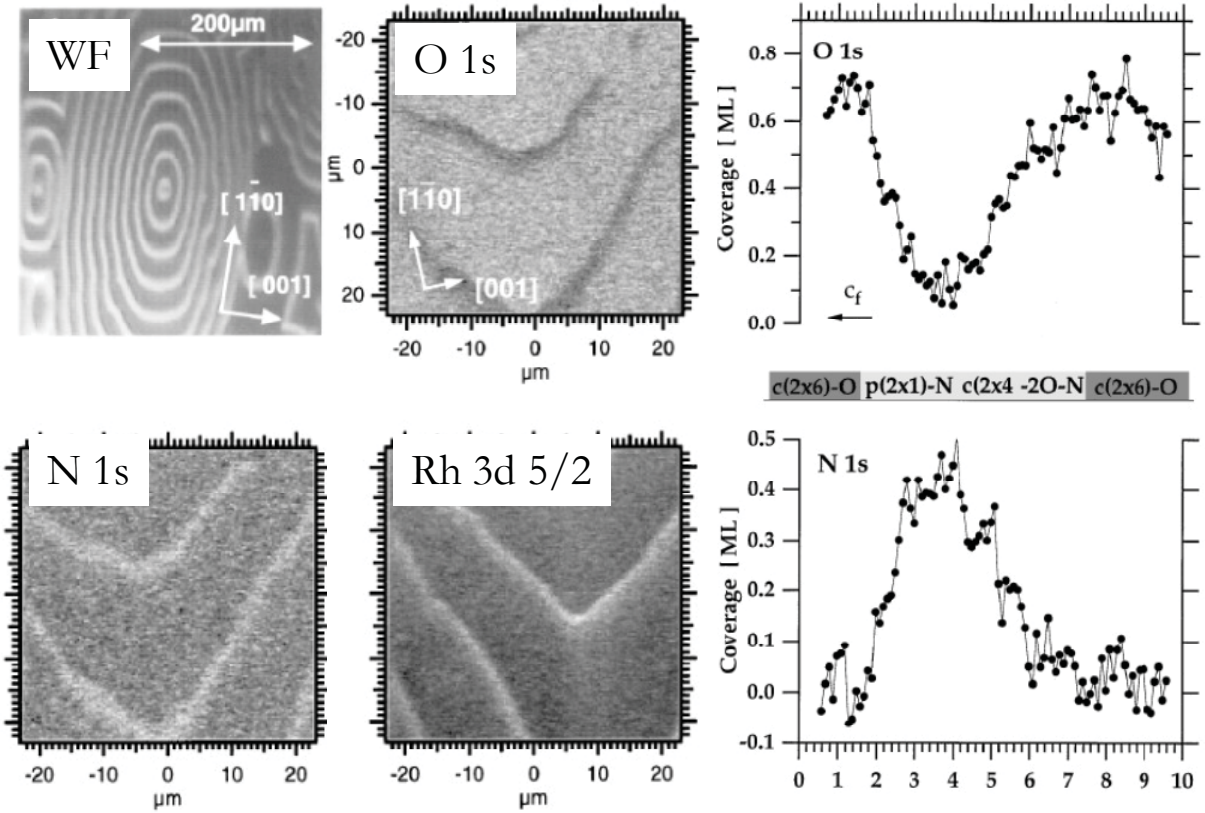

Th. Schmidt et al, Chem. Phys. Lett. 318, 549 (2000)

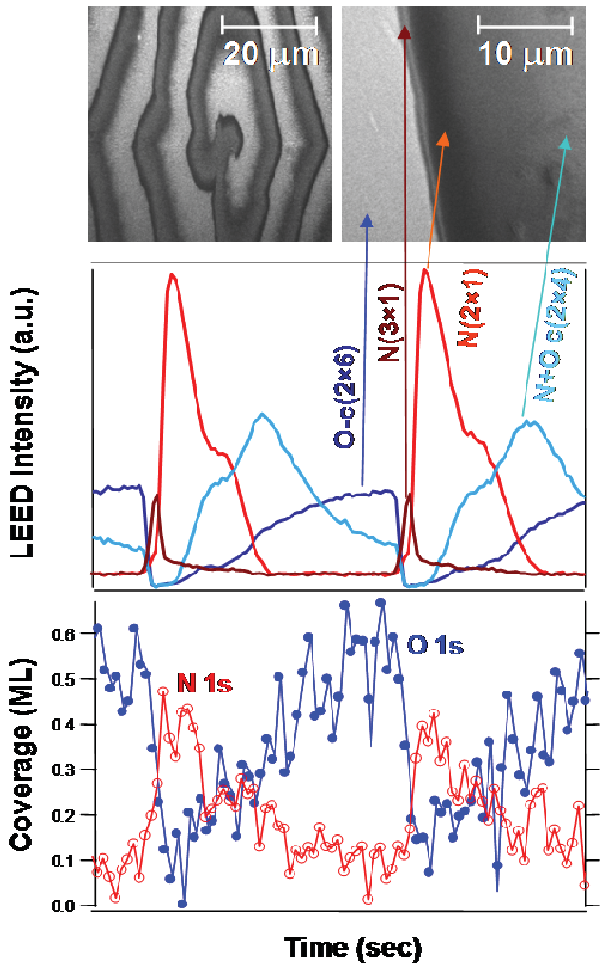

Reaction diffusion patterns: $NO+H_2$ /Rh(110)

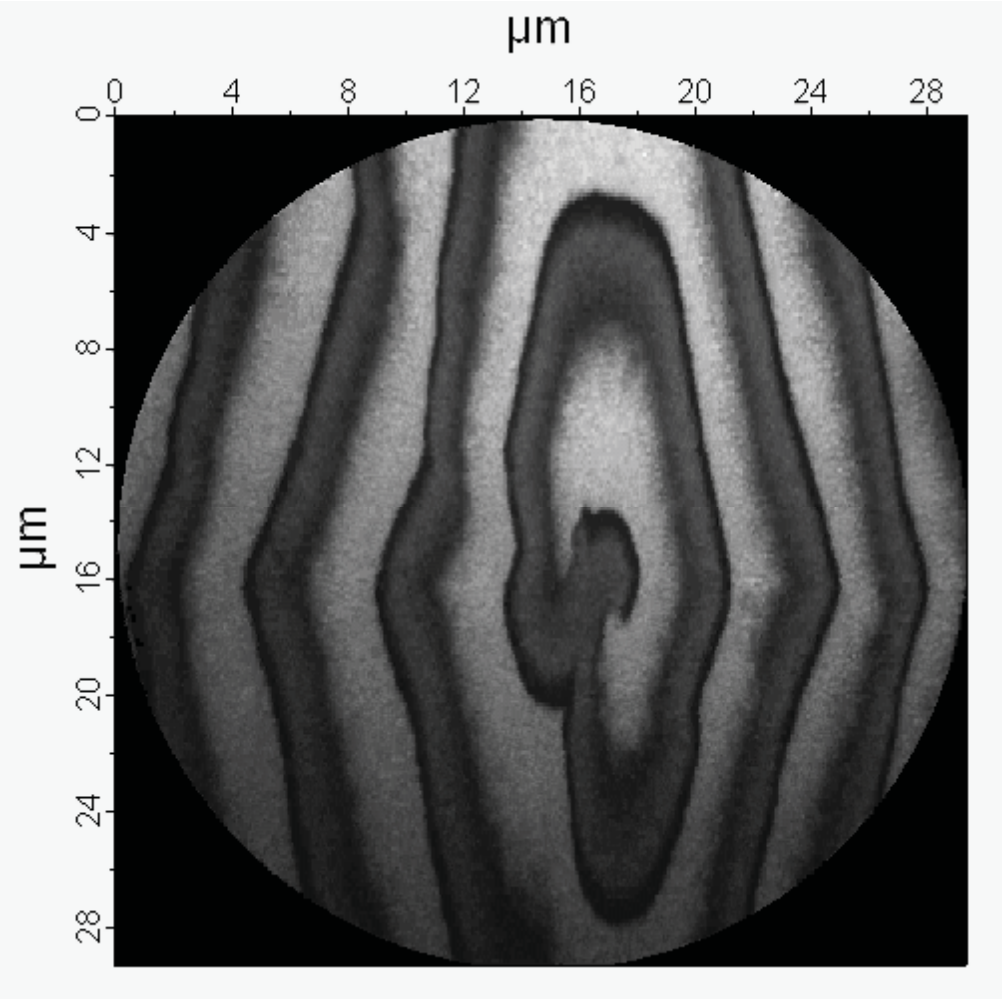

Structure + composition

(LEEM, micro-LEED)

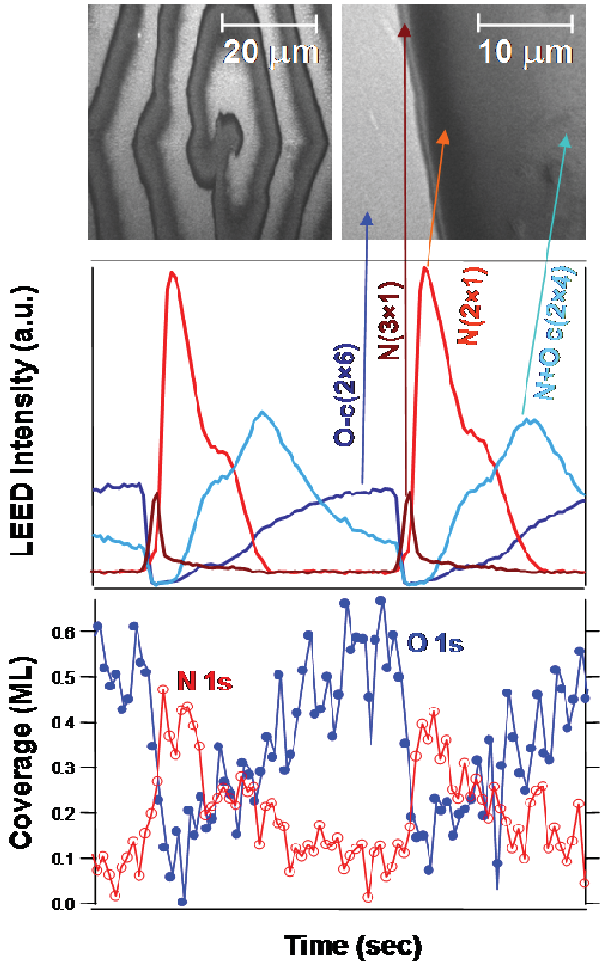

K / NO+H_2 /Rh(110)

– Mass transport by reaction fronts, K accumulation and depletion

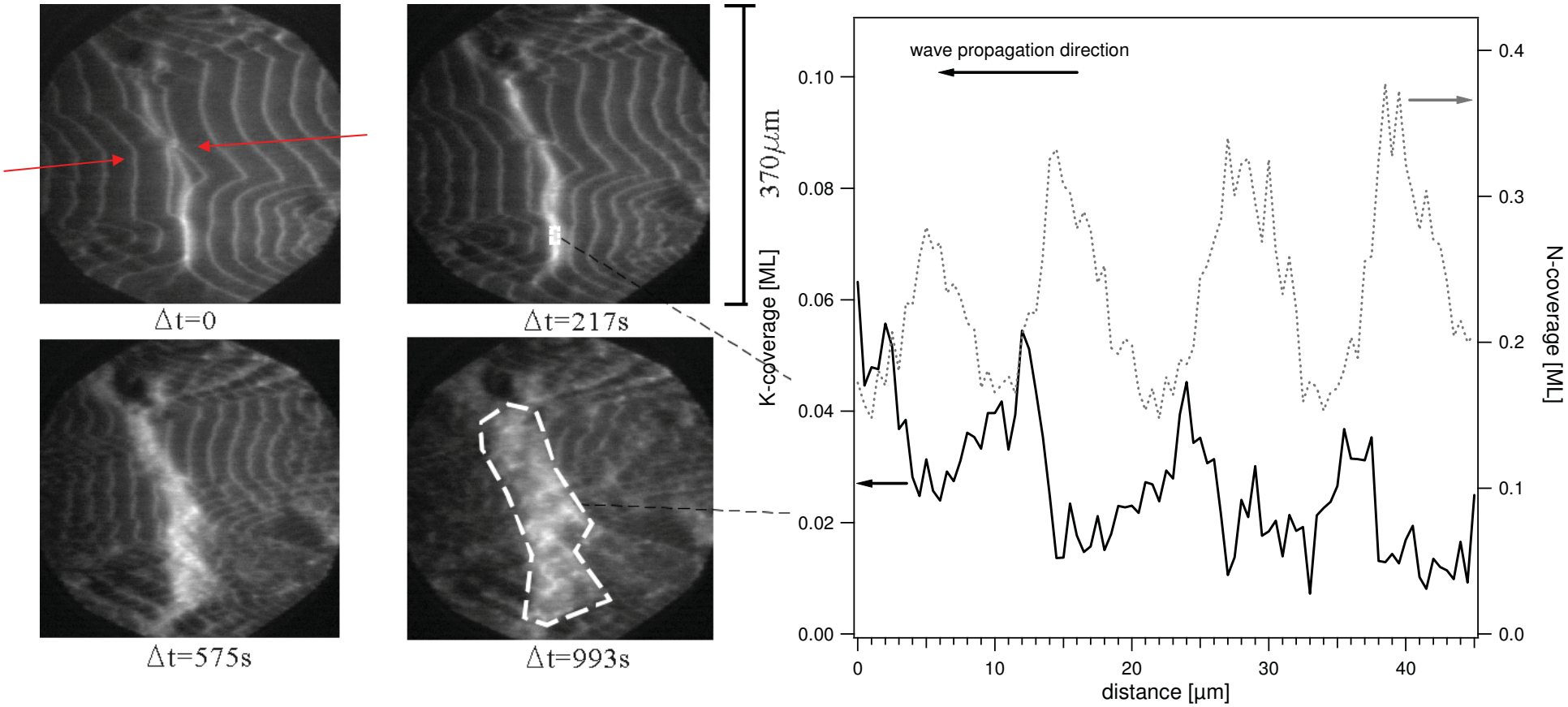

L. Honget al. Phys. Rev. E 78, 055203 (2008).

Reactivity

- Au mass transport during water formation reaction on Rh(110)

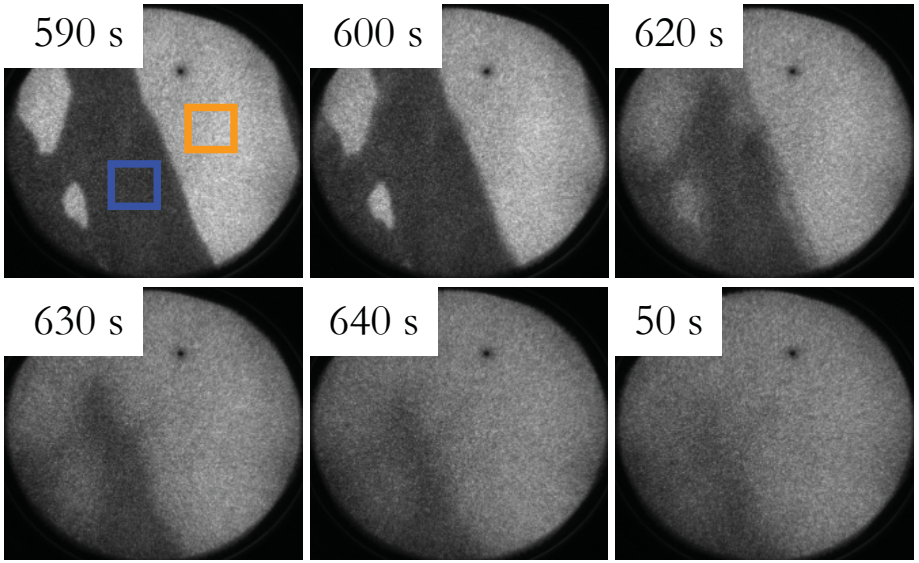

XPEEM Au 4f $_{7/2}$

field of view 10 μm

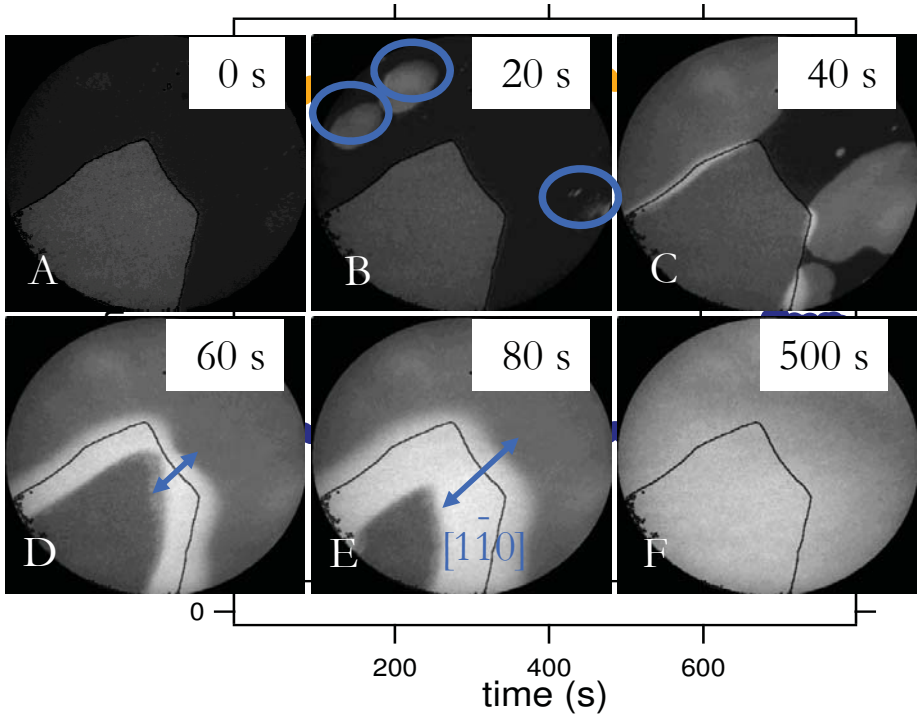

Characterisation of nano-structured surfaces by XPEEM and LEEM methods

Au/TiO_2(110): controlling growth by substrate stoichiometry

Creation of ordered oxygen vacancies

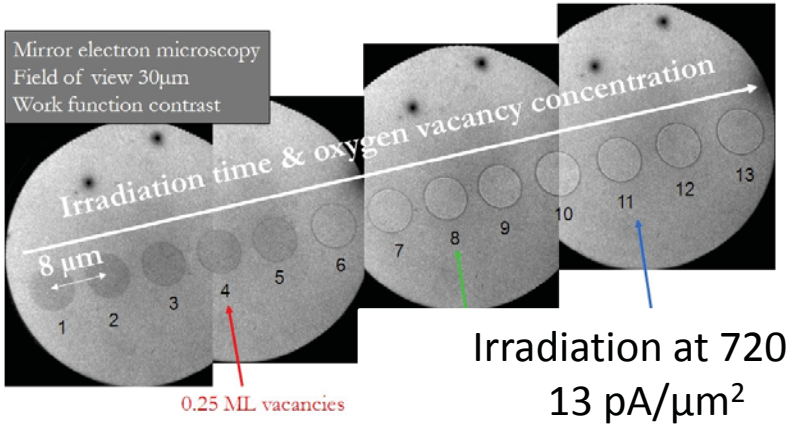

MEM
Work Function

Irradiation at 720 K
13 pA/µm²

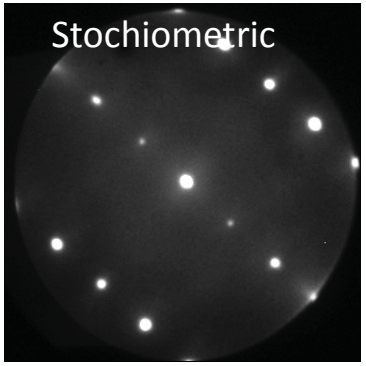

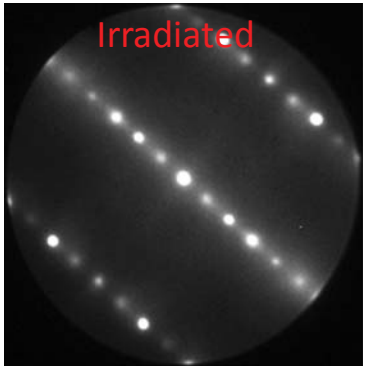

µ-LEED
structure

(1x1) (1x2)

Au growth on TiO_2(110)

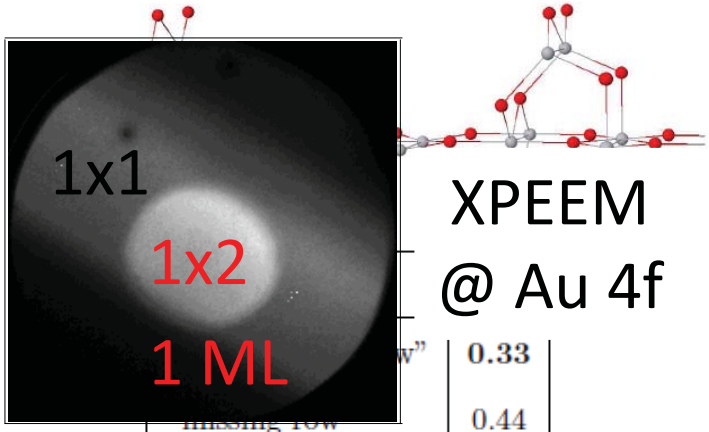

XPEEM
@ Au 4f

0.33
0.44
0.76
0.61
0.57

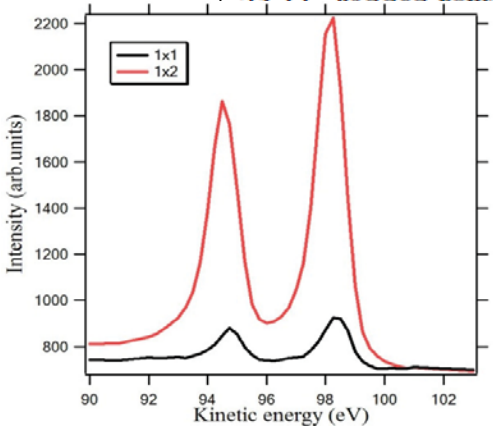

/ µ-XPS
ition with
Zheleva
eading

Condens. Matter 19, 082202 (2007); *Phys. Rev. B* 76, 155413 (2007).

Collaboration with A. Kijena and T. Pabisiack (Wroclaw)

Surface Oxygen on Ag : *e-beam "Lithography"*

Full oxidation of Ag using NO_2 does not occur:

$$NO_2 \rightarrow NO_{ad} + O_{ad}$$

Instead: e-beam (60 eV) stimulated desorption of NO_{ad} works at RT!

Low T: NO_{ad} stays, prevents oxidation

High T: NO_{ad} desorbs,

but Ag_2O unstable.

LEED reveqas path towards Ag_2O under e-beam

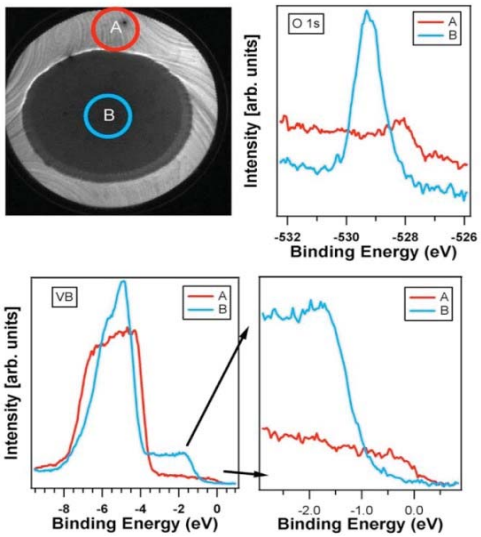

A: metallic Ag

B: Ag_2O

S. Günther *et al.*, *App. Phys. Lett.* 93, 233117 (2008).

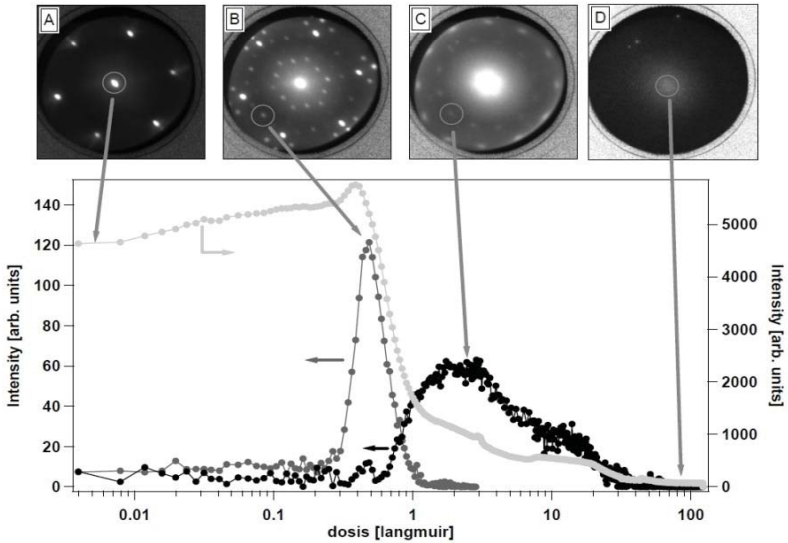

S. Günther *et al.*, *Chem. Phys. Chem.* 2010.

Surface Oxygen on Ag : *photon-beam "Lithography"*

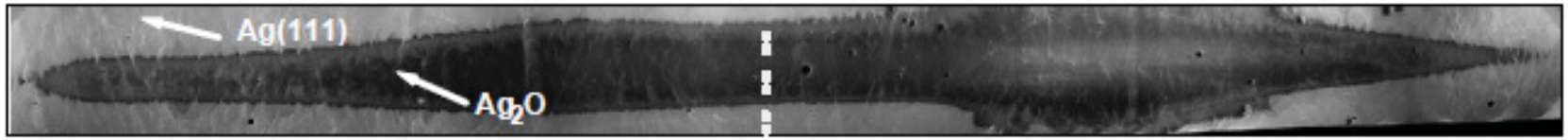

MEM 28 µm x 350 µm; after 130 L NO_2;

hv = 40 eV

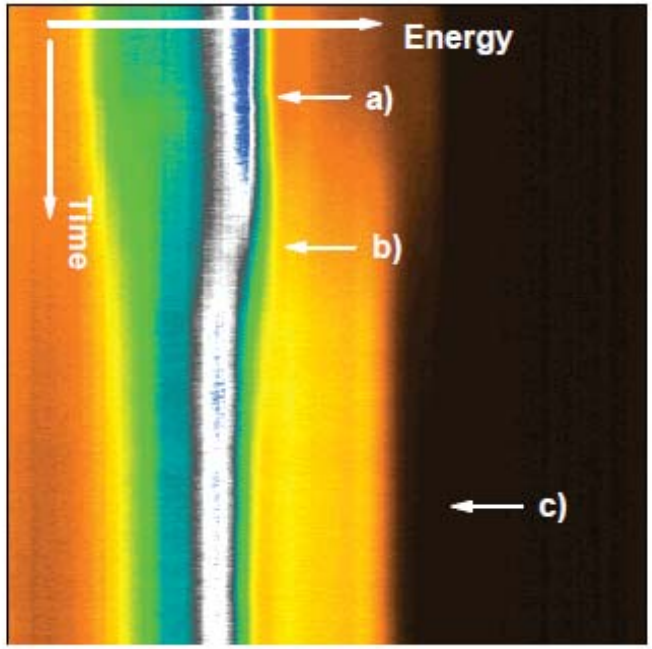

-9 eV

4 eV

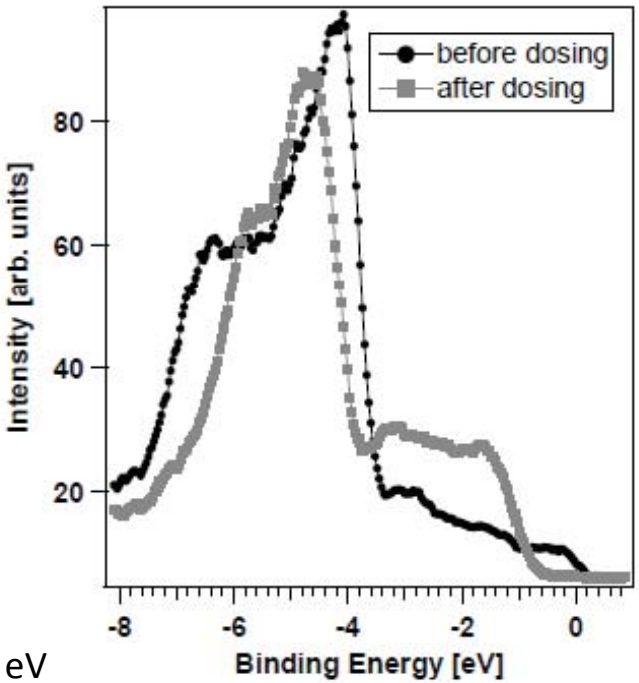

(a) Start of NO2 adsorption, *t = 0 s,*

(b) t = 210 s, p(NO_2) =1.8×10^{-7} mbar, 17 L NO_2,

(c) t = 540 s, p(NO_2) =2.5×10^{-7} mbar, 67 L NO_2.

S. Günther *et al.*, *Chem. Phys. Chem.* 2010.

Corrugation in suspended and supported exfoliated graphene: a LEEM, LEED and ARPES study

Exfoliated graphene: thickness determination by LEEM

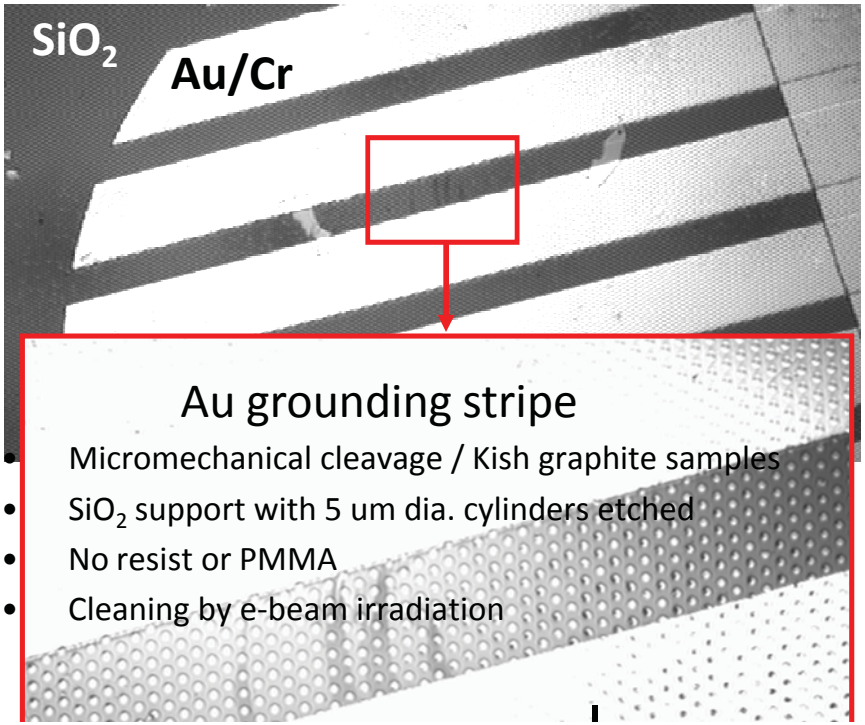

- Micromechanical cleavage / Kish graphite samples
- SiO_2 support with 5 um dia. cylinders etched
- No resist or PMMA
- Cleaning by e-beam irradiation

Thickness is revealed by modulations of the electron reflectivity at low electron energies. This is commonly understood as an inteference process, similar to that occurring in a Fabry-Perot interferometer. The number of recorded minima determine the film thickness.

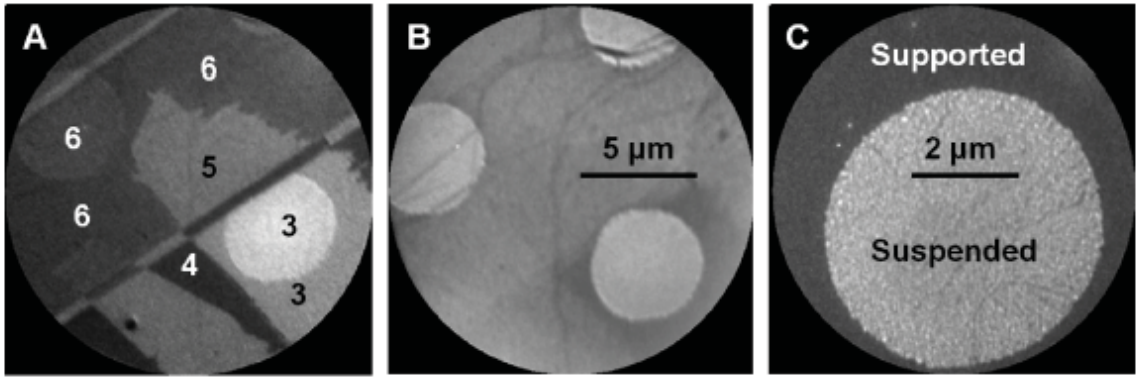

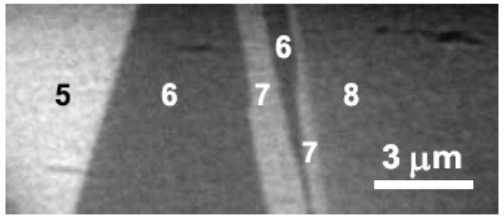

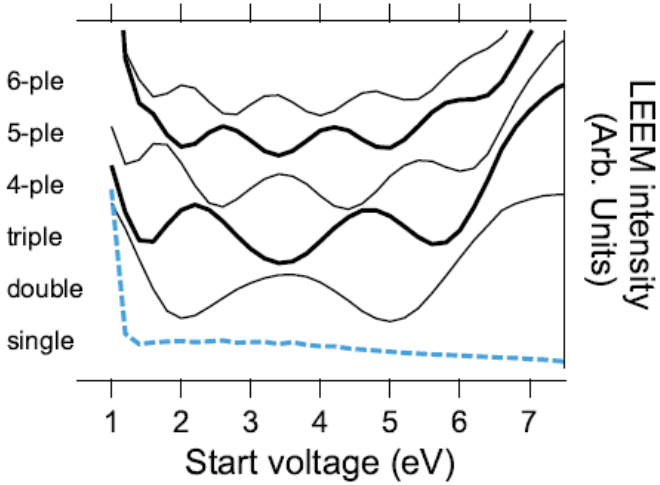

LEED measurements reveal corrugation in graphene

$$S(\mathbf{k}) = (\eta k_\perp^{-1/\alpha})^2 F_\alpha(k_\parallel \eta k_\perp^{-1/\alpha})$$

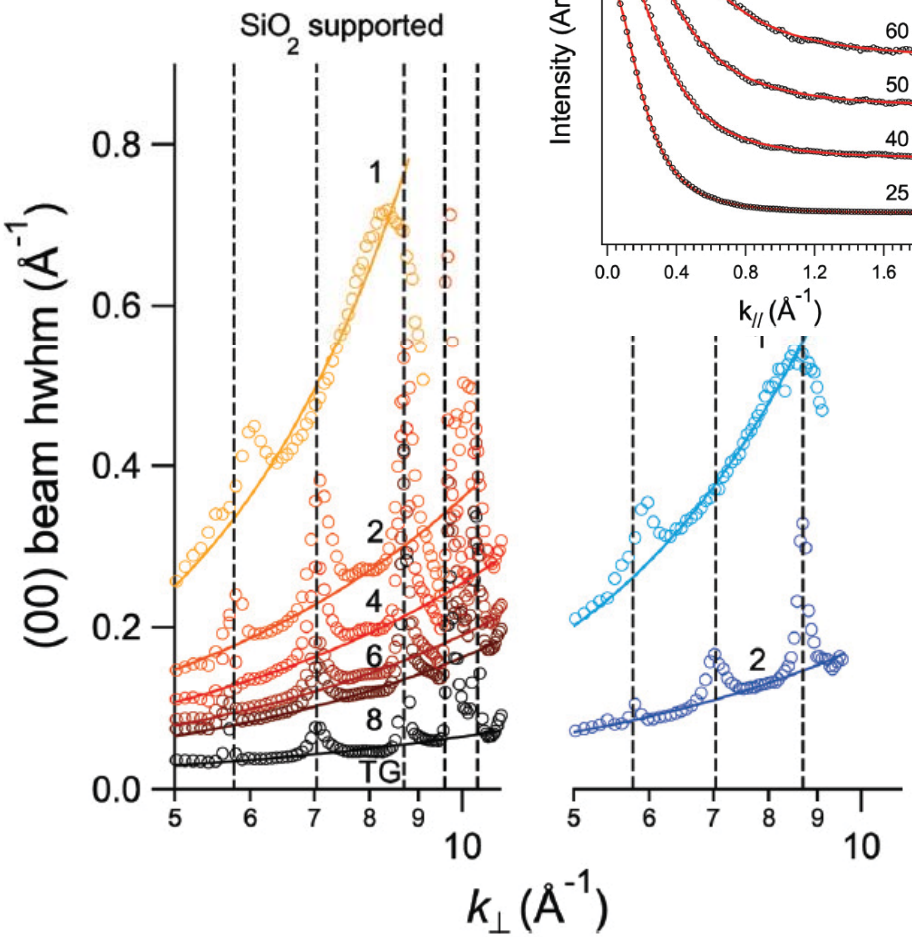

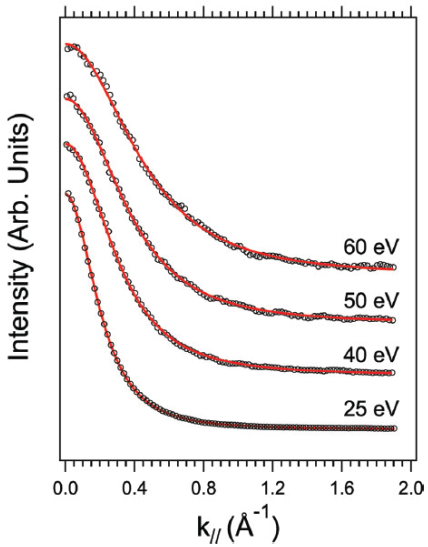

$$\text{hwhm}\ (00) = Z_g \eta^{-1} (k_\perp)^{1/\alpha}$$

α= roughness exponent w = interface width

η= roughness parameter ξ = lateral correlation length

	SiO_2-supported		suspended	
ness (layers)	α	η	α	η
1	0.49 ± 0.04	77 ± 20	0.54 ± 0.02	84 ± 11
2	0.80 ± 0.04	64 ± 6	0.80 ± 0.05	144 ± 25
3	0.80 ± 0.06	81 ± 14	0.82 ± 0.06	131 ± 24
4	0.77 ± 0.07	104 ± 28		
6	0.80 ± 0.05	133 ± 25		
8	0.80 ± 0.05	157 ± 25		
TG	0.87 ± 0.07	327 ± 70		

1. (00) peak width shows a distinct behaviour on SiO_2-supported and suspended G.
2. Smoother morphology of multi-layers with increasing thickness.

VOL. 4 ▪ NO. 8 ▪ 4879–4889 ▪ 2010 ACSNANO

Microprobe ARPES

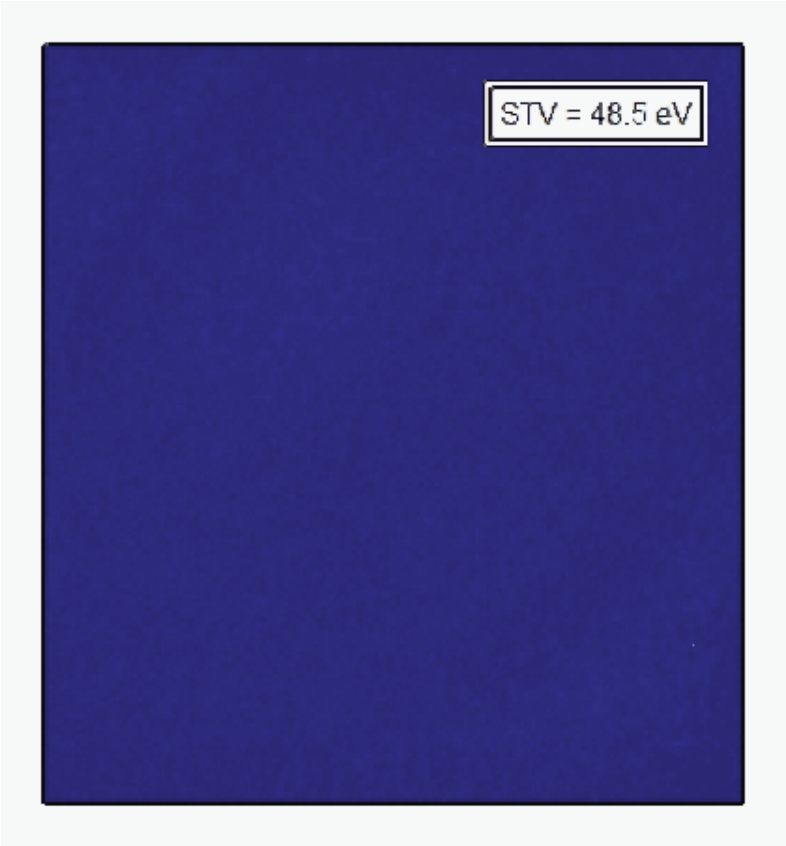

Micro-ARPES from Supported and Suspended graphene

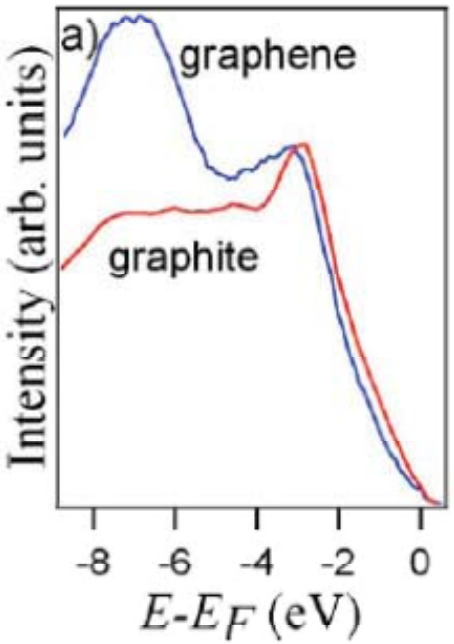

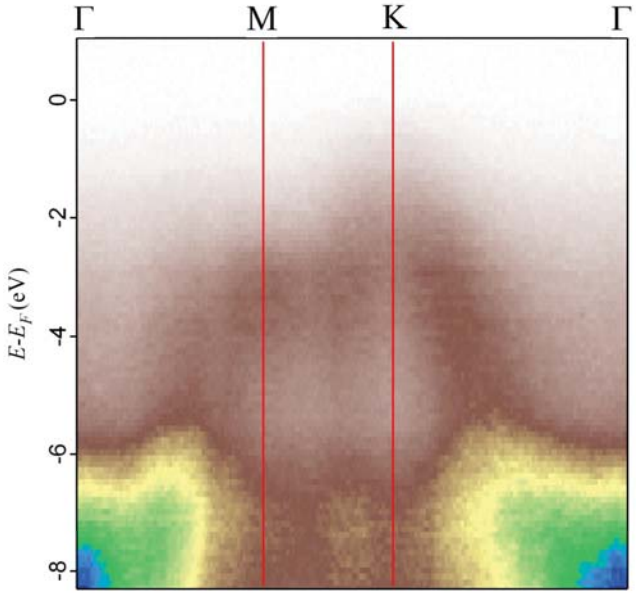

Supported Graphene

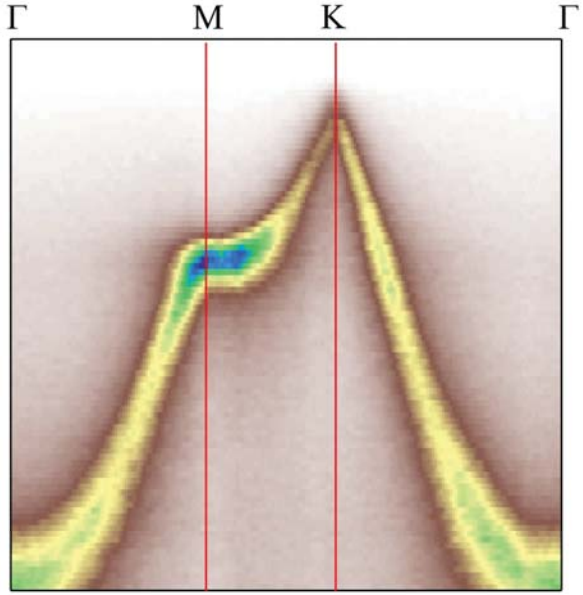

Suspended Graphene

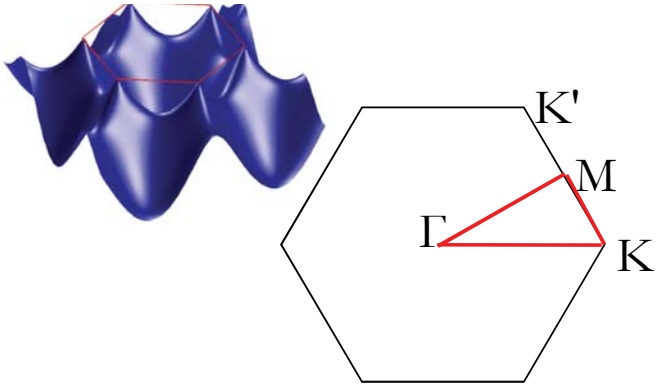

No SiO_2 photoelectrons

Significantly narrower peaks

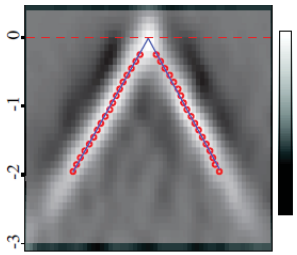

$\langle v_F \rangle = 1.1 \times 10^6$ m/s

E_d = with 25 meV from E_F

(300 meV on SiO_2)

 hv = 85 eV K. Knox et al, PRB 2011

measuring quasi-particle lifetime

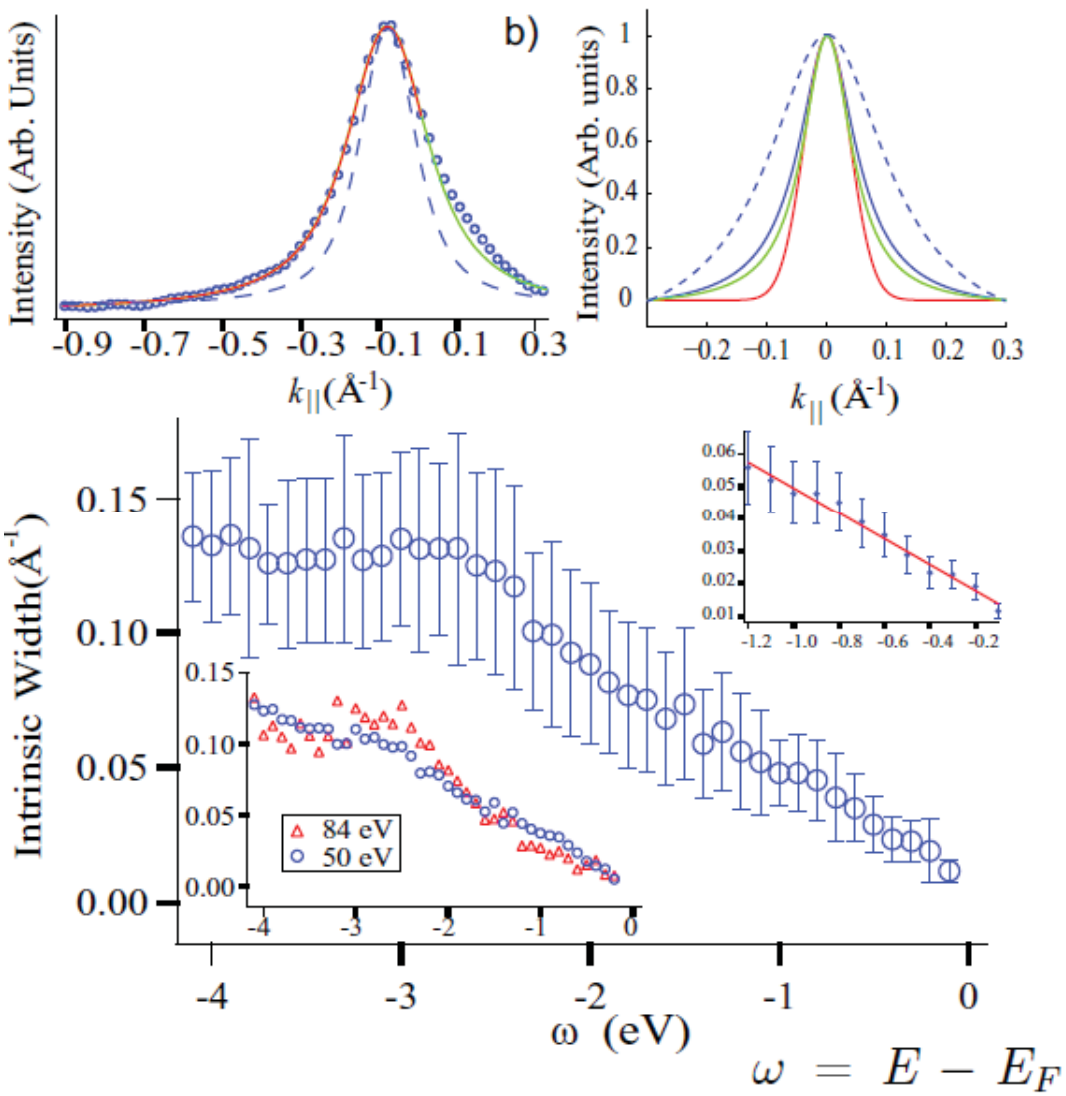

By carryng out diffraction profile we could obtain the intrinsic ARPES line width in a fit. This has allowed us to separate corrugation from lifetime broadening effects, confirming that the electronic structure of suspended EG is that of ideal, undoped graphene. These measurements validate the picture that suspended graphene behaves as a marginal Fermi liquid, showing a quasiparticle lifetime that scales as $(E-E_F)^{-1}$, in accord with theory.

K. Knox et al, PRB 2011

6. Magnetic Imaging by PEEM

- Magnetic domains in thin films: understanding of magnetic state in correlation with structure and morphology
- FM/AFM interfaces; exchange bias; understanding of interfacial spin pinning; understanding of AFM spin structure
- Magnetisation dynamics

Magnetic imaging basics: XMCD

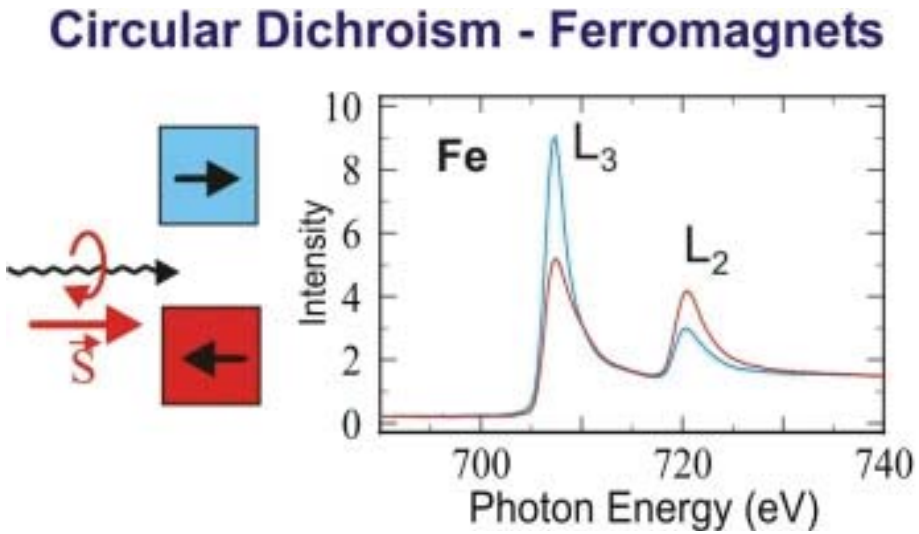

X-ray magnetic circular dichroism (XMCD) is the dependence of *x-ray absorption* on the relative orientation of the local magnetization and the polarization vector of the circularly polarized light

✓Element sensitive technique

✓ Secondary imaging with PEEM determine large probing depth (10 nm), buried interfaces.

✓sum rules allows measuring orbital and spin moments

MnAs/GaAs

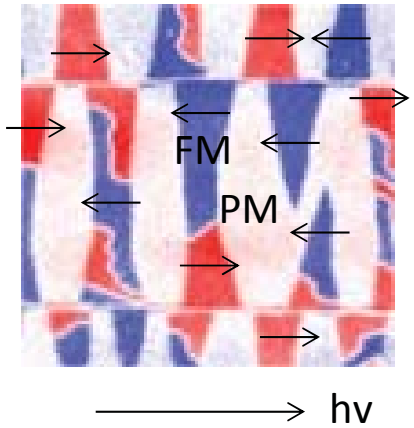

Magnetic domain imaging

At resonance, the secondary electron yield is proportional to the dot product between the magnetization direction and the photon helicity vector, which is parallel or anti-parallel to the beam propagation direction according to the handedness of the circular polarization

SPELEEM microscope

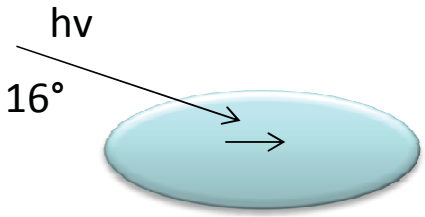

Owing to the illumination geometry, we are sensitive to the *in plane* component of M

XMCD principles

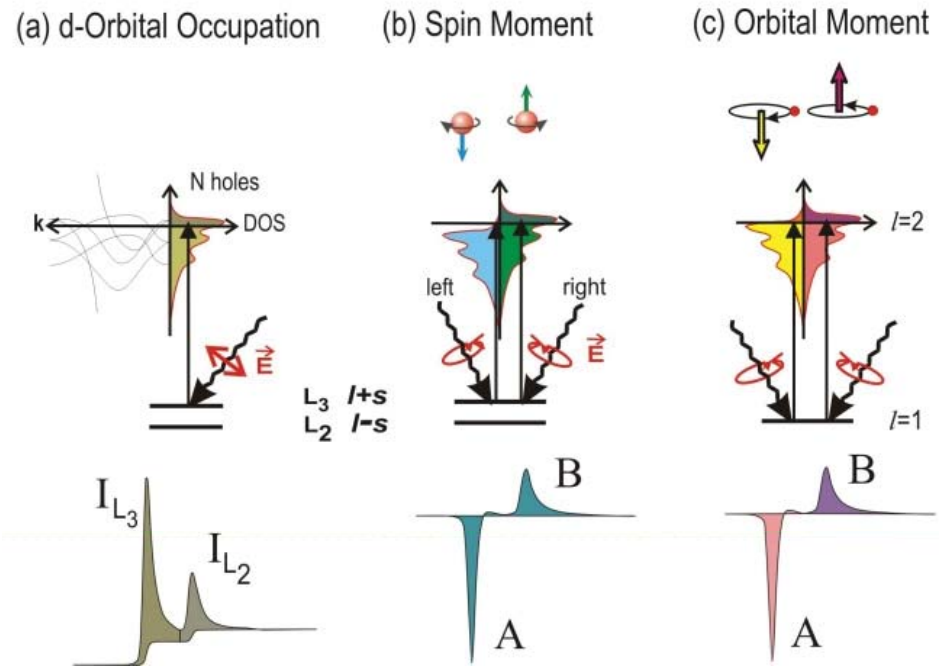

- We **PROBE** 3d elements by exciting 2p into unfilled 3d states

Dominant channel: 2p → 3d

White line intensity of the L3 and L2 resonances with the number N of empty d states (holes). So 3d electrons determine the magnetic properties.

- The spin moment is given by the imbalance of spin-up and spin-down electrons (holes).
- By using circularly polarized radiation, the angular momentum of the photon can be transferred in part to the spin through the spin-orbit coupling. Photoelectrons with opposite spins are created in the cases of left and right handed polarization. Spin polarization is opposite also for $p_{3/2}$ (L_3) and $p_{1/2}$ (L2) levels.
- The spin-split valence shell is thus a detector for the spin of the excited photoelectron. The size of the dichroism effect scales like cosθ, where θ is the angle between the photon spin and the magnetization direction.
- **Refs: IBM. J . Res. Develop. 42, 73 (1998) and J. Magn. Magn. Mater. 200, 470 (1999).**

XMCD principles

Experimental Confirmation of the X-Ray Magnetic Circular Dichroism Sum Rules for Iron and Cobalt

PRL 75, 152; 1995

C. T. Chen,[1] Y. U. Idzerda,[2] H.-J. Lin,[1,*] N. V. Smith,[1,†] G. Meigs,[1] E. Chaban,[1] G. H. Ho,[3,*] E. Pellegrin,[1] and F. Sette[1,‡]

SUM RULES

$$m_{\text{orb}} = -\frac{4\int_{L_3+L_2}(\mu_+ - \mu_-)\,d\omega}{3\int_{L_3+L_2}(\mu_+ + \mu_-)\,d\omega}(10 - n_{3d}), \quad (1)$$

$$m_{\text{spin}} = -\frac{6\int_{L_3}(\mu_+ - \mu_-)\,d\omega - 4\int_{L_3+L_2}(\mu_+ - \mu_-)\,d\omega}{\int_{L_3+L_2}(\mu_+ + \mu_-)\,d\omega} \times (10 - n_{3d})\left(1 + \frac{7\langle T_z\rangle}{2\langle S_z\rangle}\right)^{-1}, \quad (2)$$

$\langle T_z\rangle$ is the expectation value of the magnetic dipole operator

$\langle S_z\rangle$ is equal to half of m_{spin}

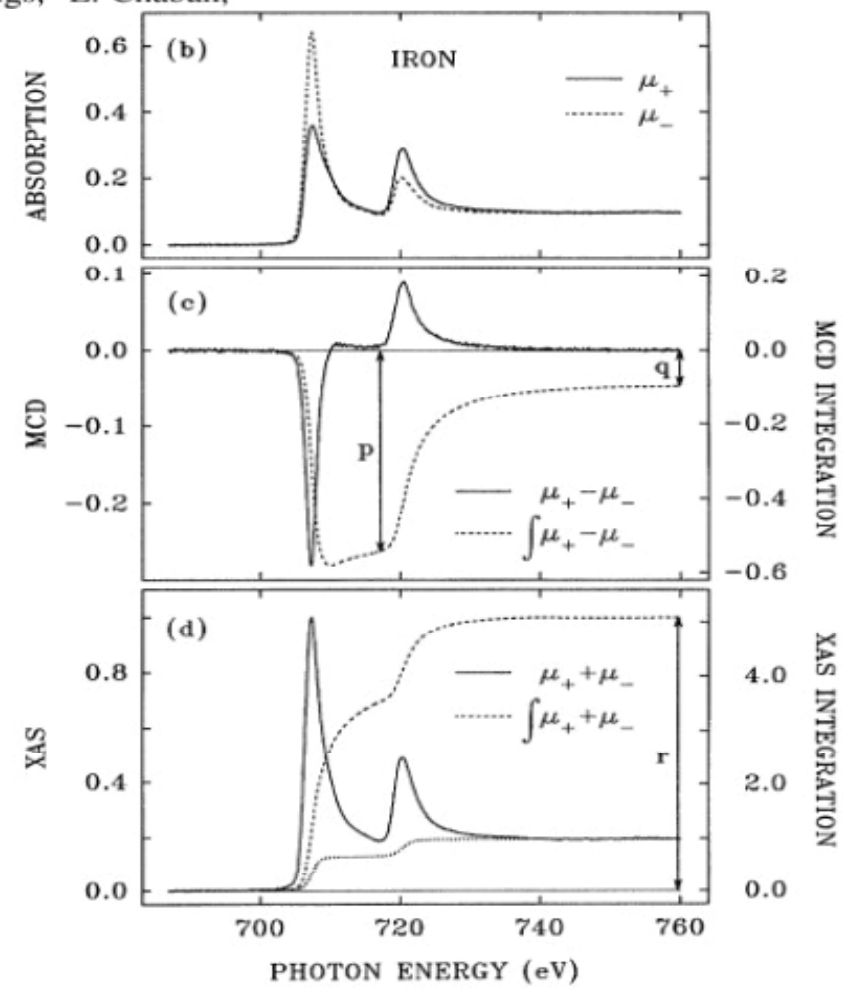

REFERENCES

B. T. Thole, P. Carra, F. Sette, and G. van der Laan, Phys. Rev. Lett. 68, 1943 (1992); P. Carra, B. T. Thole, M. Altarelli, and X.Wang, Phys. Rev. Lett. 70, 694 (1993), J.Stöhr et al, Phys. Rev. Lett. 75 (1995) 3748.

Nano-characterization by XMCD-PEEM (imaging)

MAGNETIC STATE using XMCD & XMLD

Co nanodots on Si-Ge

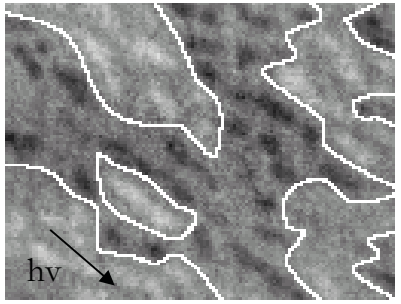

Co - L_3 edge

A. Mulders et al, Phys. Rev. B 71, 214422 (2005).

patterned structures

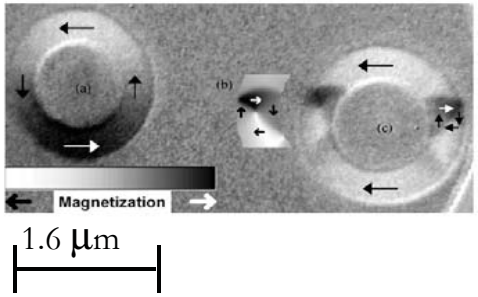

pulse injection

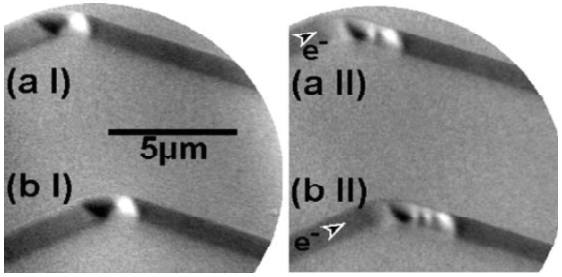

M. Klaeui et al, PRL , PRB 2003 - 2010

domain wall motion induced by spin currents

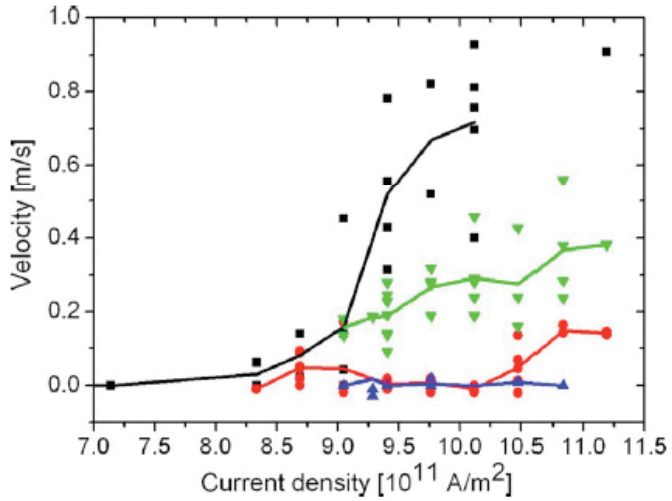

Laufemberg et al, APL 88, 232507(2006).

Spin configturations in Heusler alloys

$La_{0.7}Sr_{0.3}MnO_3$

Multi-domain to flux-closure states (favored by the shape anisotropy) with decreasing element size, with a thickness-dependent crossover at the micrometer scale.

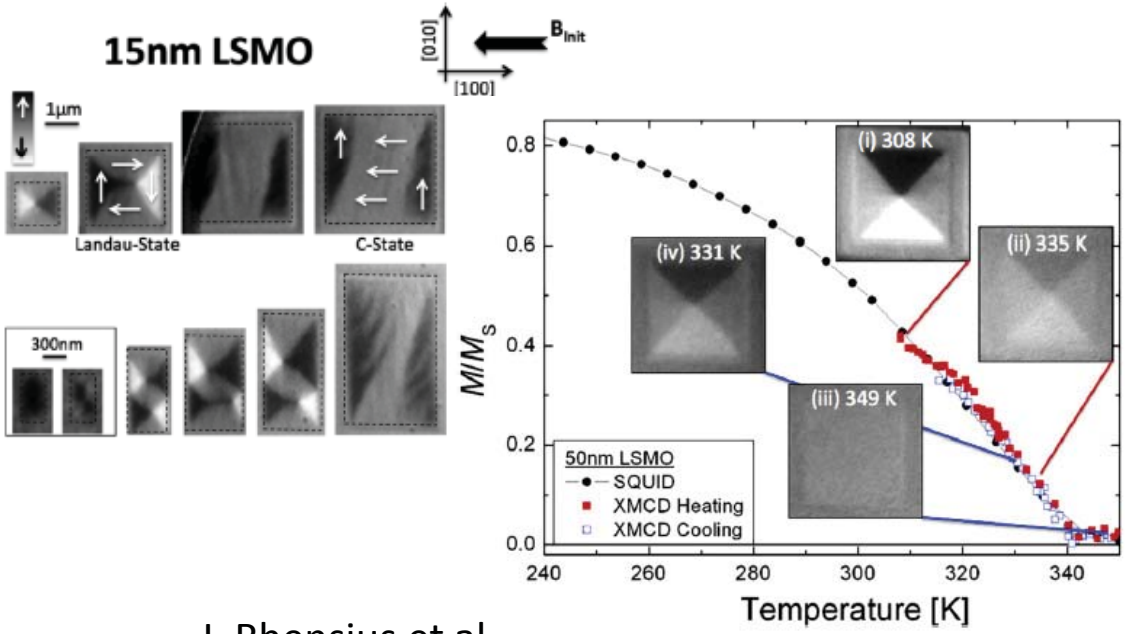

J. Rhensius et al

Appl. Phys. Lett. 99, 062508 (2011)

$Co_2FeAl_{0.4}Si_{0.6}$ rings

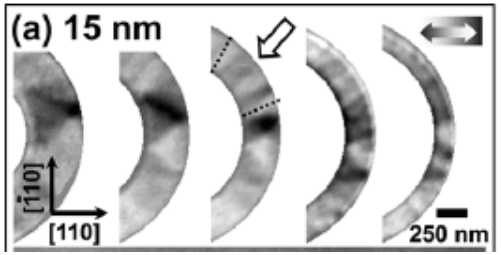

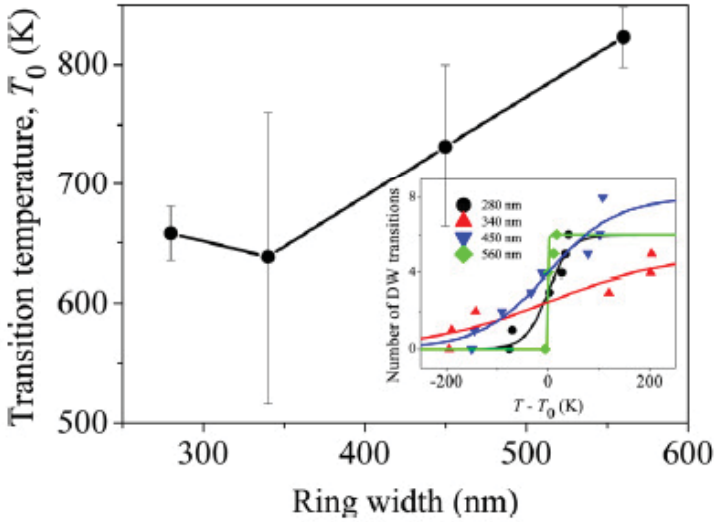

C.A.S. Vaz et al

Appl. Phys. Lett. 99, 182510 (2011)

Magnetic Imaging – present capability

nano-magnetism of (Ga,Fe)N films

Fe L3 edge (chemical)

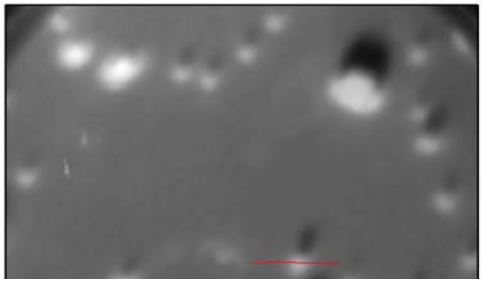

Fe L3 edge (XMCD)

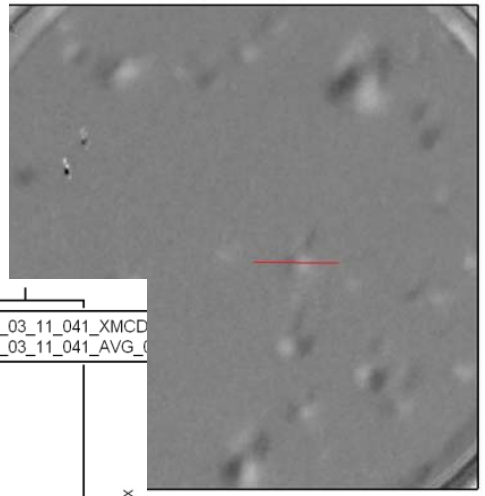

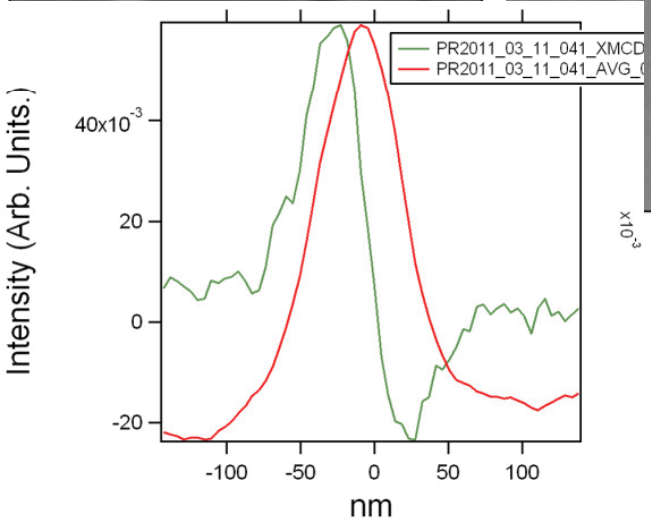

I Kowalik, D. Arvanitis, M.A. Niño et al., in preparation

Magnetization in NiPd nanostructures

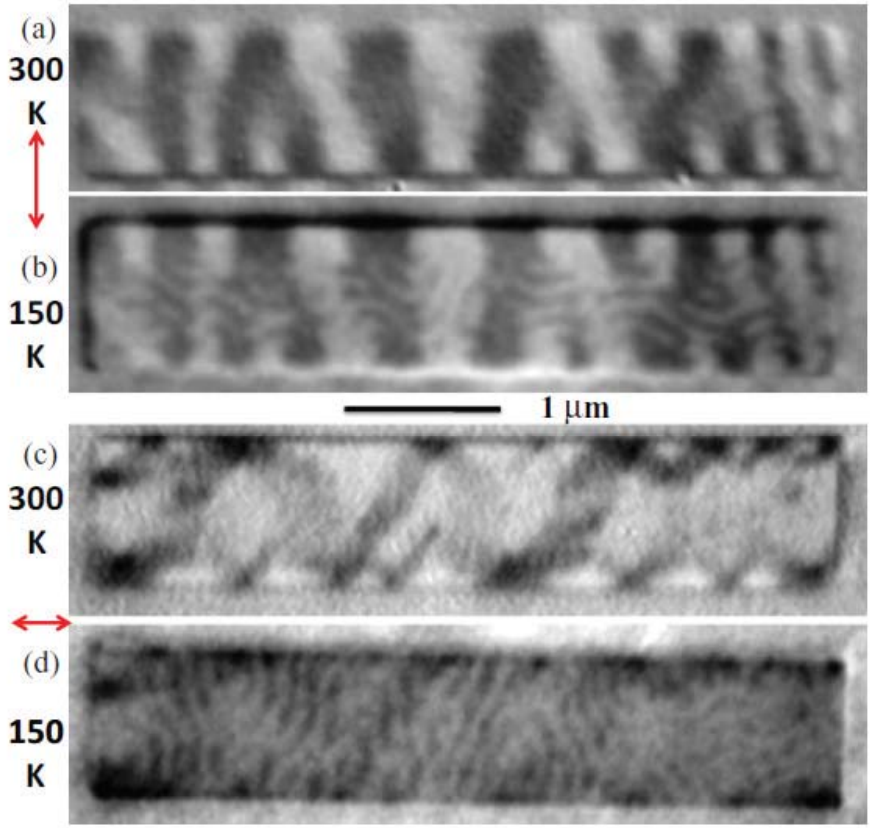

J.-Y. Chauleau, Phys. Rev. B 84, 094416 (2011)

Magnetic imaging basics: XMLD

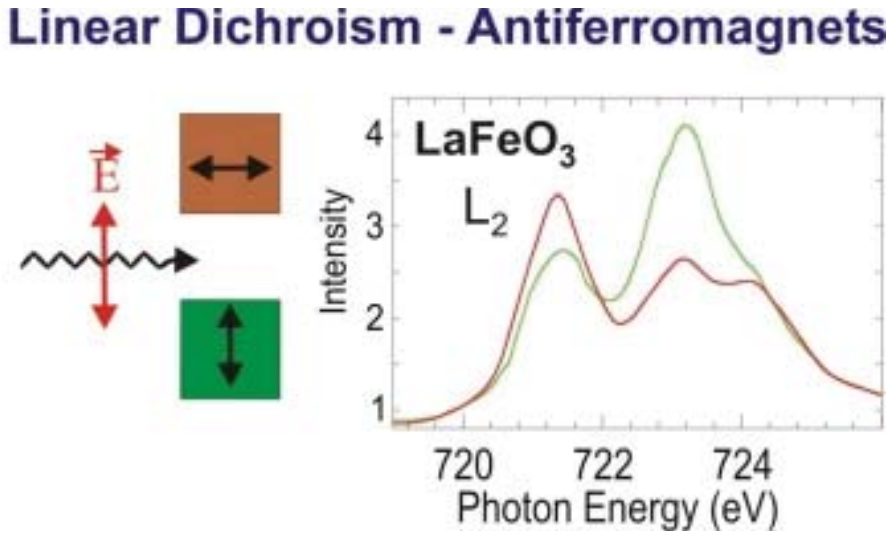

In the presence of spin order the spin-orbit coupling leads to preferential charge order relative to the spin direction, which is exploited to determine spin axis in antiferromagnetic systems.

✓Element sensitive technique

✓ Secondary imaging with PEEM determine large probing depth (10 nm), buried interfaces.

✓Applied in AFM systems (oxides such as NiO)

Absorption intensity at resonance

$$I(\vartheta,\theta,T) = a + b(3\cos^2\vartheta - 1)\langle Q_{zz}\rangle + c(3\cos^2\theta - 1)\langle M^2\rangle_T + d\sum_{i,j}\langle \hat{s}_i \cdot \hat{s}_j\rangle_T$$

1st term: quadrupole moment, i.e.electronic charge (not magnetic!)

2nd term determines XMLD effect; Θ is the angle between E and magnetic axis A; XMLD max for E || A; M reflects long range magnetic order

SPELEEM microscope

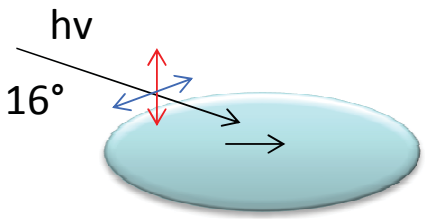

Linear vertical and linear horizontal polarization of the photon beam are used

Applications of XMCD and XMLD

Direct observation of the alignment of ferromagnetic spins by antiferromagnetic spins

F. Nolting*, A. Scholl*, J. Stöhr†, J. W. Seo‡§, J. Fompeyrine§, H. Siegwart§, J.-P. Locquet§, S. Anders*, J. Lüning†, E. E. Fullerton†, M. F. Toney†, M. R. Scheinfein‖ & H. A. Padmore*

Nature, 405 (2000), 767.

Figure 1 Images and local spectra from the antiferromagnetic and ferromagnetic layers for 1.2-nm Co on $LaFeO_3/SrTiO_3(001)$. **a**, Fe L-edge XMLD image; **b**, Co L-edge XMCD image. The contrast in the images arises from antiferromagnetic domains in $LaFeO_3$ (**a**) and ferromagnetic domains in Co (**b**) with in-plane orientations of the antiferromagnetic axis and ferromagnetic spins as indicated below the images. The spectra shown underneath were recorded in the indicated areas and illustrate the origin of the intensity contrast in the PEEM images.

ferromagnet/antiferromagnet Co/LaFeO3 bilayer, demonstrating interface exchange coupling between the two materials

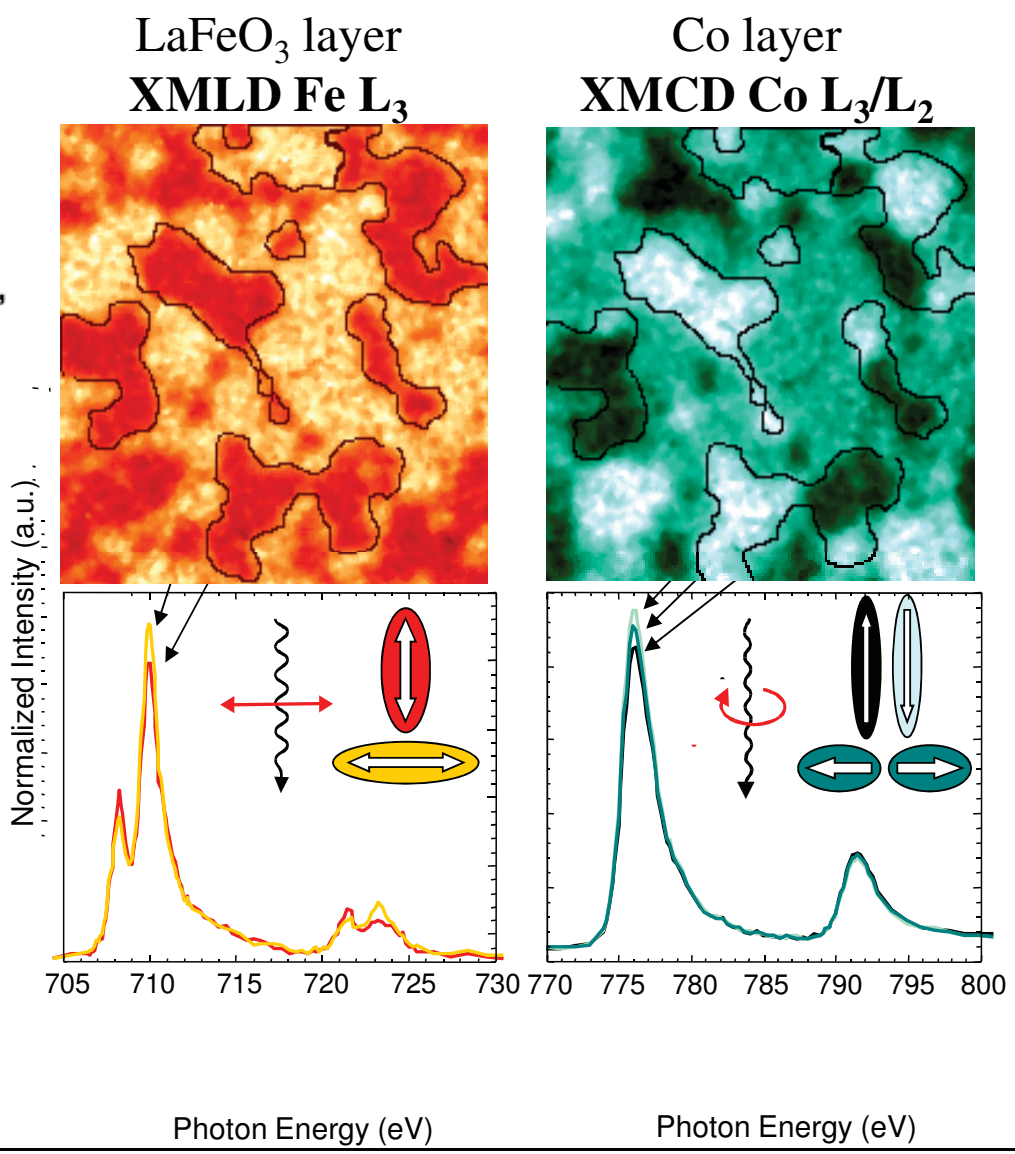

Antiferromagnetic domain imaging using AFM-LEEM

- NiO model system with well known bulk magnetic domain structure.
- 12 possible AFM domains ("T") in a bulk NiO single crystal

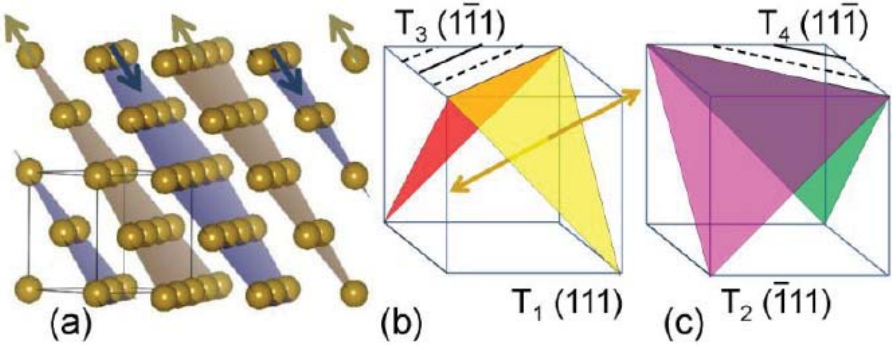

- Coherent exchange scattering: Palmberg et al: Phys. Rev.Lett. 21, 682 (1968).

Darkfield LEEM on half order spots

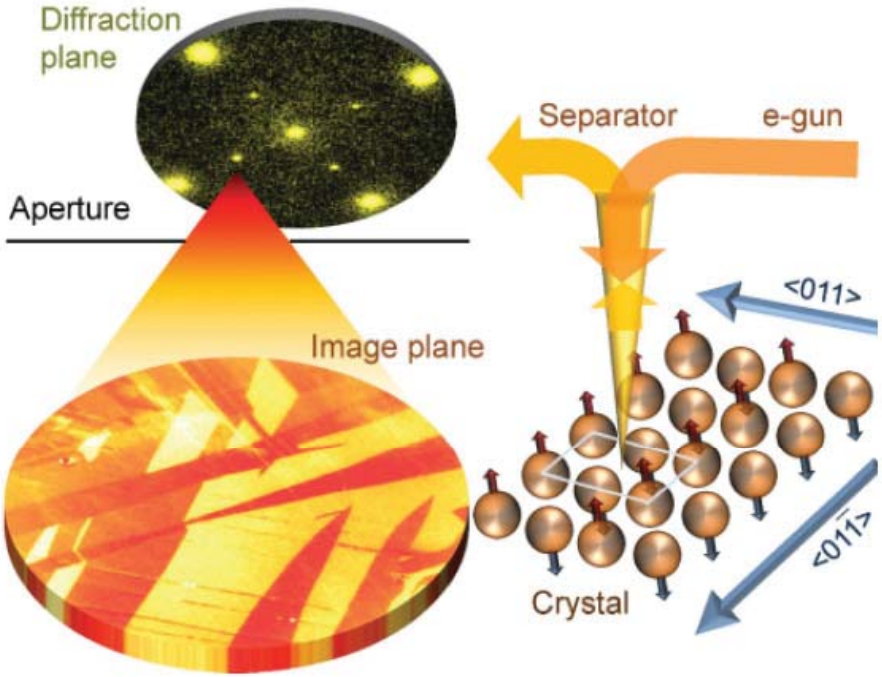

AFM-LEEM vs XMLD PEEM

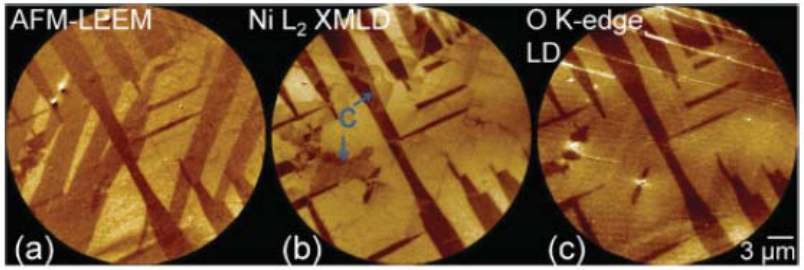

K. Menon et al, PRB 84, 132402 (2011), rapid comm.

Antiferromagnetic domain imaging using AFM-LEEM

Cleaved NiO

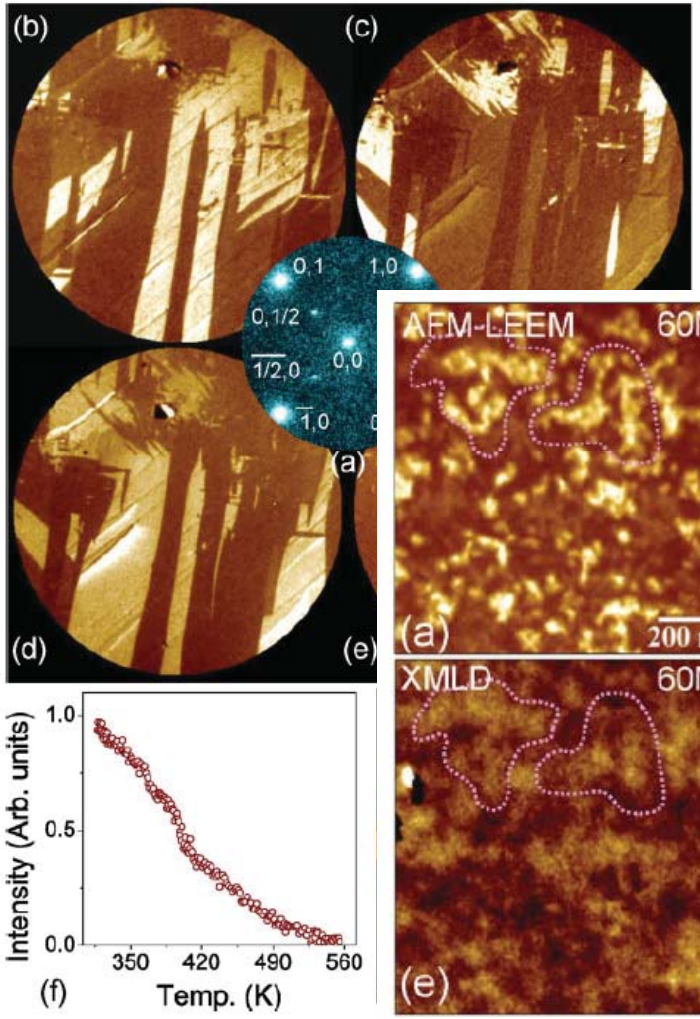

NiO/Ag(100) in-situ growth

T domain identification;

Evolution vs time,

Sample temperature;

High surface sensitivity;

High lateral resolution;

Complementary to PEEM

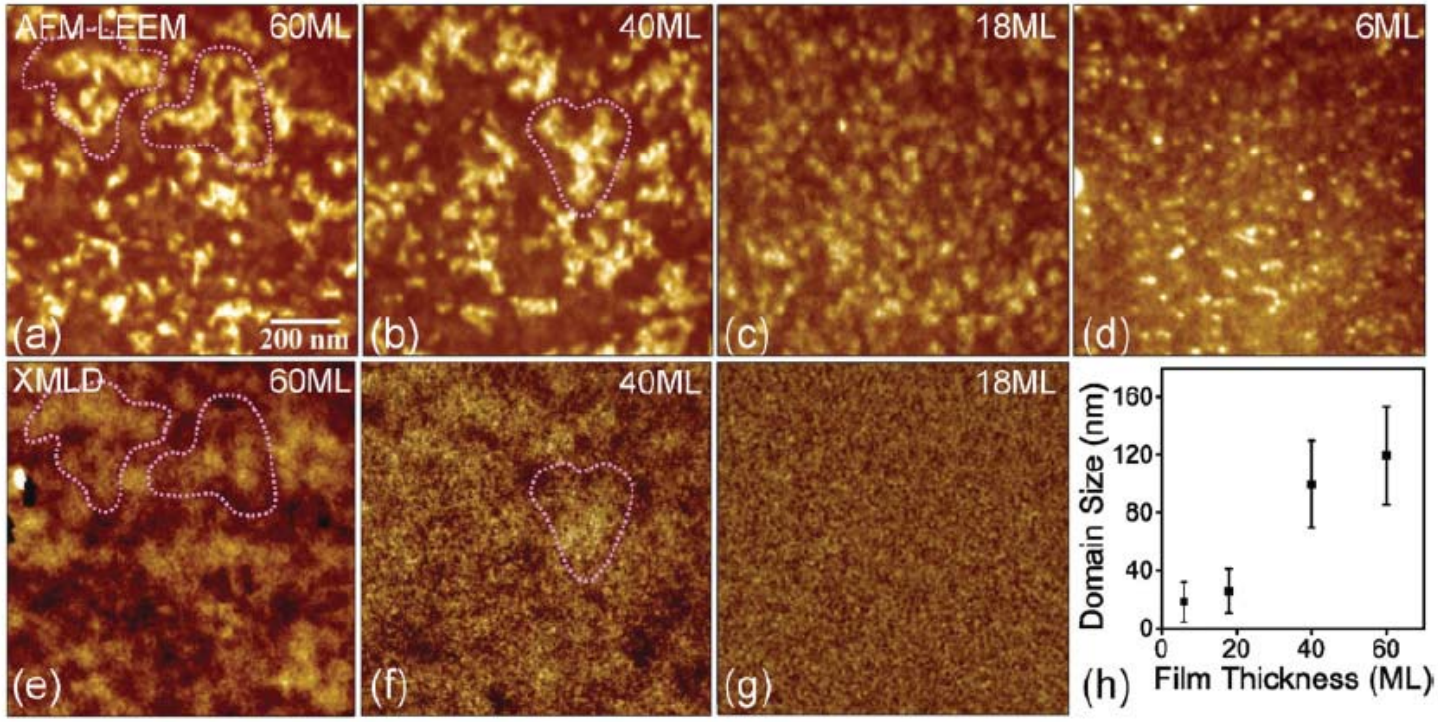

K. Menon et al, PRB 84, 132402 (2011), rapid comm.

MnAs/GaAs(100): epitaxial films

- Two phases coexist at RT
  - Hexagonal α phase (FM)
  - Orthorombic β phase (PM)

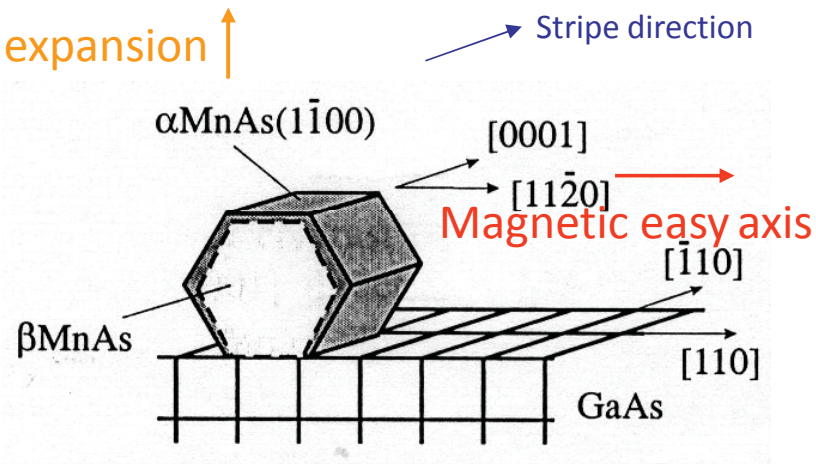

Very large misfit along [0001] direction
→ coincidence lattice

7% misfit along [11-20] direction → strain
Strain relaxation expansion normal to the film

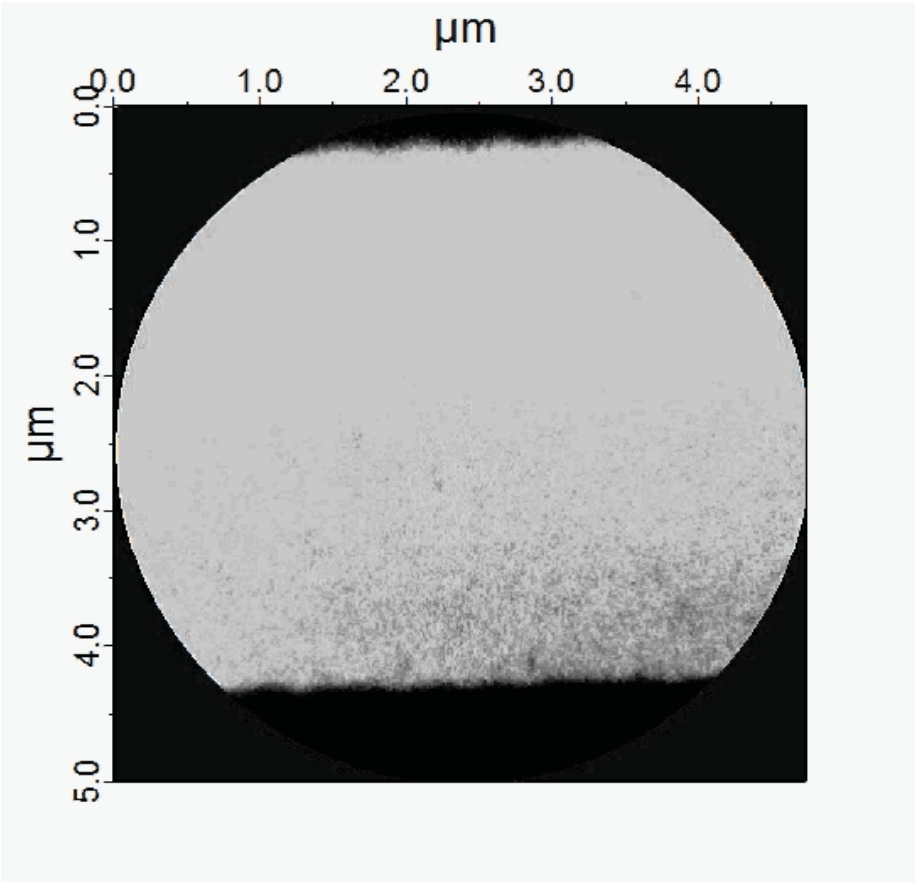

180 nm MnAs

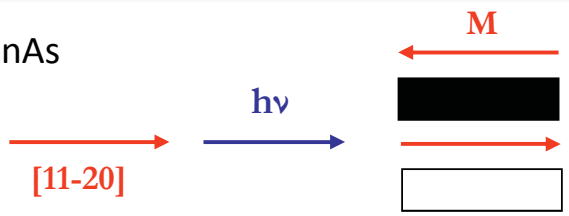

Limited probing depth of XMCD: domain strucutre of stripes

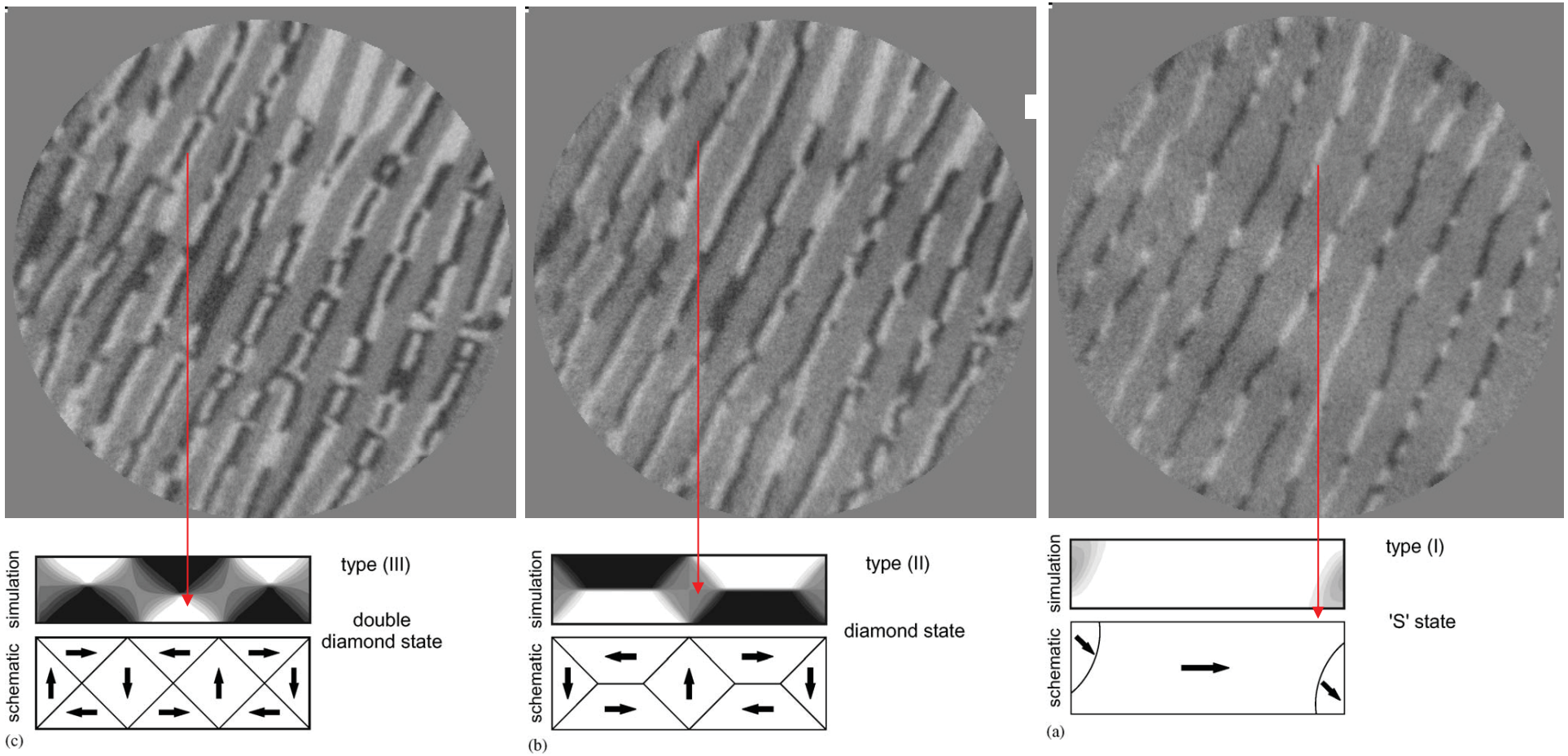

Experiment: Straight walls; Head to head domains

Simulation: Cross sectional cut: diamond state

180 nm MnAs

R. Engel-Herbert et al,
J. Magn. Magn. Mater. 305 (2006) 457

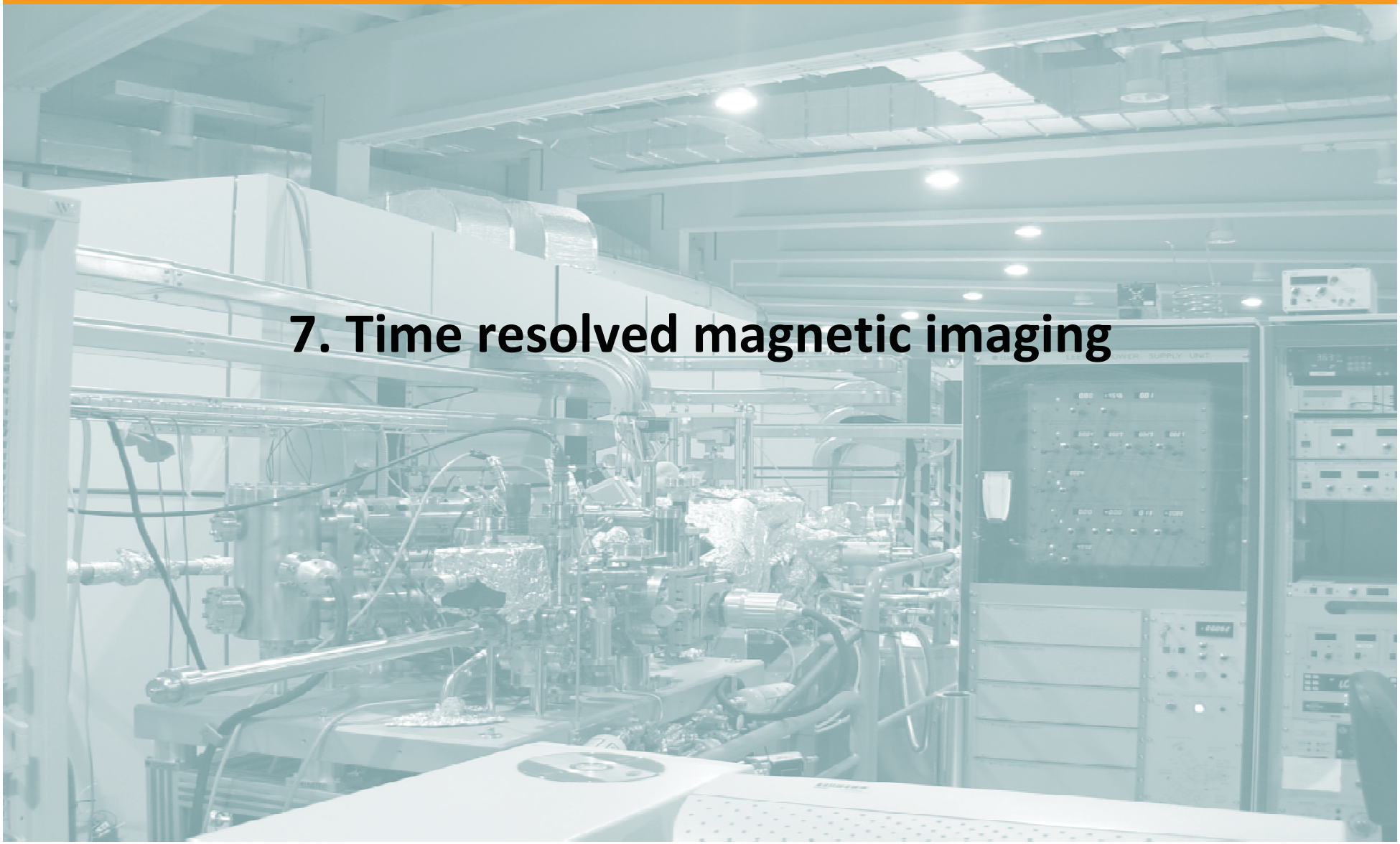

7. Time resolved magnetic imaging

Motivation of time resolved magnetic imaging

- Switching processes (magnetisation reversal) in magnetic elements (in spin valves, tunnel junction)
  - Nucleation, DW propagation or both?
  - Effect of surface topography, morphology crystalline structure etc.
  - Domain dynamics in Landau flux closure structures.
- response of vortices, domains, domain walls in Landau closure domains in the precessional regime
- Stroboscopic technique:
  - only reversible processes can be studied by pump – probe experiments
  - Spatial and time resolution are still limited

Time resolved PEEM techniques for magnetic imaging

Stroboscopic experiments combine high lateral resolution of PEEM with high time resolution, taking advantage of pulsed nature of synchrotron radiation

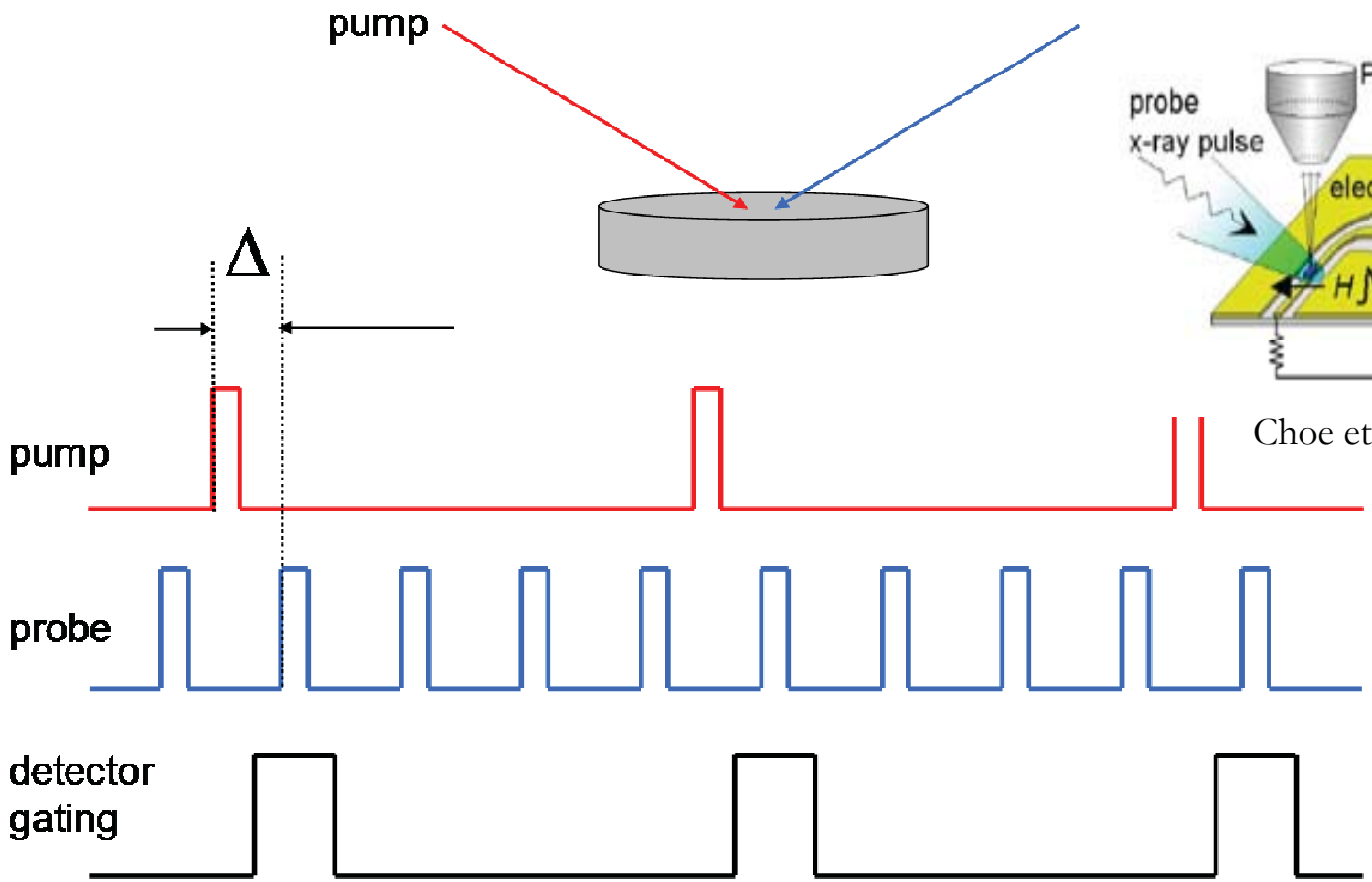

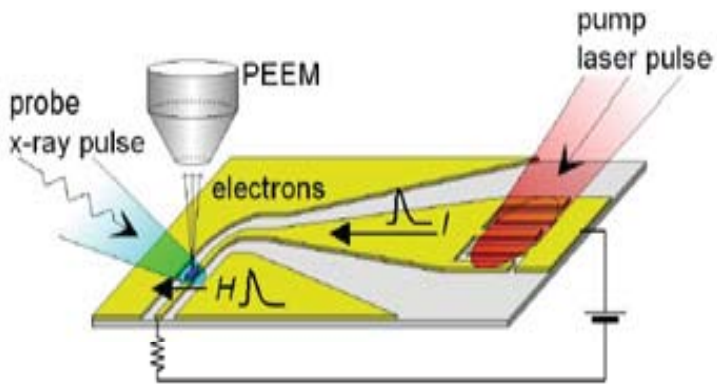

Choe et Al, Science, 304 (2004), 420

Magnetic excitations in LFC structures

PRL 94, 217204 (2005)

Quantitative Analysis of Magnetic Excitations in Landau Flux-Closure Structures Using Synchrotron-Radiation Microscopy

J. Raabe,[1,*] C. Quitmann,[1] C. H. Back,[2] F. Nolting,[1] S. Johnson,[1] and C. Buehler[1]

The time dependent magnetization is described by the phenomenological Landau-Lifshitz-Gilbert equation

$$\frac{d}{dt}\vec{M} = -\gamma_0 \vec{M} \times \vec{H}_{\text{eff}} + \frac{\alpha}{M}\left(\vec{M} \times \frac{d}{dt}\vec{M}\right).$$

The first term describes the precession of the magnetization $\vec{M}$ about the total effective field $\vec{H}_{\text{eff}}$. The second term describes the relaxation back into the equilibrium state using the dimensionless damping parameter α.

torque $\vec{T} = -\gamma_0 \vec{M} \times \vec{H}_{\text{eff}}$

xmcd

t_i-t_0

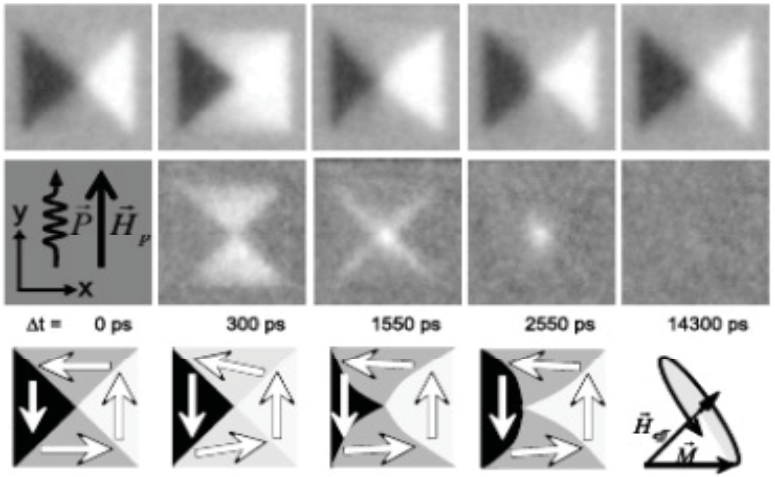

Quantitative measurement of:

- Vortex displacement (max 750 nm)
- Domain wall displacement and buldging
- Vortex velocity (~ 700 m/s)
- Quantitative time-dependent magnetisation
- Fourier analysis

Magnetic excitations in LFC structures

PRL **94**, 217204 (2005)

Quantitative Analysis of Magnetic Excitations in Landau Flux-Closure Structures Using Synchrotron-Radiation Microscopy

J. Raabe,[1,*] C. Quitmann,[1] C. H. Back,[2] F. Nolting,[1] S. Johnson,[1] and C. Buehler[1]

The time dependent magnetization is described by the phenomenological Landau-Lifshitz-Gilbert equation

$$\frac{d}{dt}\vec{M} = -\gamma_0 \vec{M} \times \vec{H}_{\mathrm{eff}} + \frac{\alpha}{M}\left(\vec{M} \times \frac{d}{dt}\vec{M}\right).$$

The first term describes the precession of the magnetization $\vec{M}$ about the total effective field $\vec{H}_{\mathrm{eff}}$. The second term describes the relaxation back into the equilibrium state using the dimensionless damping parameter α.

torque $\vec{T} = -\gamma_0 \vec{M} \times \vec{H}_{\mathrm{eff}}$

xmcd

t_i-t_0

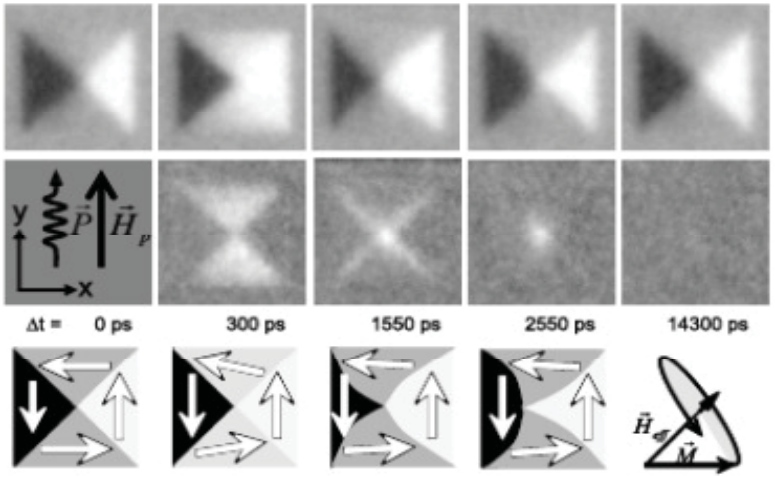

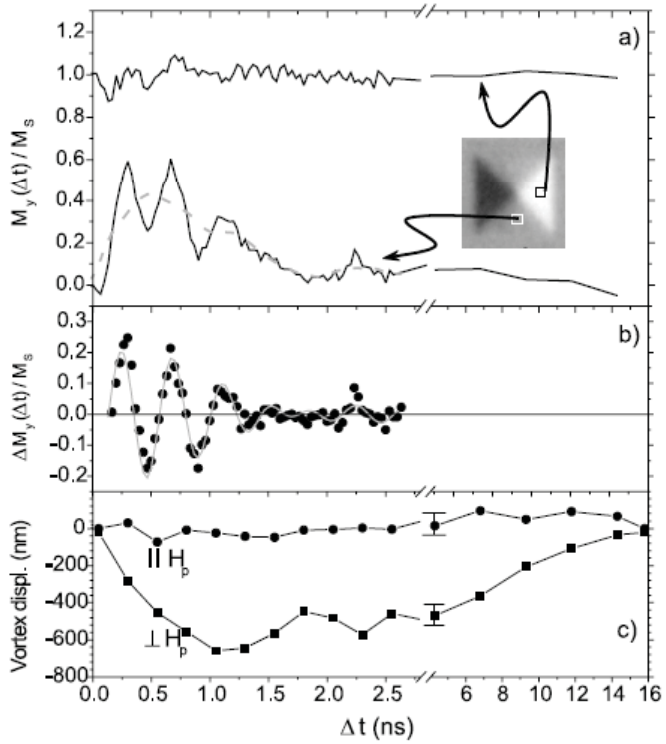

References on time resolved XMCD-PEEM

[8.1] Choe S-B, Acermann Y, Scholl A, Bauer A, Doran A, Stöhr J and Padmore H A 2004 *Science* **304** 420

[8.2] Schneider C M, Kuksov A, Krasyuk A, Oelsner A, Neeb D, Nepijko S A, Schönhense G, Mönch I, Kaltofen R, Morais J, de Nadaï C and Brookes N B 2004 *Appl. Phys.Lett.* **85** 2562

[8.3] Schneider C M, Krasyuk A, Nepijko S A, Oelsner A and Schönhense G 2006 *J. Magn. Magn. Mater.* **304** 6

[8.4] Krasyuk A, Wegelin F, Nepijko S A, Elmers H J and Schönhense G 2005 *Phys. Rev. Lett.* **95** 207201,

[8.5] Raabe J, Quitmann C, Back C H, Nolting F, Johnson S, and Buehler C, 2005 *Phys. Rev. Lett.* **94** 217204.

[8.6] Buess M, Raabe J, Perzlmaier K, Back C H and Quitmann C 2006 *Phys. Rev. B* **74** 100404

[8.7] Kuch W, Vogel J, Camarero J, Fukumoto K, Pennec Y, Pizzini S, Bonfim M and Kirschner J 2004 *Appl. Phys. Lett.* **85** 440

[8.8] Vogel J, Kuch W, Hertel R, Camarero J, Fukumoto K, Romanens F, Pizzini S, Bonfim M, Petroff F, Fontaine A and Kirschner J 2005 *Phys. Rev. B* **72** 220402

[8.9] Fukumoto K, Kuch W, Vogel J, Romanens F, Pizzini S, Camarero J, Bonfim M and Kirschner J 2006 *Phys. Rev. Lett.* **96** 097204

[8.10] Pennec Y, Camarero J, Toussaint J C, Pizzini S, Bonfim M, Petroff F, Kuch W, Offi F, Fukumoto K, Nguyen Van Dau F and Vogel J 2004 *Phys. Rev. B* **69** 180402

Spectromicroscopy with the XPEEM microscope

- XPEEM
  - » Chemical maps
  - » Chemical state (core level shifts)
  - » High versatility
  - » Limitation: size (< 30 nm) and flux: aberration corrected?
- LEEM, micro-LEED
  - » Structure
  - » Study of dynamic processes
- XMCD and XMLD PEEM
  - » Magnetic state in nanostructures and thin films
  - » Element sensitivity
  - » Thin films and buried interfaces
  - » High lateral and time resolution